TABLE OF CONTENTS

Page

LIST OF TABLES

Page

LIST OF FIGURES

LIST OF ABREVIATIONS

3GPP	3rd Generation Partnership Project
4G	4th Generation
5G	5th Generation
BS	Base Station
CA	Carrier Aggregation
CDF	Cumulative Distribution Function
CoMP	Coordinated Multi-Point
CSI	Channel State Information
D2D	Device-to-Device
DL	Down-Link
eNB	evolved Node-B
HetNet	Heterogenous Network
LoS	Line-of-Sight
LTE	Long Term Evolution
LTE-A	LTE Advanced
M2M	Machine-to-Machine
MCN	Multi-hop Cellular Networks
MIMO	Multiple-Input-Multiple-Output
MME	Mobility Management Entity

clicours.com

ODMA	Opportunity Driven Multiple Access
OFDMA	Orthogonal Frequency-Division Multiple Access
PDF	Probability Density Function
QoS	Quality-of-Service
REN	Relay Enhanced Network
RSS	Received Signal Strength
RWP	Random Way Point
SDO	Standards Development Organizations
SINR	Signal-to-Interference-plus-Noise-Ratio
SISO	Single-Input-Single-Output
TDD	Time-Division Duplexing
TM	Transmission Mode
UE	User Equipment
UL	Up-Link
UMTS	Universal Mobile Telecommunications System
V-MIMO	Virtual-MIMO
VoIP	Voice-over-IP
WiMax	Worldwide Interoperability for Microwave Access

LISTE OF SYMBOLS AND UNITS OF MEASUREMENTS

α	Path loss exponent
λ	Density of the Rayleigh distribution of the transition length
$\mathbb{E}[R]$	Expected value of random variable R
$\mathbb{V}[R]$	Variance operator of random variable R
C_n	n handover region
μ	Processing time of the handover process
Φ	Ordered set of tangent directions
ϕ_n	nth element of Φ
Ψ	Ordered set of critical directions
ψ_n	nth element of Ψ
σ_s	Standard deviation of s_{ij}
σ_s^2	Shadowing variance
σ_z	Standard deviation of z_{ij}
σ_z^2	Fast fading variance
θ	Direction of movement
θ_{tn}	nth Tangent direction
c	Propagation constant
d_{ij}	Distance between transmitter i and receiver j
d_{pn}	nth perpendicular distance

d_{pT}	Distance threshold of the handover algorithm
d_p	Distance of the moving entity from the map
$dA(r,\theta)$	Area element at (r,θ)
$f_R(r)$	PDF of random variable R
$F_R(r)$	CDF of random variable R
H	Set of perpendicular distance variables
h_{ij}	Channel gain between transmitter i and receiver j
K	A unitless constant that depends on the antennas characteristics
L_i	Random transition length at ith transition
N	Number of handovers
$n_{\mathrm{i}}^{\mathrm{R}}$	Received noise at receiver i in dedicated mode
$n_{\mathrm{i}}^{\mathrm{R}}$	Received noise at receiver i in reuse mode
$n_{\mathrm{i}}^{\mathrm{R}}$	Received noise at receiver i in cellular mode
N_0	Spectral density of white Gaussian noise
N_c	Maximum number of possible intersection points
N_d	Maximum number of possible critical directions
N_p	Maximum number of possible perpendicular points
N_t	Maximum number of possible tangent points
$P_{C_n}(\theta)$	Probably of being in C_n region in the direction of θ
P_{i}	Transmit power of transmitter i

$P_S(.)$	PDF of pause time
$P_V(.)$	PDF of velocity
R_{C}	Overall throughput of the network in cellular mode
r_{C}	Cell radius
R_{D}	Overall throughput of the network in dedicated mode
R_{R}	Overall throughput of the network in reuse mode
r_{cn}	nth intersection distance
R_H	Handover rate
S	Pause time
S_{ij}	Log-normal shadow fading variable for communication channel between transmitter i and receiver j
s_{ij}	Zero mean Gaussian random variable
S_i	Random pause time at $i+1$th waypoint
S_T	Sojourn time
T	Transition time
T_d	Running delay of the handover algorithm
T_p	Period time
$\mathrm{UE_c}$	Cellular UE
$\mathrm{UE_d}$	Destination UE
$\mathrm{UE_s}$	Source UE
v	Velocity of the moving entity

V_i	Random velocity of moving entity at *i*th transition
X	Distance variable
x	Converted distance variable
X_{c}	Horizontal coordinate of the cellular UE
X_{d}	Horizontal coordinate of the destination UE
$x_{\mathrm{i}}^{\mathrm{C}}$	Transmitted signal from transmitter i in cellular mode
$x_{\mathrm{i}}^{\mathrm{D}}$	Transmitted signal from transmitter i in dedicated mode
$x_{\mathrm{i}}^{\mathrm{R}}$	Transmitted signal from transmitter i in reuse mode
X_{s}	Horizontal coordinate of the source UE
X_{cn}	Vertical coordinate of the *n*th intersection point
X_{cn}	Horizontal coordinate of the *n*th intersection point
X_{pn}	Horizontal coordinate of the *n*th perpendicular point
X_{tn}	Horizontal coordinate of the *n*th tangent point
X_i	Vertical coordinate of the moving entity
Y	Distance variable
y	Converted distance variable
Y_{c}	Vertical coordinate of the cellular UE
Y_{d}	Vertical coordinate of the destination UE
$y_{\mathrm{i}}^{\mathrm{C}}$	Received signal at receiver i in cellular mode
$y_{\mathrm{i}}^{\mathrm{D}}$	Received signal at receiver i in dedicated mode

y_i^R	Received signal at receiver i in reuse mode
Y_s	Vertical coordinate of the source UE
Y_{pn}	Vertical coordinate of the nth perpendicular point
Y_{tn}	Vertical coordinate of the nth tangent point
Y_i	Horizontal coordinate of the moving entity
Z	Distance variable
z	Converted distance variable
z_{ij}	Gaussian fast fading variable for communication channel between transmitter i and receiver j

INTRODUCTION

The ever-increasing mobile traffic in recent years has induced service providers and telecommunications industries to develop new techniques and designs to provide higher data rates with guaranteed Quality-of-Service (QoS) and smaller prices (CISCO, 2015) for their customers in their everyday cellular communications. Relying solely on the traditional cellular networking cannot provide these qualities to the users. Therefore, in the last decade, providers and industrial telecommunication companies have developed new techniques and designs, such as cognitive radio (Mitola and Maguire, 1999; Liang *et al.*, 2008), Femtocells (Chandrasekhar *et al.*, 2008; Claussen *et al.*, 2008), Device-to-Device (D2D) communications (Doppler *et al.*, 2009; Janis *et al.*, 2009; Doppler *et al.*, 2011, 2010), Carrier Aggregation (CA) (Yuan *et al.*, 2010), Coordinated Multi-Point (CoMP) (Irmer *et al.*, 2011), Relay-Enhanced Networks (REN) (Salem *et al.*, 2010), and Heterogeneous Networks (HetNet) (Damnjanovic *et al.*, 2011) for 4th-generation (4G) Long Term Evolution (LTE), LTE–Advanced (LTE-A), and 5th-Generation (5G) systems. These schemes provide users with more capabilities on their User Equipments (UEs), much higher data rates and less latency (Osseiran *et al.*, 2011; Asadi *et al.*, 2014; Andrews *et al.*, 2014; Li and Guo, 2014; Mumtaz and Rodriguez, 2014; Song *et al.*, 2015).

The D2D transmission is one of the features proposed for 5G networks that enables paired UEs to communicate directly with each other without unnecessary routing of traffic through the network infrastructure (Doppler *et al.*, 2009, 2011; Janis *et al.*, 2009; Doppler *et al.*, 2010). In Fig. 0.1 a simple D2D transmission has been compared with the traditional cellular network.

Such a transmission provides four types of gains (Lei *et al.*, 2012; da S. Rêgo *et al.*, 2012; Phunchongharn *et al.*, 2013; Asadi *et al.*, 2014; Mumtaz and Rodriguez, 2014; Song *et al.*, 2015; Panagopoulos, 2015):

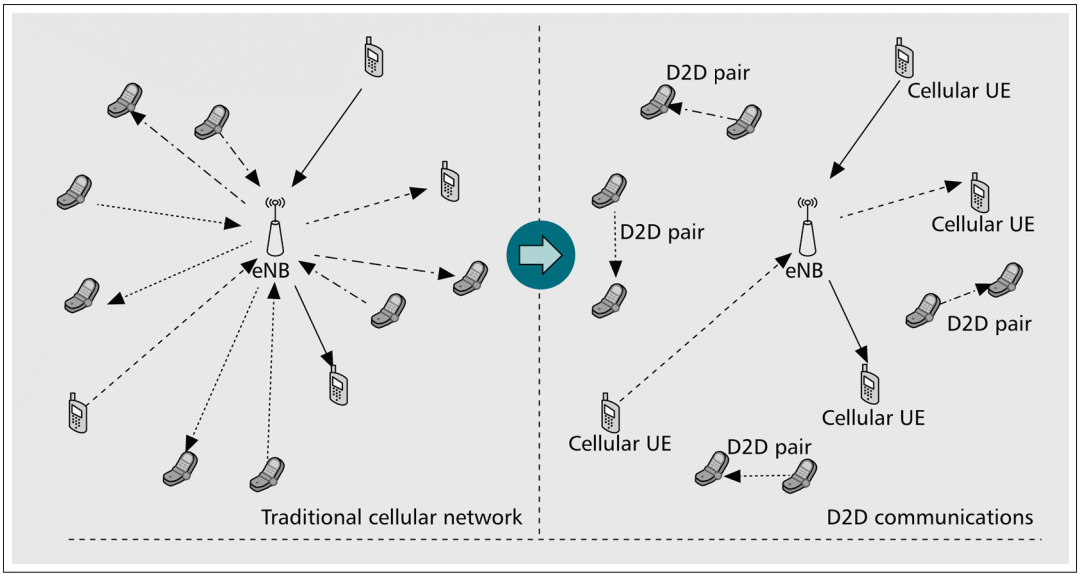

Figure 0.1 D2D transmissions underlaying a traditional cellular wireless communications system
Taken from Phunchongharn *et al.* (2013)

- Proximity gain: where the short range communication using a D2D link enables high bit rates, low delays, and low power-consumption;
- Hop gain: where D2D transmission uses one hop rather than two hops (i.e. communicating via evolved Node-B (eNB) in which case both Up-Link (UL) and Down-Link (DL) resources are used);
- Reuse gain: where D2D and cellular links can simultaneously share the same radio resources;
- Pairing gain: which facilitates new types of wireless local-area services.

There are three possible Transmission Modes (TM) for D2D enabled UEs: reuse, dedicated, and cellular modes. The first two TMs are using direct transmission between paired UEs, while the last is the traditional cellular transmission. In the reuse mode the same frequency resource is reused by both D2D paired UEs and other cellular transmission in the network, which causes interference at the receivers. However, in the dedicated and cellular modes different resources are dedicated to each D2D transmission and cellular transmission, hence no interference ap-

pears at receivers. In order to start communication, D2D UEs should decide among these three different TMs (Doppler *et al.*, 2010; Liu *et al.*, 2012b,a; Song *et al.*, 2015; Panagopoulos, 2015; Wang and Tang, 2016; Huang *et al.*, 2016), or they could also apply a mixed mode mechanism in which each D2D link can utilize multiple modes through mode switching or resource multiplexing (Feng *et al.*, 2015; Tang and Ding, 2016). Such a decision process is called the mode selection. Fig. 0.2 shows these three possible modes in a D2D enabled 5G network.

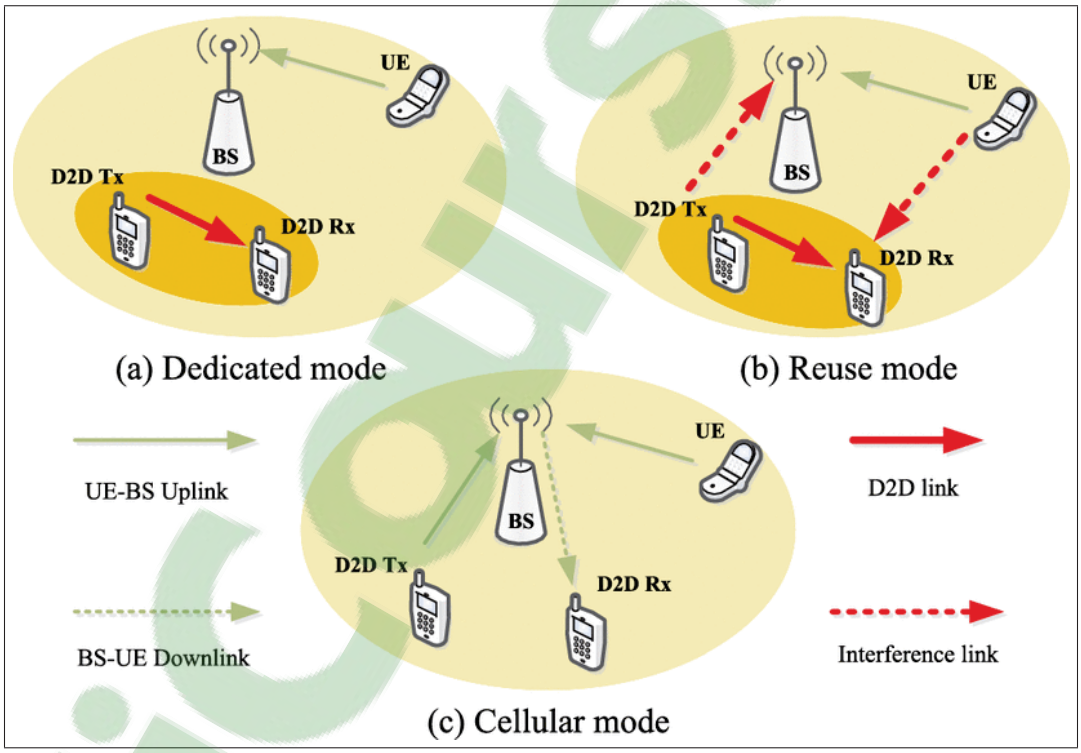

Figure 0.2 Three different TMs in D2D enabled networks
Taken from Feng *et al.* (2015)

For single mode selection, the decision is made periodically based on a specific criterion, such as the overall throughput of the network. In other words, the TM which gives the highest throughput is selected. It has been shown that for a fixed transmission power, channel conditions, and noise power, the TM to be selected depends on the location of entities in the network (Morattab *et al.*, 2015).

In this work, to the best of our knowledge, we show for the first time that there are certain geographical regions characterized by the fact that movement of one entity inside any particular region, while other entities are fixed, does not change the selected TM for the D2D UEs' communication. We find the function that define the borders of such regions analytically for two different scenarios in which the communication channel between the network entities is a Line-of-Sight (LoS) path-loss channel or when it experiences fading. We denote the set of these regions and the borders between them as the mode selection map of the D2D enabled network. Then we use these results to propose a vertical handover mechanism to enable a smooth transmission in the network while UEs are moving.

Motivation

In our recent work (Morattab *et al.*, 2015), we studied the possible mode selection technique for a network where entities use Multiple-Input-Multiple-Output (MIMO) techniques. In that work, we observed that there are certain regions in the network that if the cellular UE is located there, always a specific TM is selected by paired D2D UEs. Such regions were also shown in (Doppler *et al.*, 2009) implicitly where the main objective was to maximize the overall throughput of the network through mode selection for single antenna UEs in the network. In both studies, the resulted map is achieved numerically by calculating the throughput for each TM at a specific point in the network, and the TM that gives the highest overall throughput in this point is indicated. Fig. 0.3 shows the resulting map achieved by running a numerical point by point mode selection algorithm for single antenna and multiple antenna cases presented in (Doppler *et al.*, 2010) and (Morattab *et al.*, 2015) respectively.

This study is motivated by the following questions brought up from our observations of (Doppler *et al.*, 2010) and our work (Morattab *et al.*, 2015):

- Is there any analytical approach to derive these geographical regions?

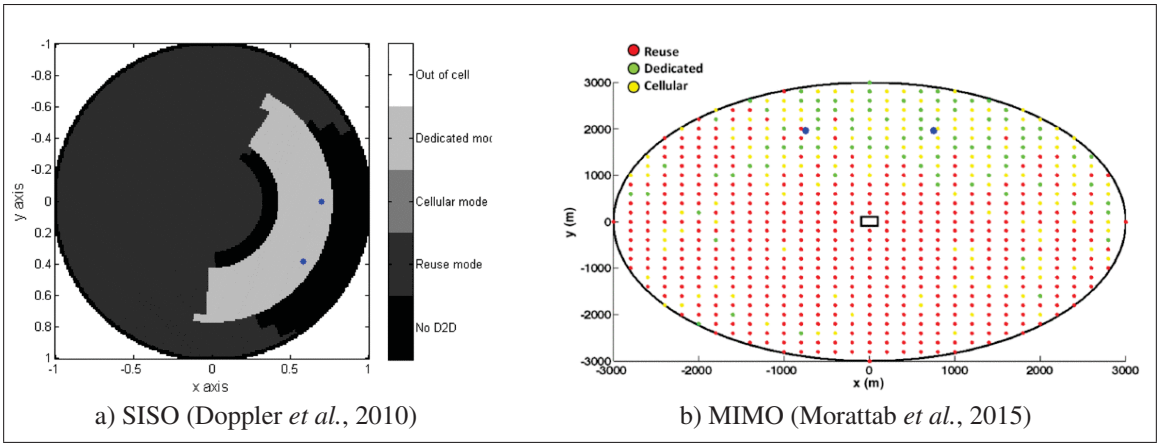

a) SISO (Doppler *et al.*, 2010) b) MIMO (Morattab *et al.*, 2015)

Figure 0.3 Mode selection map numerically resulted from mode selection algorithm for Single-Input-Single-Output (SISO) and MIMO cases

- What factors affect the shape of these regions?
- Being analytically calculated, what are the applications that can take advantage of such regions?

To better understand the set of issues we are going to solve in this work, the summary of these issues is presented in the following Section.

Problem Overview

In this work, we study possible techniques to derive the mode selection map of a D2D enabled 5G network. Relying on our results to find such a map, we study the problem of vertical handover, where movement of the cellular UE causes the TM change in the concurrent communication between the paired D2D UEs. The issues in each part of this study are summarized as follows.

Mode Selection Map

As discussed earlier, a pair of D2D UEs can communicate using the reuse, dedicated, and cellular modes. In general, this communication can be parallel with a subset of other transmissions,

but for simplicity in our study we only allow a single cellular UE to be in transmission in UL with eNB. The movement of any of the UEs might cause a TM change of the D2D pair due to the amount of interference the receiving UE of the D2D pair experiences. Fig. 0.4 shows a specific case where the cellular UE moves in the network while the D2D paired UEs are fixed.

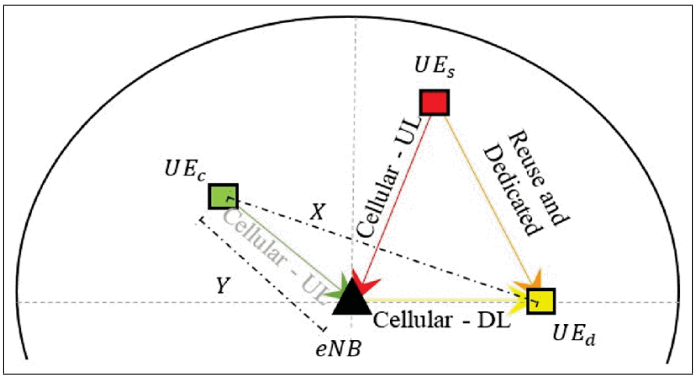

Figure 0.4 A D2D enabled network consisting a paired D2D UEs, UE_s and UE_d, and a cellular UE, UE_c
Taken from Morattab *et al.* (2016)

Our observation of the simulation results in (Doppler *et al.*, 2010; Morattab *et al.*, 2015), brought the idea of having possible disjoint regions to which a specific TM is dedicated. More specifically we address the problem of finding regions in the network where if the moving UE is located there, the paired UEs, i.e. UE_s and UE_d, keep their TM. It should be noted that Fig. 0.4 shows the case where the cellular UE, i.e. UE_c, is moving in the network while UE_s and UE_d are fixed.

The first issue regarding the mode selection map derivation is the mathematical modeling of the problem for different cases in which one of the UEs in the network move while other UEs are fixed. The modeling phase include the steps that should be taken to determine mode selection map equations. The solution to the equations in each case requires different approach due to the type of the equation and the non-linearity appears there. Finally, in our work we study

the mode selection map for two different networks which communication channels experience fading or not. Each case requires different modeling and solution steps.

Mobility Management and Handover

Due to the limited transmission range in D2D communication, a handover mechanism is required to take the responsibility for a possible TM change between the paired D2D UEs and to achieve a seamless communications for the paired D2D UEs when the mobility of the entities in the network, which are synchronized in resource allocation and mode selection process, reduces the performance of the network.

In this work, we use the results from the mode selection map derivation process for handover mechanism. This requires to first identify proper decision parameters and then calculate their value as a function of network variables. Another issue is the presentation of the vertical handover to include the decision parameters as well as practical limitations of the transition between modes. Finally, to evaluate the performance of the handover algorithm some performance metrics should be presented and be calculated.

Objectives

The general objective of this work is to develop analytical approaches for derivation of the mode selection map of a simple D2D enabled network and use its results to achieve a vertical handover mechanism. Therefore, the first main objective is to develop an analytical framework to find the mode selection map of a simple D2D enabled network. This approach should consider different communication channel conditions in terms of fading presence as well as different scenarios where any of the UEs in the network might move.

The second main objective is to utilize the mode selection map in the development of a vertical handover mechanism. Here, a subset of decision parameters should be calculated analytically

for triggering the handover execution. Moreover, to evaluate the performance of the handover procedure, specific metrics should be calculated analytically.

The two main objectives are decomposed into the following specific objectives:

- Study and analysis of mode selection in D2D enabled networks;
- Develop a model to analytical derivation of mode selection map having LoS path-loss model and fading model for the communication channels;
- Study and analysis of handover mechanisms in D2D enabled networks;
- Develop a model to use mode selection map for a handover mechanism;
- Analytical calculation of decision parameters and performance metrics for the handover mechanism.

Methodology

In this work, we study the problem of mode selection map derivation and handover mechanisms in D2D enabled networks using analytical approaches.

In the first phase, we address the problem of the derivation of the mode selection map. For this purpose, we present two scenarios using two different channel models: 1) LoS path-loss model; 2) fading model. For LoS channel scenario, we assume to have fixed communication channels between involved entities. The overall throughput of the network for the reuse, dedicated, and cellular modes is calculated. Then to find the mode selection map, these equations should be equalized two by two and be simplified. Depending on the moving UE, there are three different cases that these equations should be solved to reach the mode selection map. These three cases are when either of UE_c or UE_s or UE_d moves while the other two UEs are fixed. In the fading channel scenario, the communication channel between the involved entities is assumed to experience fading and it is modeled as Rayleigh fading channel. Due to the probabilistic

variation of the channels the expectation of the overall throughput of the network is calculated for three TMs. Like the previous scenario these functions are equalized two by to and solved. In this work, for the fading scenario, we only consider the case where UE_c moves while UE_s and UE_d are fixed.

In the second phase, the problem of vertical handover in D2D enabled network is discussed. We develop a handover algorithm for the case when UE_c moves in the network assuming fixed LoS channels. The first scenario is dedicated to find the decision parameters which are distance from the map and intersection with the map. To find these parameters it is required to develop an analytical approach to calculate perpendicular points from the moving UE_c to the map as well as its intersection with the map when UE_c moves in a specific direction. Then in the second scenario, we use these decision parameters to present the handover mechanism. The distance threshold and the period time of the algorithm execution is also calculated. Finally to evaluate the performance of the handover mechanism we present handover rate and sojourn time and we calculate them for a D2D enabled network analytically using the derived mode selection map.

Contributions

Guided by the objectives presented in Section and using the methodology proposed in Section , this thesis makes the following important novel contributions:

- To the best of our knowledge, calculating the mode selection map when the communication channel between the network entities is modeled as LoS path-loss model without fading, for two different cases which either of the D2D paired UEs move while other UEs are fixed in the network, is treated and solved for the first time;
- To the best of our knowledge, the problem of calculating the mode selection map over a fading channel is presented for the first time in this work;

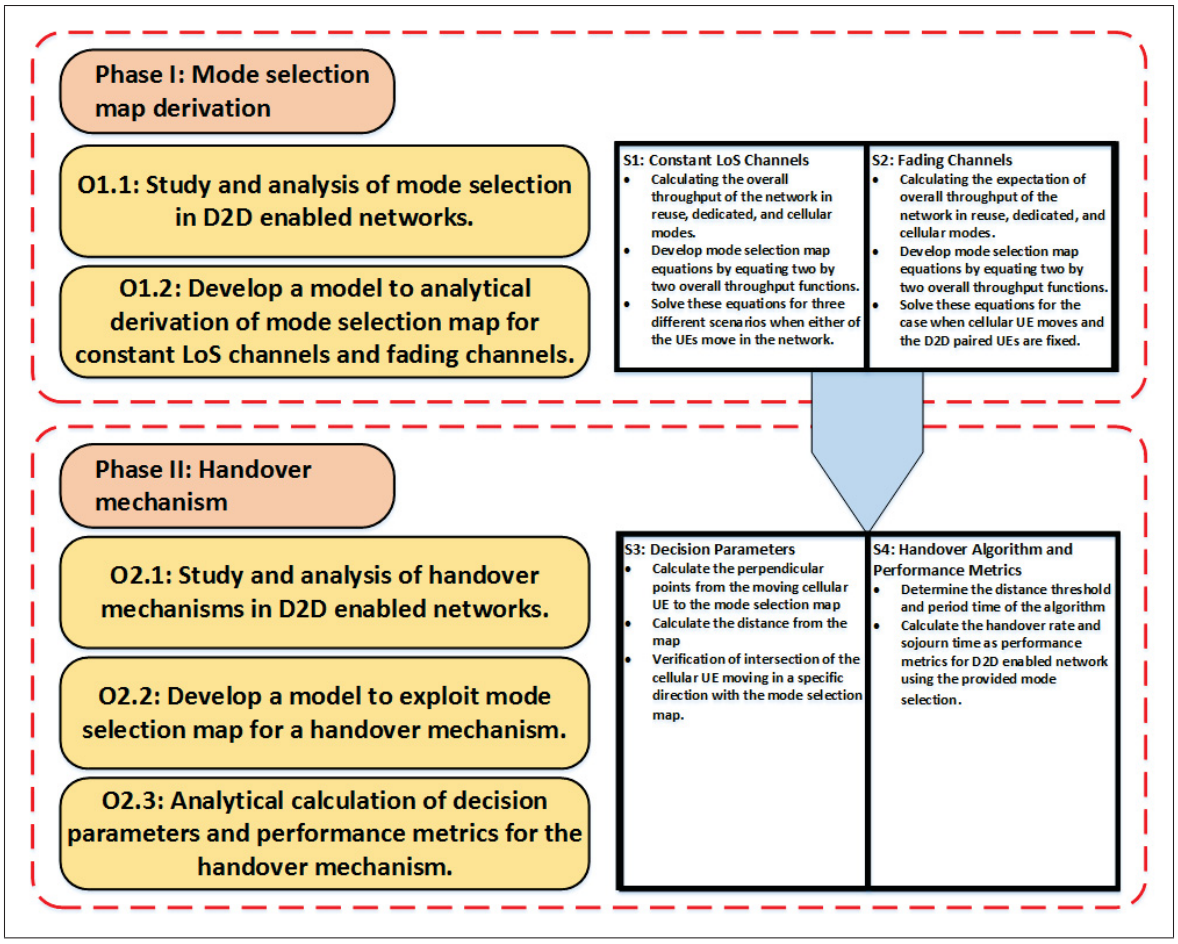

Figure 0.5 Mapping of the objectives and methodology

- A new mobility management and handover technique is proposed based on the distance from the mode selection map and the direction of the moving cellular UE is presented;
- An analytical approach to calculate the distance from the map, as the decision variable of the handover algorithm, and critical direction set is proposed;
- The performance metrics, i.e. handover rate and sojourn time, to evaluate the handover mechanism are analytically calculated.

Publications

The contributions listed in Section have been presented in three journals and two conference publications. The complete list of publications associated with this research work is presented below.

Journals

The two submitted journals (J1 and J2) corresponds to the issue of mode selection map derivation for LoS path-loss channels and fading channels respectively. These works are related to the first phase of this research work and they are presented in chapters 1 and 2 respectively. As a result of the second phase, we have the submitted journal (J3) that correspond to the vertical handover mechanism that is included in Chapter 3.

Submitted

[J1]: Morattab A., Dziong Z., Sohraby K., *Mode Selection Map in Device-to-Device Enabled Networks - An Analytical Approach,* submitted to IEEE Transactions on Vehicular Technology;

[J2]: Morattab A., Dziong Z., Sohraby K., *Mode Selection Map in D2D Enabled Cellular Networks over Fading Channels,* submitted to IEEE Transactions on Vehicular Technology;

[J3]: Morattab A., Dziong Z., Sohraby K., *Vertical Handover in D2D Enabled 5G Networks Based on Mode Selection Map,* submitted to Elsevier Journal of Network and Computer Applications.

Conferences

The conference paper (C1) presents our early achievements on using MIMO precoding/decoding in D2D enabled networks. In this the mode selection is applied by maximizing the overall throughput of the network for each TM, which results on precoding and decoding matrices, and then selecting the mode which gives the highest throughput. This work gave us the initial clue to develop techniques to derive the mode selection map. This work is attached to this

thesis and is presented in appendix I. In other published conference paper (C2), we study for the first time the mode selection derivation problem, only for the case where cellular UE moves in the network and the two D2D paired UEs are fixed. We also assume that the communication channel between the entities is LoS without fading presence. This work is also attached to this thesis and is presented in appendix II.

Published

[C1]: Morattab A., Dziong Z., Sohraby K., *An optimal MIMO mode selection method for D2D transmission in cellular networks*, Wireless and Mobile Computing, Networking and Communications (WiMob), 2015 IEEE 11th International Conference on, Pages: 392-398, October 2015, Abu Dhabi, UAE;

[C2]: Morattab A., Dziong Z., Sohraby K., *Mobility Impact on Mode Selection Map in D2D Networks – An Analytical Approach*, 2016 IEEE Wireless Communications and Networking Conference (WCNC 2016), Pages: 1-6, April 2016, Doha, Qatar.

Thesis Outline

The thesis is organized as follows: The next Chapter presents the literature review related to our addressed problems. Chapters 1-3 show the contribution of this research work.

Chapter 1: Mode Selection Map in Device-to-Device Enabled Networks - An Analytical Approach [J1]

In this chapter we show that there are certain network geographical regions characterized by the fact that movement of one entity inside any particular region, while other entities are fixed, does not change the best TM for D2D UEs' communication. The set of these regions and the borders between them form the mode selection map of the D2D enabled network. While this problem is addressed in our earlier work (Morattab *et al.*, 2016), in this chapter we develop our analytical approach for mode selection map derivation for other two cases where either of the paired D2D UEs move in the network. The resulted map can be used by eNB to assign the best

TM for the communication between D2D UEs without applying the mode selection algorithm periodically. As long as the moving entity does not leave its region, the selected mode remains the same.

Chapter 2: Mode Selection Map in D2D Enabled Cellular Networks over Fading Channels [J2]

Due to multi-path propagation and shadowing from obstacles affecting the wave propagation, the communication channels in wireless networks usually experience fading effects. Being wireless, D2D transmission is not an exception to fading, therefore, to have a reliable modeling and solid results, the fading effect should be taken into account for mode selection, performance analysis, channel modeling, or resource allocation. Likewise, a new approach to derive the mode selection map considering the presence of fading effect, for the communication channels between two entities, is required. Since the statistics of random variables, which represent fading, would not change for a long time, the resulted map could be used in applications such as mode selection, resource allocation, mobility management and handover. Such approach is the subject of this chapter and we provide an analytical framework which leads to geometrical functions describing the mode selection map of the network when fading is present. We develop this model only for the case when cellular UE moves in the network and paired D2D UEs have fixed locations.

Chapter 3: Vertical Handover in D2D Enabled 5G Networks Based on Mode Selection Map [J3]

In this chapter we propose a vertical handover technique to take the responsibility for the TM change for the communication between the paired UEs when the moving cellular UE affects the quality of transmission between them. We apply our analytical approach presented in (Morattab *et al.*, 2016), to reach the mode selection map of the network. We design the handover

algorithm, based on the resulted map, by presenting an analytical framework to find the tangent points, perpendicular points, and intersection points to the map. The resulted equations are applied to find the distance from the map and critical direction set. Our proposed algorithm uses this distance variable together with the direction of the movement, to decide the best time to start the vertical handover procedure. The critical direction set is used to calculate handover rate and sojourn time, which are the performance metrics of our handover algorithm, analytically to analyze its efficiency.

Finally, the thesis ends by conclusions that provide a summary of the addressed problems, the proposed solutions and the future research works.

LITERATURE REVIEW

As discussed before the idea of D2D transmissions is based on the concept of mixing ad-hoc wireless networks and cellular networks. It was discussed for the first time in a 3rd Generation Partnership Project (3GPP) document under the name of "Opportunity Driven Multiple Access" (ODMA) as a mean to improve the efficiency of Universal Mobile Telecommunications System (UMTS)-Time-Division Duplexing (TDD) systems (3GPP, 1999) by establishing a connection between far user and the Base Station (BS) using multi-hop relaying by other users, not a direct communication between two users that they want to communicate with each other.

The idea of direct communication between two users has been presented in (Lin and Hsu, 2000; Qiao *et al.*, 2000; Qiao and Wu, 2000) where they introduce a multi-hop transmission considering mobile devices as relays. In (Lin and Hsu, 2000) the multi-hop scenario has been compared with single-hop scenario, and it has been shown that with the same number of BSs the multi-hop technique has higher throughput in comparison with single-hop. The spatial reuse advantage of such a technique also has been analyzed in the paper. In (Qiao *et al.*, 2000; Qiao and Wu, 2000), the basic idea is to place a number of mobile relay stations within each-cell to achieve dynamic load balancing among different cells which increases the effective capacity of the system. Although they have used fixed relays to bypass the traffic of one cell to the neighbor cell, they have proposed that such a relaying method can be done using the mobile devices which make an ad-hoc network. In order to extend the cell coverage of new cellular systems, the authors in (Gruber and Li, 2004) proposed a novel routing algorithm based on ad-hoc networking which increases the distance between adjacent BSs and reduces the cost of deployment.

In (Le and Hossain, 2007), the authors discuss different challenges in Multi-hop Cellular Networks (MCN) where relays are deployed in specific location in the network to enhance the communication in UL an DL. In this work, a Virtual-MIMO (V-MIMO) technique which users or relays can make a cluster to pass the signal from source to destination in a single hop or multiple hops is discussed. The handover issue in MCN has been studied in (Cho *et al.*, 2009)

which relay stations are located either inside a cell or on the boundary between two adjacent cells. This paper also investigates the effects of the deployment position of relay stations to handover performance. It has been shown that the overall throughput of the MCN with relay stations inside a cell is higher than for those with relay stations on the boundary between two adjacent cells, whereas the opposite is observed for the throughput of cell-boundary users. (Mahmoud and Shen, 2012) proposes a fair and efficient incentive mechanism to stimulate the user cooperation in MCN. The presented mechanism uses a charging policy for source and destination nodes to deal with the problem of selfish nodes which they just make use of the cooperative nodes to relay their packets.

Since 1999 when the idea of Internet of Everything (IoE), which later called Machine-to-Machine (M2M) transmission, was presented in (Ashton, 2009), many researchers started to investigate the challenges in that area. The main issue was how to enable machines equipped with different transmission systems to communicate with each other efficiently. Although such a transmission can be done using wire-line or wireless systems, the cellular networks have been suggested to be the main infrastructure to enable machines to directly communicate with each other as it is partially standardized for LTE networks as LTE-M by Seven Standards Development Organizations (SDOs) (3GPP, 2012). D2D transmission is a special case of M2M transmission which focuses on transmission between UEs. As discussed earlier in this chapter, in previous works the transmission between users was only for routing the signal form the source user in UL to the base station or vice versa. The direct transmission between devices, without passing the signal through the base station, is discussed for the first time in (Middleton and Lilleberg, 2007). In this paper, the users in a cell are either uniformly distributed in the network or they are located in different clusters. For the mobile users located in the same cluster, it is also allowed to communicate directly with each other. It has been shown that if the clusters distance is more than a specified minimum distance they can reuse the resources while the Signal-to-Interference-plus-Noise-Ratio (SINR) of the received signal is more than a specified value. In (Kaufman and Aazhang, 2008) the authors have offered a spectrum sharing strategy between cellular and D2D users in the same scenarios as (Middle-

ton and Lilleberg, 2007). They have derived an analytical expression for the probability of existence of a single-hop D2D link that does not cause the cellular link to break, for uniformly distributed D2D users and clustered D2D users. It has been also discussed that for the first case such a D2D link can exist with significant probability, but in clustered D2D model such a link can exist with very high probability in certain user topologies. By considering multi-hop, the probability that a D2D link can exist further increases. Both (Middleton and Lilleberg, 2007; Kaufman and Aazhang, 2008) consider a beyond-3G network based on Worldwide Interoperability for Microwave Access (WiMAX) which uses Orthogonal Frequency-Division Multiple Access (OFDMA) technique for transmission.

A basic study which introduces D2D transmission as an underlay to LTE-A network is (Doppler *et al.*, 2011) where a session setup mechanism for D2D transmission and management has been proposed. It is shown that D2D transmission considerably increases the total throughput observed in the cell area, compared to the case where all D2D traffic is relayed by the cellular network. The authors further investigate the feasibility and the range of D2D transmission, and its impact to the power margins of cellular communications in (Doppler *et al.*, 2009) which their results demonstrate that by tolerating a modest increase in interference, D2D transmission with practical range becomes feasible.

To deal with the issue of mode selection, (Zulhasnine *et al.*, 2010; Doppler *et al.*, 2010; Belleschi *et al.*, 2011; Yu *et al.*, 2011; ElSawy *et al.*, 2014) have presented different approaches. (Zulhasnine *et al.*, 2010) has considered the D2D and cellular link quality and the interference situation of each possible sharing mode and finally a mode that provides the highest sum-rate while satisfying the SINR constraint of the cellular network in both single-cell and multiple-cell is selected. In their model each cell includes one D2D pair and one cellular user and they have not considered the issue of power control. In (Doppler *et al.*, 2010) the authors have presented a mode selection scheme with power control in a single cell and multi-cell scenario that includes one D2D link and one cellular user able to reuse the same resources and they are subject to spectral efficiency restrictions and maximum transmission power or energy constraints. This method enables a much more reliable D2D transmission with limited interference

to the cellular network compared to simpler mode selection procedures which forces all D2D terminals to reuse the same resources as the cellular communication. The authors in (Belleschi *et al.*, 2011) have formulated the joint mode selection, scheduling and power control task as an optimization problem in both centralized and distributed manner. They have shown that the distributed scheme performs close to the optimal scheme (centralized) both in terms of resource efficiency and user fairness. The single-cell mode selection and resource allocation algorithm also effectively extends the range for which D2D transmissions is useful. It helps to protect the cellular layer from interference from D2D links and reduces the overall power consumption in the network. In (Yu *et al.*, 2011) an optimum resource allocation and power control between the cellular and D2D connections that share the same resources have been analyzed for different resource sharing modes in both single-cell and multi-cell scenarios. In their method the cellular user with a higher channel quality will share the resource with a D2D link which causes lower interference. The authors in (ElSawy *et al.*, 2014) propose a biasing-based mode selection method for D2D-enabled cellular networks. They introduce bias value and power control cutoff threshold as two important design parameters to control the performance of the network. Their results have shown that underlay D2D communication improves the system performance in terms of spatial frequency reuse, link spectrum efficiency, and spatial spectrum efficiency, that they have been evaluated analytically.

Regarding the issue of the mode selection map, the idea is implicitly discussed for the first time in (Doppler *et al.*, 2010) where a mode selection procedure in single-cell and multi-cell environments is proposed. The map is derived numerically by optimizing all possible TMs and selecting the one that gives the highest throughput for given location of the cellular UE. In our previous work, (Morattab *et al.*, 2015), we extended the mode selection procedure in (Doppler *et al.*, 2010) assuming the UEs and eNB to use MIMO precoding. We present a method to optimally design MIMO precoders and decoders at each transmitter and receiver respectively, to reach the highest possible overall throughput for different TMs. Our results in that work shows considerable gain and efficiency in MIMO scenario compared to SISO which is discussed in (Doppler *et al.*, 2010). Derivation of the mode selection map of the network numerically using

the same point-to-point technique shows that using MIMO, the area where the dedicated and reuse modes reach the highest throughput is larger than SISO scenario. The mode selection maps in (Doppler *et al.*, 2010; Morattab *et al.*, 2015) are derived numerically by applying a point-to-point procedure which is imprecise, complex, time consuming, and inefficient. Using such methods consumes a lot of execution time and systems memory. Since, such methods are point based, the precision of resulting map is a function of the distance between two consecutive points where mode selection algorithm is applied. To deal with these issues in (Morattab *et al.*, 2016) we present an analytical approach to find the mode selection map for the case where the cellular UE moves in the network and the D2D pairs are fixed. For simplicity an LoS path-loss model is considered for the communication channel between each two entities without fading presence. We showed that the resulting geometrical functions presented in the paper could trace the mode selection map precisely for each arbitrary configuration of the network. In a recent work in (Xu *et al.*, 2016), the authors make a theoretical analysis on D2D mode selection with user mobility. Although the authors do not explicitly present a mode selection map derivation method, they define a region where its border is computed by equating the Received Signal Strength (RSS) of the cellular and reuse modes. In this work, TM between the paired D2D UEs is changed whenever one of the UEs exits a specific region. Although the authors presented an equation to reach the equi-RSS boundaries, no solution is proposed to derive the mode selection map. Except presenting a circular region as the approximation of the equation. Moreover the fading effect is missing in problem modeling and calculations. Our work in Chapter 1 extends our results presented in (Morattab *et al.*, 2016), for other two cases which either of the paired D2D UEs move in the network while the cellular UE and the other paired UE are fixed in the network. In Chapter 2, we present our analytical framework to derive the mode selection map when only cellular UE is moving in the network and the channel between each two communicating entities experiences fading.

As discussed earlier, one of the main issues in D2D enabled networks, is how to design a handover scheme that could maintain the QoS of a connection between two paired UEs and execute TM change in a seamless way whenever is needed. Some works have been done in

recent years to study this issue in different applications and scenarios (Raghothaman *et al.*, 2013; Yilmaz *et al.*, 2014; Chen *et al.*, 2015; Orsino *et al.*, 2015; Jarray and Giovanidis, 2016; Xu *et al.*, 2016). In (Raghothaman *et al.*, 2013), the authors present protocols to extend the 3GPP LTE-A system to incorporate D2D communication, including the establishing and maintaining a D2D call and procedures for efficient mobility between a traditional cellular mode and a D2D mode of operation within one cell. This work only provides a time sequence procedure for the handover mechanism without presenting a specific decision criteria. Moreover it is not explained well that the direct D2D is for the reuse mode or the dedicated mode. In (Yilmaz *et al.*, 2014), a handover mechanism based on RSS which is able to minimize the end-to-end latency and signaling overhead for the communicating D2D pairs. The authors in (Chen *et al.*, 2015), provide the same handover scenario as presented in (Yilmaz *et al.*, 2014), however unlike the previous work, several decision criteria have been taken into account to find the best time to start the handover. The issue regarding the proposed handover scheme in (Yilmaz *et al.*, 2014; Chen *et al.*, 2015) is that they do not provide performance metrics for their algorithm. In (Orsino *et al.*, 2015) a handover scheme, where D2D connectivity helps to improve the migration of users across different BSs to enhance the overall link quality experienced by the UEs is presented. Like (Yilmaz *et al.*, 2014; Chen *et al.*, 2015) the handover is for the case when D2D UEs move from one cell to other cells. The mechanism presented in this work is able to efficiently offer the attractive energy efficiency, data rate, and packet delivery ratio benefits. Moreover performance metrics of their solution by utilizing the tools from stochastic geometry are derived which is an advantage over (Yilmaz *et al.*, 2014; Chen *et al.*, 2015). In (Jarray and Giovanidis, 2016), the performance of caching in D2D networks for different degrees of node mobility is studied. In the presented scenario devices could establish connection with transmitters that have the desired content cached, however due to the mobility the link quality between receivers and transmitters is affected which results in connection drop. This work does not propose any handover mechanism and only studies the performance of the network while UEs move. Our work in Chapter 3 partially relies on the recent study presented in (Xu *et al.*, 2016), which the authors make a theoretical analysis on D2D mode selection with user mobility. As discussed earlier, an approximation of equi-RSS equations is used to define

the area which the reuse mode is always selected for the communication between the D2D pair. Another deficiency of this work is the absence of the dedicated mode to be selected by the paired D2D UEs. In this work, only cellular and reuse modes are allowed.

CHAPTER 1

MODE SELECTION MAP IN DEVICE-TO-DEVICE ENABLED NETWORKS - AN ANALYTICAL APPROACH

Armin Morattab[1], Zbigniew Dziong[1], Kazem Sohraby[2]

[1] Department of Electrical Engineering, École de Technologie Supérieure,
1100 Notre-Dame Ouest, Montreal, Quebec, Canada, H3C 1K3
[2] Department of Electrical and Computer Engineering, South Dakota School of Mines & Technology, Rapid City, SD 57701, USA
& an Adjunct in Computer Science Department, Sand Diego State University, USA

Article submitted for review in January 2017.

Abstract

Device-to-Device (D2D) transmission is one of the promising features of 5G networks enabling direct transmission between User Equipment (UE) in addition to traditional cellular transmission. Communicating UEs would be able to select among different transmission modes based on a defined criteria. In this paper, a network consisting of a communicating D2D pair and one cellular UE communicating with an evolved Node-B (eNB) is considered. For simplicity the communication channel between each two entities is modeled using a line-of-sight (LoS) path-loss model. It is assumed that the cellular UE uses uplink transmission while the paired D2D UEs would select among the reuse, dedicated, and the cellular transmission modes taking into account the overall network throughput as the mode selection criteria. We present two different cases where one of the UEs in D2D pair moves and the other UEs are fixed. For each case we develop an analytical solution to find mode selection map, which specifies the regions in the network where if the moving UE remains in the region, a specific mode is selected for communication between the D2D pair. Our analytical solution shows that the mode selection map could be defined by geometrical functions. The shape of the map depends on the transmission power of UEs and eNB, the location of fixed UEs, and the channels' condition. Our simulations verify the results of the mode selection map derivation using the proposed analytical approach.

Introduction

The deployment of the fourth generation (4G) Long Term Evolution (LTE) and LTE-Advanced (LTE-A) systems in cellular networks has provided users with more capabilities on their User Equipment (UEs) (Asadi *et al.*, 2014; Song *et al.*, 2015; Li and Guo, 2014; Mumtaz and Rodriguez, 2014). They can easily watch their desired video, surf web and make Voice-over-IP (VoIP) calls, or listen to their favorite music. In light of such advances, the number of users is increasing rapidly and they demand higher data rates with guaranteed Quality-of-Service (QoS) at lower prices (CISCO, 2015). Therefore, it is inevitable for service providers and telecommunication companies to develop new techniques and designs to satisfy customers. Device-to-Device (D2D) communication is one of the features proposed for fifth generation (5G) and beyond networks that enables UEs communicate directly with each other instead of using the traditional cellular option (Asadi *et al.*, 2014; Song *et al.*, 2015; Doppler *et al.*, 2009; Janis *et al.*, 2009; Doppler *et al.*, 2011).

There are three possible Transmission Modes (TM) for D2D UEs: reuse, dedicated, or cellular modes. The first two TMs use direct transmission between UEs, while the last is the traditional cellular transmission. The difference between the reuse and dedicated TMs is in the method of utilizing resources for D2D pair. In the reuse mode, D2D UEs and a subset of other cellular devices reuse the same resources (frequency spectrum). In the dedicated mode, only dedicated resources are allocated to D2D UEs. Communicating D2D UEs should decide among these three different TMs (Doppler *et al.*, 2010; Liu *et al.*, 2012c), or apply a mixed mode mechanism in which each D2D link can utilize multiple modes through resource multiplexing (Tang and Ding, 2016). Such a decision leads to the mode selection process.

For single mode selection, the mode selection decision is made periodically based on a specific criterion, such as the overall throughput of the network. In other words, the TM which produces the highest throughput is selected. It has been shown that in the line-of-sight (LoS) case considered in this paper, for a fixed transmission power, channel conditions, and noise power, the TM to be selected depends on the location of entities in the network (Morattab *et al.*, 2015).

In this paper, we show that there are certain regions in the network where the movement of a UE does not change the transmission mode for the D2D communication. The set of these regions and the corresponding borders form the mode selection map of the D2D network. This map can be used by eNB to predetermine and assign the best TM for communication between D2D UEs without the need to compute the mode selection algorithm periodically. As long as the entity remains in the region, the mode remains the same. Furthermore, the Mobility Management Entity (MME) can use the mode selection map to find the best policy for vertical handover when the moving entity leaves a region and enters its neighboring regions where different TM may be computed. Such applications are left for future investigation and are not discussed further in this paper.

1.1 Related Works

In our previous work, (Morattab *et al.*, 2015), we present a method to define the optimal precoder and decoders for a D2D enabled network where the entities are equipped with multiple antennas. Then a mode selection method is applied to find the best TM between the paired UEs. Finally the mode selection map of the network is derived numerically and the results for both single antenna and multiple antennas scenarios are compared.

In (Doppler *et al.*, 2010), the authors propose a mode selection procedure for resource sharing with the cellular network in a single and multi-cell environments. That paper presents a mode selection map which is derived numerically by selecting the TM which produces the highest rate for the cellular UE at specific points in the network.

The above methods for the mode selection map calculation are based on numerical results which are complex, time consuming, and inefficient. The mode selection techniques are applied to every point in the network. Using numerical methods requires a lot of computing time and systems memory. Since such methods are for each point, the precision of the map is a function of the distance between two consecutive points where mode selection algorithm is applied. Therefore in (Morattab *et al.*, 2016) we introduced the mode selection map for the first

time and developed an analysis of the map for a special case when the cellular UE is moving in the network and the D2D UEs are static.

1.2 Contributions

To determine a precise mode selection map for a network, in this paper, we extend our analytical approach in (Morattab *et al.*, 2016) to develop a comprehensive and tractable analytical framework for two other scenarios where one of the D2D UEs move while other UEs are static. The main contributions of this paper are summarized as follows:

- The problem of calculating mode selection maps for two different cases where either of the D2D UEs move while other UEs are static in the network, is treated and solved for the first time;
- Analytical solutions are provided for each case resulting in geographical borders between disjoint regions.

The remainder of the paper is organized as follows. In Section 1.3, the mathematical model of the network is presented assuming three different TMs between the D2D UEs. The formulation of overall network throughput is derived in Section 1.4. In Section 1.5, we present the construction of mode selection maps as well as the analytical approach for two different cases. In Section 1.6, simulation results for each of the two cases in Section 1.5 are provided. Finally, the conclusions are formulated in Section 1.7.

1.3 System Model

We consider a single cell D2D enabled cellular network consisting of D2D UEs, a cellular UE, and an evolved Node-B (eNB). D2D UEs are assumed to wish to communicate with each other. The D2D UEs could operate in the reuse, dedicated, or cellular modes; the cellular UE's TM is limited to the cellular mode in the Uplink (UL) direction. As it is shown in Fig. 1.1, transmission for D2D UEs is from source UE (UE_s) to destination UE (UE_d), while the cellular

UE (UE_c) transmits to eNB. It is also assumed that all entities in the network are equipped with a single antenna.

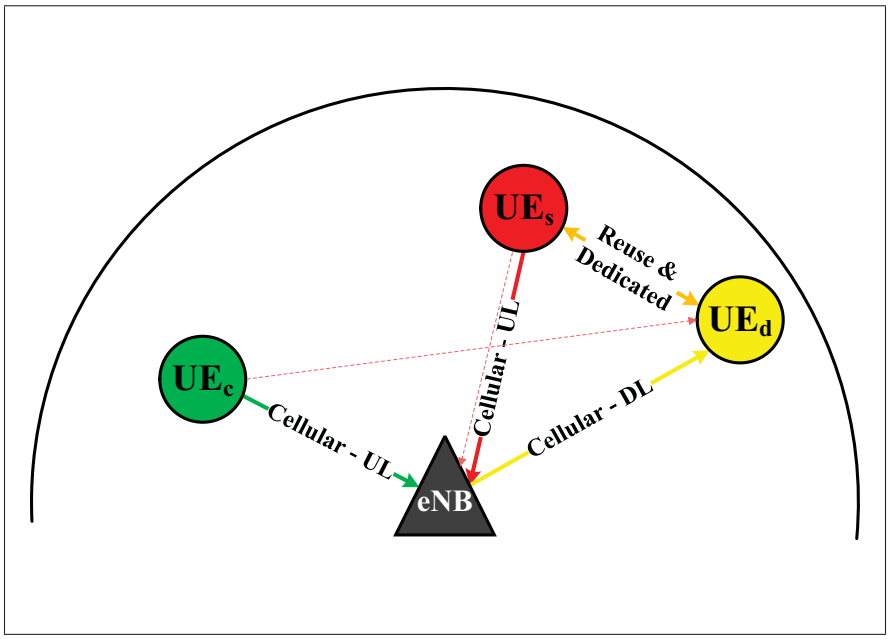

Figure 1.1 D2D enabled 5G network – LoS pathloss channels

For simplicity a simple path-loss channel model, for an LoS communication between entities, is assumed. It should be noted that fading effect is not considered in this paper and is left for future investigation. The channel gain in this case is calculated as follows:

$$h_{ij} = \sqrt{\frac{K}{d_{ij}^{\alpha}}} \tag{1.1}$$

where, d_{ij} is the distance between transmitter i and receiver j, where i is either s, c, or e, and j is either e or d. The subscripts s, c, d, and e stand for UE_s, UE_c, UE_d and eNB respectively. K is a unitless constant that depends on the antennas characteristics. α is the path loss exponent which is a function of carrier frequency, environment, obstructions, etc. The values of K and α are assumed to be the same for all cases.

We assume that, in the reuse mode, resources for UE_s-UE_d transmission are shared with the UE_c-eNB transmission. Therefore, receivers in the network will be affected by the interference from transmitters as well as the background noise. The interference channel is shown in Fig. 1.1 as red dotted lines. However, when the D2D UEs' communication is in the dedicated or cellular modes, half of the resources are assigned to the D2D UEs, and the remainder to the UE_c-eNB.

Based on the above assumptions, the received signal, y, for three different TMs between D2D UEs is as follows:

$$y_{\mathrm{d}}^{\mathrm{R}} = \sqrt{P_{\mathrm{s}}} h_{\mathrm{sd}} x_{\mathrm{s}}^{\mathrm{R}} + \sqrt{P_{\mathrm{c}}} h_{\mathrm{cd}} x_{\mathrm{c}}^{\mathrm{R}} + n_{\mathrm{d}}^{\mathrm{R}} \tag{1.2}$$

$$y_{e}^{\mathrm{R}} = \sqrt{P_{\mathrm{c}}} h_{\mathrm{ce}} x_{\mathrm{c}}^{\mathrm{R}} + \sqrt{P_{\mathrm{s}}} h_{\mathrm{se}} x_{\mathrm{s}}^{\mathrm{R}} + n_{\mathrm{e}}^{\mathrm{R}} \tag{1.3}$$

$$y_{\mathrm{d}}^{\mathrm{D}} = \sqrt{P_{\mathrm{s}}} h_{\mathrm{sd}} x_{\mathrm{s}}^{\mathrm{D}} + n_{\mathrm{d}}^{\mathrm{D}} \tag{1.4}$$

$$y_{\mathrm{e}}^{\mathrm{D}} = \sqrt{P_{\mathrm{c}}} h_{\mathrm{ce}} x_{\mathrm{c}}^{\mathrm{D}} + n_{\mathrm{e}}^{\mathrm{D}} \tag{1.5}$$

$$y_{\mathrm{e1}}^{\mathrm{C}} = \sqrt{P_{\mathrm{s}}} h_{\mathrm{se}} x_{\mathrm{s}}^{\mathrm{C}} + n_{\mathrm{e}}^{\mathrm{C}} \tag{1.6}$$

$$y_{\mathrm{d}}^{\mathrm{C}} = \sqrt{P_{\mathrm{e}}} h_{\mathrm{ed}} x_{\mathrm{e}}^{\mathrm{C}} + n_{\mathrm{d}}^{\mathrm{C}} \tag{1.7}$$

$$y_{\mathrm{e2}}^{\mathrm{C}} = \sqrt{P_{\mathrm{c}}} h_{\mathrm{ce}} x_{\mathrm{c}}^{\mathrm{C}} + n_{\mathrm{e}}^{\mathrm{C}} \tag{1.8}$$

where x is the transmitted signal, n is the white Gaussian noise with spectral density of N_0, and P is the transmitter's power. In these equations, R, D, and C superscripts represent the reuse, dedicated, or cellular modes respectively. It should be noted that when the TM of D2D UEs is cellular, the UE_s-UE_d transmission breaks into two cascade transmission, i.e. UE_s-eNB and eNB-UE_d. In this case the eNB receives two signals, one from the UE_s which is $y_{\mathrm{e1}}^{\mathrm{C}}$ and the other from UE_c which is $y_{\mathrm{e2}}^{\mathrm{C}}$.

The signals in the reuse mode in (1.2) and (1.3), include three terms. The first term represents the desired signal from the paired entity, the second term is interference from the UE_c transmitter, and the last term is noise. However, the received signals in the dedicated or cellular modes, as presented in (1.4)–(1.8), do not include interference, since the resources are not shared.

In the following section, we formulate the overall throughput, which will be used later to derive the mode selection map.

1.4 Problem Formulation

We assume that near capacity channel codes are used at transmitters, hence the overall throughput in the reuse, dedicated, and cellular modes would be almost equal to the overall capacity of the network for each mode.

$$R_{\mathrm{R}} = \log_2\left(1+\frac{|h_{\mathrm{sd}}|^2 P_{\mathrm{s}}}{|h_{\mathrm{cd}}|^2 P_{\mathrm{c}}+N_0}\right)+\log_2\left(1+\frac{|h_{\mathrm{ce}}|^2 P_{\mathrm{c}}}{|h_{\mathrm{se}}|^2 P_{\mathrm{s}}+N_0}\right) \tag{1.9}$$

$$R_{\mathrm{D}} = \frac{1}{2}\left(\log_2\left(1+\frac{|h_{\mathrm{sd}}|^2 P_{\mathrm{s}}}{N_0}\right)+\log_2\left(1+\frac{|h_{\mathrm{ce}}|^2 P_{\mathrm{c}}}{N_0}\right)\right) \tag{1.10}$$

$$R_{\mathrm{C}} = \frac{1}{4}\min\left(\log_2\left(1+\frac{|h_{\mathrm{se}}|^2 P_{\mathrm{s}}}{N_0}\right),\log_2\left(1+\frac{|h_{\mathrm{ed}}|^2 P_{\mathrm{e}}}{N_0}\right)\right)+\frac{1}{2}\log_2\left(1+\frac{|h_{\mathrm{ce}}|^2 P_{\mathrm{c}}}{N_0}\right) \tag{1.11}$$

In the above equations we assumed the bandwidth is normalized to one. Therefore, it is not shown as separate variable. It should be noted that in the reuse mode both ce and sd links reuse the same frequency resources. However, we assume that for the dedicated and cellular modes, the ce link uses half of the resources while the remaining half is used by sd and sed links respectively. The $\frac{1}{2}$ and $\frac{1}{4}$ multipliers in (1.9) and (1.10) refer to this fact. It should be noted that for the sed link, it is assumed that se and ed links use $\frac{1}{4}$ of total frequency resources and since they are cascaded with encoding at eNB, the total capacity of the sed link is calculated as the minimum of the capacities of se and ed links as shown in the first term of (1.11) on the right hand of the equation.

The mode selection map boundaries are found by equating the overall throughput expressions in (1.9)–(1.11), one by one as follows:

$$R_{\mathrm{R}} = R_{\mathrm{D}} \tag{1.12}$$

$$R_{\mathrm{R}} = R_{\mathrm{C}} \tag{1.13}$$

$$R_{\mathrm{D}} = R_{\mathrm{C}} \tag{1.14}$$

For the mode selection map, depending on which entity moves, three different cases should be considered. We have already presented an analytical approach in (Morattab *et al.*, 2016) to find the map for the case when $\mathrm{UE_c}$ moves while $\mathrm{UE_s}$ and $\mathrm{UE_d}$ are static. In the following section we present an analytical approach for the mode selection map using (1.12)–(1.14) for two other cases in which one of the paired D2D UEs moves while other UEs are static.

1.5 Mode Selection Map

As discussed in previous sections, we assume that transmission power and noise power are constant. Therefore, the only variables are the distance between network entities. We consider the following cases to derive the boundary formulations of the mode selection map:

Case I: $\mathrm{UE_s}$ moves, $\mathrm{UE_d}$ and $\mathrm{UE_c}$ are static; Network variables are $X = d_{\mathrm{sd}}$ and $Y = d_{\mathrm{se}}$;

Case II: $\mathrm{UE_d}$ moves, $\mathrm{UE_s}$ and $\mathrm{UE_c}$ are static; Network variables are $X = d_{\mathrm{sd}}$, $Y = d_{\mathrm{cd}}$, and $Z = d_{\mathrm{ed}}$.

We will realize in the following subsections that in each of these two cases, (1.12)–(1.14) lead to equations that different approaches are needed to solve them. As described above, depending on which case is discussed, each variable represents a different distance in the network. For example for the case where $\mathrm{UE_s}$ moves, Y represents d_{se} while when $\mathrm{UE_d}$ moves, it represents d_{cd}.

To simplify our solution to (1.12)–(1.14), we use the following conversions:

$$x = \frac{1}{X^{\alpha}} \tag{1.15a}$$

$$y = \frac{1}{Y^{\alpha}} \tag{1.15b}$$

$$z = \frac{1}{Z^{\alpha}} \tag{1.15c}$$

Since X, Y, and Z are distances, $x, y, z > 0$.

In this paper, a solution to (1.12)–(1.14) should produce the following:

- An explicit function that defines any of the network variables (distances) with respect to the others;
- Conditions on parameters (Channel State Information (CSI), transmit power, fixed distances, noise power, and pathloss exponent) for which solutions exist;
- Conditions on variables for which solutions exist;
- An expression which transforms variables to coordinates of the moving UE.

In the following subsections we present solutions for the mode selection map.

1.5.1 Moving UE_s

In this subsection we find the boundaries of mode selection map for the case when UE_s moves, while UE_c and UE_d are static. Therefore, as discussed in Section 1.5, the network variables would be $X = d_{sd}$ and $Y = d_{se}$ as shown in Fig.1.2. Referring to this figure, the following triangle inequalities should be satisfied:

$$X + Y \geq d_{ed} \tag{1.16}$$

$$|X - Y| \leq d_{\text{ed}} \tag{1.17}$$

For this case (1.12)–(1.14) are re-written as follows:

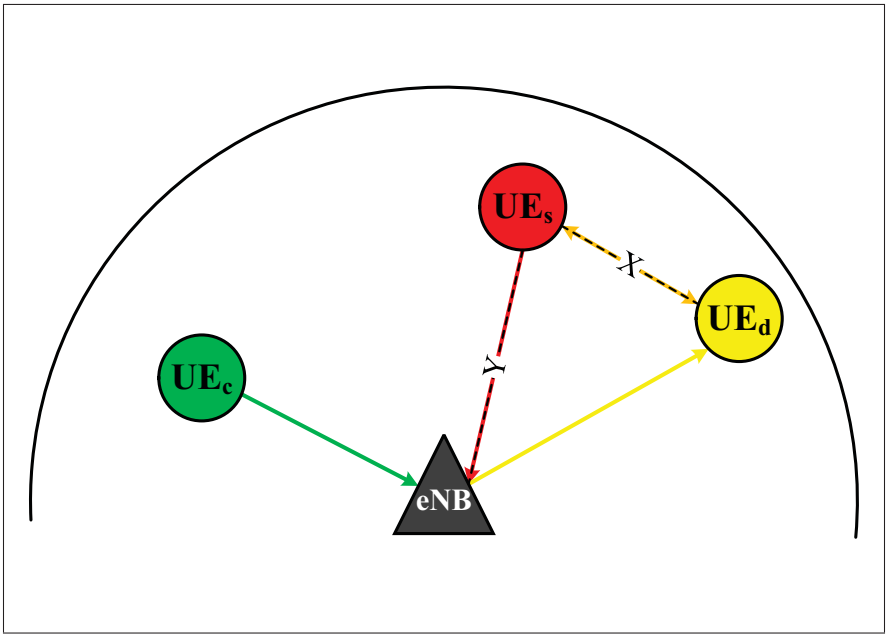

Figure 1.2 Tuple model and distance variables when UE_s moves in the network and the communication channels are modeled as LoS pathloss

$$R_{\text{R}} = \log_2\left((1 + a_1 x)\left(1 + \frac{a_2}{1 + a_3 y}\right)\right) \tag{1.18}$$

$$R_{\text{D}} = \frac{1}{2}\log_2\left((1 + a_2)\,(1 + a_4 x)\right) \tag{1.19}$$

$$R_{\text{C}} = \frac{1}{4}\log_2\left((1 + a_2)^2 \min\left(1 + a_3 y, a_5\right)\right) \tag{1.20}$$

where:

$$a_1 = \frac{K P_{\text{s}}}{|h_{\text{cd}}|^2 P_{\text{c}} + N_0} \tag{1.21a}$$

$$a_2 = \frac{|h_{ce}|^2 P_c}{N_0} \tag{1.21b}$$

$$a_3 = \frac{K P_s}{N_0} \tag{1.21c}$$

$$a_4 = \frac{K P_s}{N_0} \tag{1.21d}$$

$$a_5 = 1 + \frac{|h_{ed}|^2 P_e}{N_0} \tag{1.21e}$$

The solution to each equation in (1.12)–(1.14), for the case of moving UE_s, requires a different approach that is going to be discussed in the following subsections.

1.5.1.1 $R_R = R_D$

Referring to (1.18) and (1.19):

$$\log_2\left((1+a_1x)\left(1+\frac{a_2}{1+a_3y}\right)\right) = \frac{1}{2}\log_2\left((1+a_2)(1+a_4x)\right) \tag{1.22}$$

$$\left((1+a_1x)\left(1+\frac{a_2}{1+a_3y}\right)\right)^2 = (1+a_2)(1+a_4x) \tag{1.23}$$

Which can be written as:

$$f(x,y) = a(x)\,y^2 + b(x)\,y + c(x) = 0 \tag{1.24}$$

where:

$$a(x) = \left((1+a_1x)^2 - (1+a_4x)(1+a_2)\right)a_3^2 \tag{1.25a}$$

$$b(x) = 2\Big((1+a_1x)^2 (1+a_2) - (1+a_4x)(1+a_2) \Big) a_3 \tag{1.25b}$$

$$c(x) = (1+a_1x)^2 (1+a_2)^2 - (1+a_4x)(1+a_2) \tag{1.25c}$$

The second order function $f(x,y)$ in (1.24) has real roots if:

$$\begin{aligned} \Delta(x) &= b(x)^2 - 4a(x)c(x) \\ &= 4(1+a_2)\, a_2^2 a_3^2 (1+a_1x)^2 (1+a_4x) > 0 \end{aligned} \tag{1.26}$$

It is obvious from (1.26) that $\Delta(x)$ is always positive, for all values of $x > 0$. Therefore the two real roots of (1.24) are:

$$y = \frac{-b(x) \pm \sqrt{\Delta(x)}}{2a(x)} \tag{1.27}$$

Since $y > 0$, eight different situations are possible for (1.27), depending on the sign of $a(x)$, $b(x)$, and $c(x)$ as follows:

$$\text{if } a(x) < 0 \begin{cases} \text{if } b(x) < 0 \\ \qquad \begin{cases} \text{if } c(x) < 0, \text{No positive solution} & \text{(1.28a)} \\ \text{if } c(x) > 0,\ y = \dfrac{-b(x) - \sqrt{\Delta(x)}}{2a(x)} & \text{(1.28b)} \end{cases} \\ \text{if } b(x) > 0 \\ \qquad \begin{cases} \text{if } c(x) < 0,\ y = \dfrac{-b(x) \pm \sqrt{\Delta(x)}}{2a(x)} & \text{(1.28c)} \\ \text{if } c(x) > 0,\ y = \dfrac{-b(x) - \sqrt{\Delta(x)}}{2a(x)} & \text{(1.28d)} \end{cases} \end{cases}$$

$$\text{if } a(x) > 0 \begin{cases} \text{if } b(x) < 0 \\ \qquad \begin{cases} \text{if } c(x) < 0,\ y = \dfrac{-b(x) + \sqrt{\Delta(x)}}{2a(x)} & \text{(1.28e)} \\ \text{if } c(x) > 0,\ y = \dfrac{-b(x) \pm \sqrt{\Delta(x)}}{2a(x)} & \text{(1.28f)} \end{cases} \\ \text{if } b(x) > 0 \\ \qquad \begin{cases} \text{if } c(x) < 0,\ y = \dfrac{-b(x) + \sqrt{\Delta(x)}}{2a(x)} & \text{(1.28g)} \\ \text{if } c(x) > 0, \text{No positive solution} & \text{(1.28h)} \end{cases} \end{cases}$$

To choose the proper solution among eight possible choices in (1.28a)–(1.28h), we should find the sign of $a(x)$, $b(x)$, and $c(x)$ for different values of X (or x). The results for the sign of $a(x)$ is summarized as follows:

- for $0 < X < X_1$, $a(x) > 0$

- for $X_1 < X$, $a(x) < 0$

where:

$$X_1 = \sqrt[\alpha]{\frac{2a_\mathrm{a}}{-b_\mathrm{a} + \sqrt{b_\mathrm{a}^2 + 4a_\mathrm{a}c_\mathrm{a}}}} \tag{1.29a}$$

$$a_\mathrm{a} = a_1^2 \tag{1.29b}$$

$$b_\mathrm{a} = 2a_1 - a_2a_4 - a_4 \tag{1.29c}$$

$$c_\mathrm{a} = a_2 \tag{1.29d}$$

and for the sign of $b(x)$:

- if $a_4 > 2a_2$,
  - for $0 < X < X_2$, $b(x) < 0$
  - for $X_2 < X$, $b(x) > 0$
- if $a_4 < 2a_2$, for all $0 < X$, $b(x) > 0$

where:

$$X_2 = \sqrt[\alpha]{\frac{a_1^2}{a_4 - 2a_1}} \tag{1.30}$$

and finally for the sign of $c(x)$:

- if $\Delta_\mathrm{c} < 0$, for $0 < X$, $c(x) > 0$
- if $\Delta_\mathrm{c} > 0$,
  - if $b_\mathrm{c} < 0$,
    - for $0 < X < X_3$, $c(x) > 0$

  - for $X_3 < X < X_4$, $c < 0$
  - for $X_4 < X$, $c(x) > 0$
- if $b_c > 0$, for $0 < X$, $c(x) > 0$

where:

$$X_3 = \frac{2a_c}{-b_c + \sqrt{\Delta_c}} \tag{1.31a}$$

$$X_4 = \frac{2a_c}{-b_c - \sqrt{\Delta_c}} \tag{1.31b}$$

$$\Delta_c = b_c^2 - 4a_c c_c \tag{1.31c}$$

$$a_c = a_1^2(1 + a_2) \tag{1.31d}$$

$$b_c = 2a_1 - 2a_1 a_2 - a_4 \tag{1.31e}$$

$$c_c = a_2 \tag{1.31f}$$

As discussed earlier, the triangle inequalities that should be satisfied are (1.16) and (1.17).

The solution boundaries would be symmetric to the line which passes through eNB and UE_d. To find coordinates of UE_s, i.e. (X_s,Y_s), where (1.24) is satisfied, we apply the following conversion:

$$X_s = -\frac{X^2 - Y^2 - d_{ed}^2}{2d_{ed}} \frac{X_d}{d_{ed}} \mp \sqrt{Y^2 - \left(\frac{X^2 - Y^2 - d_{ed}^2}{2d_{ed}}\right)^2} \frac{Y_d}{d_{ed}} \tag{1.32a}$$

$$Y_s = \pm\sqrt{Y^2 - \left(\frac{X^2 - Y^2 - d_{ed}^2}{2d_{ed}}\right)^2} \frac{X_d}{d_{ed}} + \frac{X^2 - Y^2 - d_{ed}^2}{2d_{ed}} \frac{Y_d}{d_{ed}} \tag{1.32b}$$

In the next subsection we discuss the solution for (1.13), when UE_s moves.

1.5.1.2 $R_{\mathbf{R}} = R_{\mathbf{C}}$

We develop this equation referring to (1.18) and (1.20) as follows:

$$\log_2\left((1+a_1x)\left(1+\frac{a_2}{1+a_3y}\right)\right) = \frac{1}{4}\log_2\left((1+a_2)^2\min\left(1+a_3y,a_5\right)\right) \tag{1.33}$$

$$\left((1+a_1x)\left(1+\frac{a_2}{1+a_3y}\right)\right)^4 = (1+a_2)^2\min\left(1+a_3y,a_5\right) \tag{1.34}$$

The min(.) function is a piecewise function which operates as follows:

$$\min\left(1+a_3y,a_5\right) = \begin{cases} 1+a_3y, \text{for } 0 < y < y_1 & \text{(1.35a)} \\ a_5 \quad \text{, for } y_1 < y & \text{(1.35b)} \end{cases}$$

where:

$$y_1 = \frac{a_5 - 1}{a_3} \tag{1.36}$$

If (1.35a) is the case, (1.34) becomes:

$$\left((1+a_1x)\left(1+\frac{a_2}{1+a_3y}\right)\right)^4 = (1+a_2)^2(1+a_3y) \tag{1.37}$$

Then the solution to the above equation is as follows:

$$x = \frac{1}{a_1}\left(\frac{\sqrt[4]{(1+a_2)^2\,(1+a_3 y)^5}}{1+a_2+a_3 y} - 1\right) \tag{1.38}$$

If (1.35b) is the case, (1.34) would be developed as:

$$\left((1+a_1 x)\left(1+\frac{a_2}{1+a_3 y}\right)\right)^4 = (1+a_2)^2\, a_5 \tag{1.39}$$

Then the solution to above equation would be as follows:

$$x = \frac{1}{a_1}\left(\left(\sqrt[4]{(1+a_2)^2\, a_5}\right)\left(\frac{1+a_3 y}{1+a_2+a_3 y}\right) - 1\right) \tag{1.40}$$

To have both solutions in (1.38) and (1.40) valid, the $x > 0$ condition should be satisfied. Applying this inequality on (1.38) produces:

$$\frac{1}{a_1}\left(\frac{\sqrt[4]{(1+a_2)^2\,(1+a_3 y)^5}}{1+a_2+a_3 y} - 1\right) > 0 \tag{1.41}$$

which leads to the following:

$$f(t) = \frac{(1+a_2)^2\, t^5}{(a_2+t)^4} > 1 \tag{1.42}$$

where:

$$t = 1 + a_3 y \tag{1.43a}$$

Generally y can change between 0 and ∞, therefore t from (1.43a) correspondingly changes between 1 and ∞. To analyze the behavior of $f(t)$ for $t > 1$ we find its derivative as follows:

$$f'(t) = \frac{(1+a_2)^2(5a_2t^4+t^5)}{(a_2+t)^5} \tag{1.44a}$$

As could be seen $f'(t)$ is positive for $t > 1$, therefore $f(t)$ is strictly increasing for $t > 1$. Moreover referring to (1.42), $f(1) = \frac{1}{(1+a_2)^2} < 1$ and $\lim_{t\to\infty} f(t) = \infty$. From intermediate value theorem since $f(t)$ is continuous for $t \in [1,\infty)$, there is a $t = t_0 > 1$ such that $f(t_0) = 1$, and since $f(t)$ is strictly increasing, t_0 is unique. For $t_0 < t$, $f(t) > 1$ and therefore (1.42) is satisfied. We can calculate t_0 by solving $f(t) = 1$ numerically using methods such as Newton-Raphson.

We call y_0 as the corresponding value of y for t_0. The summary of sign determination for the solution x in (1.38), for $y > 0$, is presented as follows:

- if $y_0 < y_1$,
  - for $0 < y < y_0$, $x < 0$
  - for $y_0 < y < y_1$, $x > 0$
- if $y_1 < y_0$, for $0 < y < y_1$, $x < 0$

As shown above, only for values of $y_0 < y < y_1$, $x > 0$ is satisfied.

Applying this condition on (1.40) we have the following :

$$\frac{1}{a_1}\left(\left(\sqrt[4]{(1+a_2)^2 a_5}\right)\left(\frac{1+a_3y}{1+a_2+a_3y}\right)-1\right) > 0 \tag{1.45}$$

$$y > y_2 \tag{1.46}$$

where:

$$y_2 = \frac{1}{a_3}\left(\frac{a_2}{\sqrt[4]{a_5\,(1+a_2)^2}-1}-1\right) \tag{1.47}$$

Signs for the solution x in (1.40), for $y > 0$, is summarized as follows:

- if $y_2 < 0$, for $y_1 < y$, $x > 0$
- if $0 < y_2$,
  - if $y_2 < y_1$, for $y_1 < y$, $x > 0$
  - if $y_1 < y_2$,
    - for $y_1 < y < y_2$, $x < 0$
    - for $y_2 < y$, $x > 0$

Similar to the results in Section 1.5.1.1, the solution boundaries would be symmetric to the line passing through eNB and $\mathrm{UE_d}$. To find $(X_\mathrm{s},Y_\mathrm{s})$ coordinates, we apply (1.32a) and (1.32b) conversions X and Y that satisfy the triangle inequalities.

1.5.1.3 $R_\mathbf{D} = R_\mathbf{C}$

Following this equation using (1.19) and (1.20):

$$\frac{1}{2}\log_2\left((1+a_2)(1+a_4x)\right) = \frac{1}{4}\log_2\left((1+a_2)^2\min\left(1+a_3y,a_5\right)\right) \tag{1.48}$$

$$x = \frac{1}{a_4}\left(\sqrt{\min\left(1+a_3y,a_5\right)}-1\right) \tag{1.49}$$

The min(.) function in (1.49) is represented as follows:

$$\min\left(1+a_3 y, a_5\right) = \begin{cases} 1+a_3 y, \text{for } 0 < y < y_1 & \text{(1.50a)} \\ a_5 \quad \text{, for } y_1 < y & \text{(1.50b)} \end{cases}$$

where:

$$y_1 = \frac{a_5 - 1}{a_3} \tag{1.51}$$

The solution to (1.49) is summarized as follows:

$$\text{for } 0 < y < y_1 \quad , \quad x = \frac{\sqrt{1+a_3 y} - 1}{a_4} \tag{1.52a}$$

$$\text{for } y_1 < y \quad , \quad x = \frac{\sqrt{a_5} - 1}{a_4} \tag{1.52b}$$

Like the results achieved in Section 1.5.1.1 and 1.5.1.2, here also the solution boundaries would be symmetric to the line which passes through eNB and UE_d. To find (X_s, Y_s) coordinates, we apply (1.32a) and (1.32b) on achieved X and Y that satisfy the triangle inequalities.

1.5.2 Moving UE_d

In this subsection we find the boundaries of mode selection map for the case when UE_d moves, while UEc and UE_s are static. Unlike the cases presented in (Morattab *et al.*, 2016) and 1.5.1, where there were two distance variables in (1.12)–(1.14), here three distance variables as shown in Fig.1.3 will appear. These variables, as discussed earlier in Section (1.5), are $X = d_{sd}$, $Y = d_{cd}$, and $Z = d_{ed}$ and due to the following relations, they are not independent from each other:

$$\text{if } |X_s Y_c - X_c Y_s| \neq 0, Z = \sqrt{\frac{-B'(X,Y) \pm \sqrt{B'(X,Y)^2 - 4A'C'(X,Y)}}{2A'}} \tag{1.53a}$$

$$\text{if } |X_s Y_c - X_c Y_s| = 0, Z = \sqrt{\frac{Y_c\left(X^2 - d_{se}^2\right) - Y_s\left(Y^2 - d_{ce}^2\right)}{Y_c - Y_s}} \tag{1.53b}$$

where for (1.53a), we have:

$$A' = d_{cs}^2 \tag{1.54a}$$

$$\begin{aligned} B'(X,Y) = &-\left(\left(d_{cs}^2 + d_{ce}^2 - d_{se}^2\right)X^2 + \left(d_{cs}^2 + d_{se}^2 - d_{ce}^2\right)Y^2 - 4d_{se}^2 d_{ce}^2\right. \\ &\left. - \left(d_{cs}^2 - \left(d_{se}^2 + d_{ce}^2\right)\right)\left(d_{se}^2 + d_{ce}^2\right) + 4\left(X_s Y_c - X_c Y_s\right)^2\right) \end{aligned} \tag{1.54b}$$

$$\begin{aligned} C'(X,Y) = &\, d_{ce}^2 X^4 - \left(d_{cs}^2 + d_{se}^2 - d_{ce}^2\right) d_{ce}^2 X^2 + \left(d_{cs}^2 - \left(d_{se}^2 + d_{ce}^2\right)\right) X^2 Y^2 \\ &+ d_{se}^2 Y^4 - \left(d_{cs}^2 + d_{ce}^2 - d_{se}^2\right) d_{se}^2 Y^2 + d_{ce}^2 d_{se}^2 d_{cs}^2 \end{aligned} \tag{1.54c}$$

Referring to Fig.(1.3), the following triangle inequalities should be satisfied between X, Y, and Z:

$$X + Y \geq d_{cs} \tag{1.55}$$

$$|X - Y| \leq d_{cs} \tag{1.56}$$

$$X + Z \geq d_{se} \tag{1.57}$$

$$|X - Z| \leq d_{se} \tag{1.58}$$

Similar to the previous cases, (1.12)–(1.14) can be represented as follows:

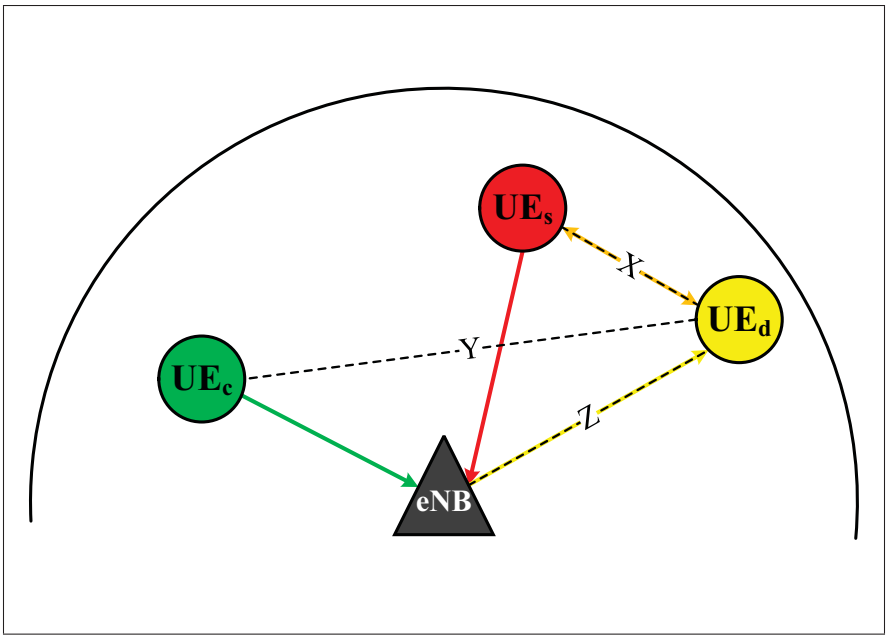

Figure 1.3 Tuple model and distance variables when UE_d moves in the network and the communication channels are modeled as LoS pathloss

$$R_R = \log_2\left(\left(1+\frac{a_1 x}{1+a_2 y}\right)a_3'\right) \tag{1.59}$$

$$R_D = \frac{1}{2}\log_2\left((1+a_1 x)\,a_3''\right) \tag{1.60}$$

$$R_C = \frac{1}{2}\log_2\left(a_3''\right)+\frac{1}{4}\log_2\left(\min\left(a_4, 1+a_5 z\right)\right) \tag{1.61}$$

where:

$$a_1 = \frac{KP_s}{N_0} \tag{1.62a}$$

$$a_2 = \frac{KP_c}{N_0} \tag{1.62b}$$

$$a_3 = \frac{{a_3'}^2}{a_3''} \tag{1.62c}$$

$$a_3' = 1 + \frac{|h_{ce}|^2 P_c}{|h_{se}|^2 P_s + N_0} \tag{1.62d}$$

$$a_3'' = 1 + \frac{|h_{ce}|^2 P_c}{N_0} \tag{1.62e}$$

$$a_4 = 1 + \frac{|h_{se}|^2 P_s}{N_0} \tag{1.62f}$$

$$a_5 = \frac{K P_e}{N_0} \tag{1.62g}$$

and x, y, and z are defined as in (1.15a)–(1.15c) respectively.

Referring to (1.59) and (1.61), note that in order to solve (1.13), all three variables appear in the equation, while (1.12) and (1.14) includes just two of variables. This causes more complex solution for the former equation.

In the following three parts solution to the mode selection map boundaries is determined.

1.5.2.1 $R_{\mathbf{R}} = R_{\mathbf{D}}$

Represent this equation as follows:

$$\log_2\left(\left(1 + \frac{a_1 x}{1 + a_2 y}\right) a_3'\right) = \frac{1}{2}\log_2\left((1 + a_1 x)\, a_3''\right) \tag{1.63}$$

$$\left(1 + \frac{a_1 x}{1 + a_2 y}\right)^2 a_3 = (1 + a_1 x) \tag{1.64}$$

Solving for the unknowns, (1.64) leads to find the roots of a second order equation as follows:

$$f(x,y) = a(x)y^2 + b(x)y + c(x) = 0 \tag{1.65}$$

where:

$$a(x) = a_2^2 \left(a_3 - (1 + a_1 x)\right) \tag{1.66a}$$

$$b(x) = 2 \left(a_2 \left(1 + a_1 x\right) \left(a_3 - 1\right)\right) \tag{1.66b}$$

$$c(x) = \left(1 + a_1 x\right) \left(\left(1 + a_1 x\right) a_3 - 1\right) \tag{1.66c}$$

The second order equation in (1.65) has a solution if the following condition is satisfied:

$$\Delta(x) = 4 a_1^2 a_2^2 a_3 x^2 \left(1 + a_1 x\right) > 0 \tag{1.67}$$

which is always true for $x > 0$.

To find the positive solution to the second order equation in (1.65), the same conditions presented in (1.28a)–(1.28h) is applied.

To find the sign of $a(x)$ as presented in (1.66a), note the following:

- if $1 < a_3$,
  - for $0 < X < X_1$, $a(x) < 0$
  - for $X_1 < X$, $a(x) > 0$
- if $a_3 < 1$, for $X > 0$, $a(x) < 0$

where:

$$X_1 = \sqrt[\alpha]{\frac{a_1}{a_3 - 1}} \tag{1.68}$$

For the sign of $b(x)$:

- if $1 < a_3$, for $X > 0$, $b(x) > 0$
- if $a_3 < 1$, for $X > 0$, $b(x) < 0$

For the sign of $c(x)$:

- if $a_3 > 1$, for $X > 0$, $c(x) > 0$
- if $a_3 < 1$,
  - for $0 < X < X_2$, $c(x) > 0$
  - for $X_2 < X$, $c(x) < 0$

where:

$$X_2 = \sqrt[\alpha]{\frac{a_1 a_3}{1 - a_3}} \tag{1.69}$$

The solution boundaries would be symmetric to the line passing through UE_c and UE_s. To find coordinates UE_d, i.e. (X_d, Y_d), where (1.65) is satisfied, apply the following conversion of X and Y that satisfy the triangle inequalities presented in (1.55) and (1.56):

$$X_d = -\frac{X^2 - Y^2 - d_{cs}^2}{2d_{cs}} \frac{X_s}{d_{cs}} \mp \sqrt{Y^2 - \left(\frac{X^2 - Y^2 - d_{cs}^2}{2d_{cs}}\right)^2} \frac{Y_s}{d_{cs}} + X_c \tag{1.70a}$$

$$Y_d = \pm\sqrt{Y^2 - \left(\frac{X^2 - Y^2 - d_{cs}^2}{2d_{cs}}\right)^2} \frac{X_s}{d_{cs}} + \frac{X^2 - Y^2 - d_{cs}^2}{2d_{cs}} \frac{Y_s}{d_{cs}} + Y_c \tag{1.70b}$$

In the next subsection we discuss the solution to (1.13), for the case when UE_d moves.

1.5.2.2 $R_R = R_C$

Referring to (1.59) and (1.61):

$$\log_2\left(\left(1+\frac{a_1x}{1+a_2y}\right)a_3'\right)=\frac{1}{2}\log_2(a_3'')+\frac{1}{4}\log_2\left(\min\left(a_4,1+a_5z\right)\right) \tag{1.71}$$

$$\left(1+\frac{a_1x}{1+a_2y}\right)^4 a_3^2=\min\left(a_4,1+a_5z\right) \tag{1.72}$$

Here, three distance variables exist, unlike (1.48) and (1.49), where just two were present.

Continue our as follows:

$$\frac{a_1x}{1+a_2y}=\sqrt[4]{\frac{\min\left(a_4,1+a_5z\right)}{a_3^2}}-1 \tag{1.73}$$

Then we define $a_3'(z)$ as:

$$a_3'(z)=\sqrt[4]{\frac{\min\left(a_4,1+a_5z\right)}{a_3^2}}-1 \tag{1.74}$$

$$=\begin{cases}\sqrt[4]{\dfrac{a_4}{a_3^2}}-1 & \text{,for } 0<Z<Z_1 \quad (1.75a)\\ \sqrt[4]{\dfrac{1+a_5z}{a_3^2}}-1 & \text{,for } Z_1<Z \quad (1.75b)\end{cases}$$

where:

$$Z_1=\sqrt[\alpha]{\frac{a_5}{a_4-1}} \tag{1.76}$$

Referring to (1.73), since the left hand side is always positive, $a_3'(z)$ should also be positive. Otherwise, there would be no solution for the equation. Applying this condition on (1.75a):

$$a_3^2 < a_4 \tag{1.77}$$

and on (1.75b):

$$z > \frac{a_3^2 - 1}{a_5} \tag{1.78}$$

Using (1.15c), the condition in (1.78) becomes:

- if $0 < a_3 < 1$, $Z > 0$
- if $1 < a_3$, $Z < Z_2$

where:

$$Z_2 = \sqrt[\alpha]{\frac{a_5}{a_3^2 - 1}} \tag{1.79}$$

As discussed above, for $1 < a_3$, in order for (1.75b) to be positive, $Z < Z_2$ should be satisfied. On the other hand, the following condition should be satisfied:

$$Z_1 < Z_2 \tag{1.80a}$$

$$\Rightarrow \sqrt[\alpha]{\frac{a_5}{a_4 - 1}} < \sqrt[\alpha]{\frac{a_5}{a_3^2 - 1}} \tag{1.80b}$$

$$\Rightarrow a_3^2 < a_4 \tag{1.80c}$$

Combining the results in (1.74), (1.75a), and (1.75b) and the results for positive $a_3'(z)$ above produces:

$$a_3'(z)$$

$$= \begin{cases} \text{if } 0 < a_3^2 < 1 & (1.81a) \\ \sqrt[4]{\dfrac{a_4}{a_3^2}} - 1 \qquad \text{,for } 0 < Z < Z_1 & (1.81b) \\ \sqrt[4]{\dfrac{1+a_5 z}{a_3^2}} - 1 \text{,for } Z_1 < Z & (1.81c) \\ \text{if } 1 < a_3^2 < a_4 & (1.81d) \\ \sqrt[4]{\dfrac{a_4}{a_3^2}} - 1 \qquad \text{,for } 0 < Z < Z_1 & (1.81e) \\ \sqrt[4]{\dfrac{1+a_5 z}{a_3^2}} - 1 \text{,for } Z_1 < Z < Z_2 & (1.81f) \end{cases}$$

It should be noted that according to (1.77) and (1.78), (1.73) have solution only if $a_3^2 < a_4$.

Using the calculations above, the solution which depends on the values of parameters and the interval to which Z belongs, is as follows:

$$\text{if } 0 < a_3 < 1$$

$$\begin{cases} y = \dfrac{1}{a_2}\left(\dfrac{a_1 x}{\sqrt[4]{\frac{a_4}{a_3^2}} - 1}\right) \qquad \text{,for } 0 < Z < Z_1 & (1.82a) \\ \dfrac{a_1 x}{1+a_2 y} = \sqrt[4]{\dfrac{(1+a_5 z)}{a_3^2}} - 1 \text{,for } Z_1 < Z & (1.82b) \end{cases}$$

if $1 < a_3 < \sqrt{a_4}$

$$\begin{cases} y = \dfrac{1}{a_2}\left(\dfrac{a_1 x}{\sqrt[4]{\frac{a_4}{a_3^2}} - 1}\right) \text{ ,for } 0 < Z < Z_1 & \text{(1.82c)} \\ \dfrac{a_1 x}{1 + a_2 y} = \sqrt[4]{\dfrac{(1 + a_5 z)}{a_3^2}} - 1, \text{for } Z_1 < Z < Z_2 & \text{(1.82d)} \end{cases}$$

The solution provided in (1.82a) and (1.82c) is straightforward, since y is a linear function of x. However it should be noted that only the values of X and Y which leads to Z such that $0 < Z < Z_1$ are acceptable. For this (1.53a) or (1.53b) are used to find the values of Z.

To solve (1.82b) and (1.82d), we develop the following equation to find Z as a function of X and Y as follows:

$$Z = \sqrt[\alpha]{\frac{A''(X)Y^{4\alpha} + B''(X)Y^{3\alpha} + C''(X)Y^{2\alpha} + D''(X)Y^{\alpha} + E''(X)}{F''(X)Y^{4\alpha} + G''(X)Y^{3\alpha} + H''(X)Y^{2\alpha} + I''(X)Y^{\alpha} + J''(X)}} \tag{1.83}$$

where:

$$A''(X) = a_5 X^{4\alpha} \tag{1.84a}$$

$$B''(X) = 4a_2 a_5 X^{4\alpha} \tag{1.84b}$$

$$C''(X) = 6a_2^2 a_5 X^{4\alpha} \tag{1.84c}$$

$$D''(X) = 4a_2^3 a_5 X^{4\alpha} \tag{1.84d}$$

$$E''(X) = a_2 a_5 X^{4\alpha} \tag{1.84e}$$

$$F''(X) = a_3 \left(X^{\alpha} + a_1\right)^4 - X^{4\alpha} \tag{1.84f}$$

$$G''(X) = 4a_2\left(a_3^2\left(X^\alpha + a_1\right)^3 - X^{3\alpha}\right)X^\alpha \tag{1.84g}$$

$$H''(X) = 6a_2^2\left(a_3^2\left(X^\alpha + a_1\right)^2 - X^{2\alpha}\right)X^{2\alpha} \tag{1.84h}$$

$$I''(X) = 4a_2^3\left(a_3^2\left(X^\alpha + a_1\right) - X^\alpha\right)X^{3\alpha} \tag{1.84i}$$

$$J''(X) = a_2\left(a_3^2 - 1\right)X^{4\alpha} \tag{1.84j}$$

By equating (1.83) and (1.53a) or (1.83) and (1.53b) separately, the following solutions are achieved for $Z_1 < Z < Z_2$:

if $|X_s Y_c - X_c Y_s| \neq 0$,

$$\sqrt[\alpha]{\frac{A''(X)Y^{4\alpha} + B''(X)Y^{3\alpha} + C''(X)Y^{2\alpha} + D''(X)Y^\alpha + E''(X)}{F''(X)Y^{4\alpha} + G''(X)Y^{3\alpha} + H''(X)Y^{2\alpha} + I''(X)Y^\alpha + J''(X)}} = \sqrt{\frac{-B'(X,Y) \pm \sqrt{B'(X,Y)^2 - 4A'C'(X,Y)}}{2A'}} \tag{1.85a}$$

if $|X_s Y_c - X_c Y_s| = 0$,

$$\sqrt[\alpha]{\frac{A''(X)Y^{4\alpha} + B''(X)Y^{3\alpha} + C''(X)Y^{2\alpha} + D''(X)Y^\alpha + E''(X)}{F''(X)Y^{4\alpha} + G''(X)Y^{3\alpha} + H''(X)Y^{2\alpha} + I''(X)Y^\alpha + J''(X)}} = \sqrt{\frac{Y_c\left(X^2 - d_{se}^2\right) - Y_s\left(Y^2 - d_{ce}^2\right)}{Y_c - Y_s}} \tag{1.85b}$$

Finding close form solutions, which produces Y as a function of X from the above is not followed in this paper. Therefore, the solution is obtained numerically using Newton-Raphson method. It should be noted that the resulting X and Y are only acceptable if they satisfy $Z_1 < Z$ when $0 < a_3 < 1$ and $Z_1 < Z < Z_2$ when $1 < a_3 < \sqrt{a_4}$. Having X and Y, (1.53a) or (1.53b) are used to find Z.

To find the mode selection map boundaries, apply (1.70a) and (1.70b) to convert accepted X and Y which satisfy the triangle inequalities in (1.55) and (1.56) to (X_d, Y_d) coordinates.

It should be noted that since Z, which is a function of X and Y, limits the solutions to (1.82a)–(1.82d), the resulting mode selection map boundaries would not be generally symmetric.

1.5.2.3 $R_D = R_C$

Referring to (1.60) and (1.61):

$$\frac{1}{2}\log_2(1+a_1x) = \frac{1}{4}\log_2(\min(a_4, 1+a_5z)) \tag{1.86}$$

$$(1+a_1x)^2 = \min(a_4, 1+a_5z) \tag{1.87}$$

The solution to (1.87) is straightforward, since the min(.) could be broken into a piecewise function as follows:

$$\min(a_4, 1+a_5z) = \begin{cases} 1+a_5z, \text{for } 0 < z < z_1 & \text{(1.88a)} \\ a_4 \quad\quad \text{, for } z_1 < z & \text{(1.88b)} \end{cases}$$

where:

$$z_1 = \frac{a_4 - 1}{a_5} \tag{1.89}$$

and the solution is:

$$X = \begin{cases} \sqrt[\alpha]{\dfrac{a_1}{\sqrt{a_4}-1}} & \text{,for } 0 < Z < Z_1 \quad (1.90a) \\ \sqrt[\alpha]{\dfrac{a_1}{\sqrt{1+a_5 Z^{-\alpha}}-1}} & \text{,for } Z_1 < Z \quad (1.90b) \end{cases}$$

where Z_1 is determined by converting z_1 using (1.15c).

To find the mode selection map boundaries, apply the following conversions on the solution pair X and Z that satisfy the triangle inequalities in (1.57) and (1.58) to determine the (X_d,Y_d) coordinates:

$$X_\mathrm{d} = -\frac{X^2 - Z^2 - d_\mathrm{se}^2}{2d_\mathrm{se}} \frac{X_\mathrm{s}}{d_\mathrm{se}} \mp \sqrt{Z^2 - \left(\frac{X^2 - Z^2 - d_\mathrm{se}^2}{2d_\mathrm{se}}\right)^2} \frac{Y_\mathrm{s}}{d_\mathrm{se}} \quad (1.91a)$$

$$Y_\mathrm{d} = \pm\sqrt{Z^2 - \left(\frac{X^2 - Z^2 - d_\mathrm{se}^2}{2d_\mathrm{se}}\right)^2} \frac{X_\mathrm{s}}{d_\mathrm{se}} + \frac{X^2 - Z^2 - d_\mathrm{se}^2}{2d_\mathrm{se}} \frac{Y_\mathrm{s}}{d_\mathrm{se}} \quad (1.91b)$$

It should be noted that since the solution just includes x and z variables, the mode selection boundaries would be symmetric to the line passing through eNB and $\mathrm{UE_s}$.

1.6 Numerical Results

To illustrate the application of the approach in Section 1.5, we present the mode selection map of the D2D enabled network showed in Fig. 1.1. Then to validate the results from that approach, we apply a point-to-point mode selection map derivation. We divide the area of the network into a matrix of points where the vertical and horizontal distances between two neighbor points is 25m. We place the moving UE at each point and take the same a_is as used for analytical approach simulations. Then to find the overall throughput of the network for all three modes at that point, we use (1.18)–(1.20) for moving $\mathrm{UE_s}$, and (1.59)–(1.61) for moving $\mathrm{UE_d}$. Finally, the mode that gives the highest overall throughput is assigned to that specific

point. For simplicity we assign red, yellow, and green for reuse, dedicated, and cellular modes respectively. We apply this procedure for all the points in the area of the network.

We assume that UEs and eNB have fixed power and use a single antenna for their communication. Moreover, as discussed earlier, the communication channel between any two entities is modeled as a LoS path-loss channel. The parameters of our simulation are summarized in Table 1.1. For the two different cases presented in Section 1.5, results are presented separately as follows:

Table 1.1 Simulation parameters for mode selection map derivation in LoS pathloss channel

Parameter	**Value**
Cell radius: r_{C}	3 km
$\mathrm{UE_c}$'s position: $(X_{\mathrm{c}},Y_{\mathrm{c}})$	$(-1000,1000)$
$\mathrm{UE_s}$'s position: $(X_{\mathrm{s}},Y_{\mathrm{s}})$	$(250,1500)$
$\mathrm{UE_d}$'s position: $(X_{\mathrm{d}},Y_{\mathrm{d}})$	$(1500,250)$
UE's maximum power: P_{c}, P_{s}, P_{d}	23dBm
eNB's maximum power: P_{e}	46dBm
Pathloss exponent: α	3 (for urban areas)

1.6.1 Moving $\mathrm{UE_s}$

Relying on the results from Section 1.5.1 for the mode selection map for (1.12)–(1.14) in the moving $\mathrm{UE_s}$ case, using the values from Table 1.1, the simulation results are shown in Fig. 1.4a and Fig. 1.5.

Fig. 1.4a shows the equi-rate boundaries derived analytically as discussed in Section 1.5.1 when $\mathrm{UE_s}$ is moving in the network. As could be seen the boundaries divide the area of the network into disjoint regions. To find the map using the analytically derived boundaries, we take an arbitrary point in each disjoint region and find the mode which gives the highest overall throughput there, then we assign all points in that specific region to the same mode. The

result of this approach is shown in Fig. 1.4b. In this figure, the red, green, and yellow zones represent regions where the reuse, cellular, and dedicated modes produces the highest overall throughput respectively. For example if UE_s is located in the yellow region and remains there while moving, the selected TM for the D2D UE pair would be the dedicated. Finally Fig. 1.4c, shows the resulted map using the point-to-point approach discussed earlier. As could be seen the map derived analytically is the same as the one achieved using the point to point method. However using the analytical method, the resulted map is more precise, and it takes less processing time to achieve it.

To check the validity of the resulted equi-rate boundaries using the analytical method in the case when UE_s moves in the network, they are compared with simulation results from the point-to-point method as shown in Fig. 1.5. As could be seen the equi-rate boundaries derived analytically matches the boundaries found using the point-to-point method.

1.6.2 Moving UE_d

In this subsection we present results relying on the approach from Section 1.5.2 that defines the mode selection map for each case related to (1.12)–(1.14) when UE_d moves. The values from Table 1.1 are applied. The simulation results are shown in Fig. 1.6 and Fig. 1.7.

Fig. 1.6a shows the equi-rate boundaries derived analytically as presented in Section 1.5.1. As discussed earlier in 1.5.2, the boundary curves are only symmetric for (1.12) and (1.14), while for (1.13) since generally three different dependent distance variables appear in the equations the result is asymmetric. We use the same techniques as discussed in Section 1.6.1, to achieve the analytically derived mode selection map as shown in Fig. 1.6b, as well as finding the mode selection map using the point-to-point method as shown in Fig. 1.6c. In this case also the point-to-point simulation map validates our analytically derived map.

Again to check the validity of the resulted equi-rate boundaries using the analytical method in the case when UE_d moves in the network, they are compared with simulation results from the

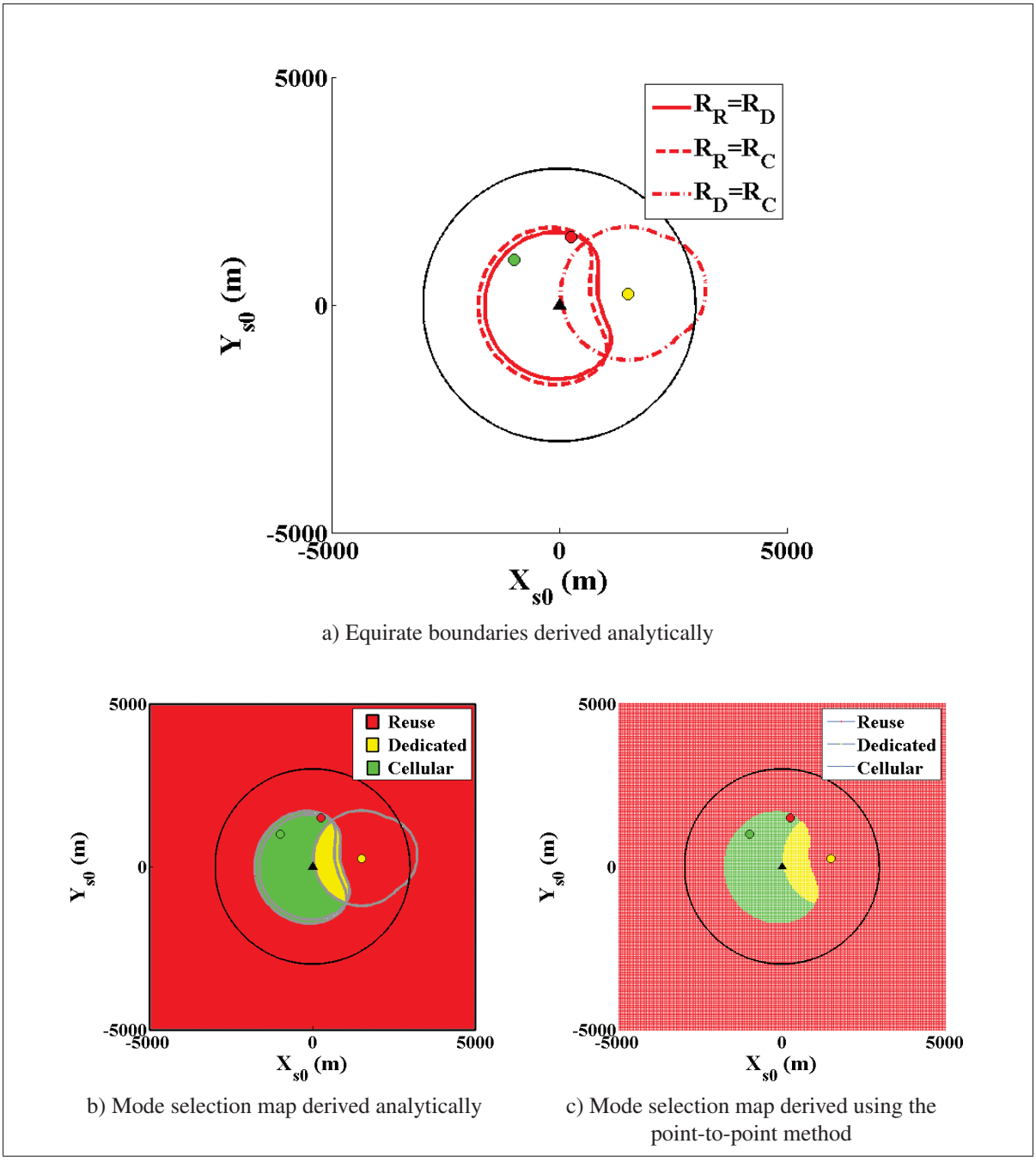

a) Equirate boundaries derived analytically

b) Mode selection map derived analytically

c) Mode selection map derived using the point-to-point method

Figure 1.4 Mode selection map and its boundaries when UE_s moves in the network and the communication channels are modeled as LoS pathloss

point-to-point method as shown in Fig. 1.7. As could be seen the equi-rate boundaries derived analytically matches the boundaries found using the point-to-point method.

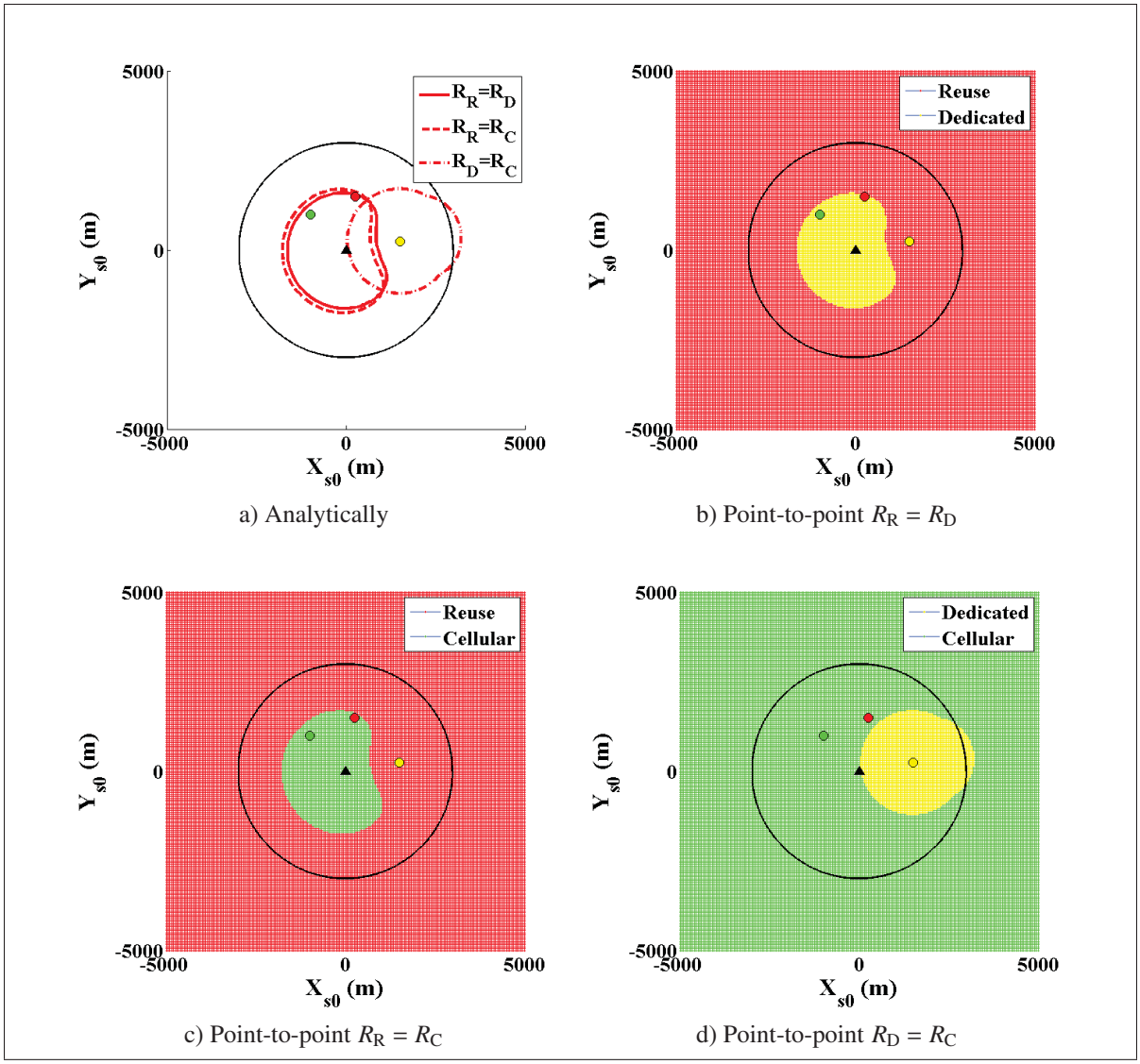

a) Analytically

b) Point-to-point $R_R = R_D$

c) Point-to-point $R_R = R_C$

d) Point-to-point $R_D = R_C$

Figure 1.5 Comparison of equirate boundaries derived analytically and from point-to-point simulation approaches, when UE_s moves in the network and the communication channels are modeled as LoS pathloss

1.7 Conclusion

In this work, we propose an analytical solution for determining the mode selection map in single cell D2D enabled 5G network consisting of a D2D UE pair, one cellular UE, and one eNB. While the cellular UE communicates with eNB in UL, D2D UEs select their TM among the reuse, dedicated, and cellular modes by choosing the one which results in the highest overall

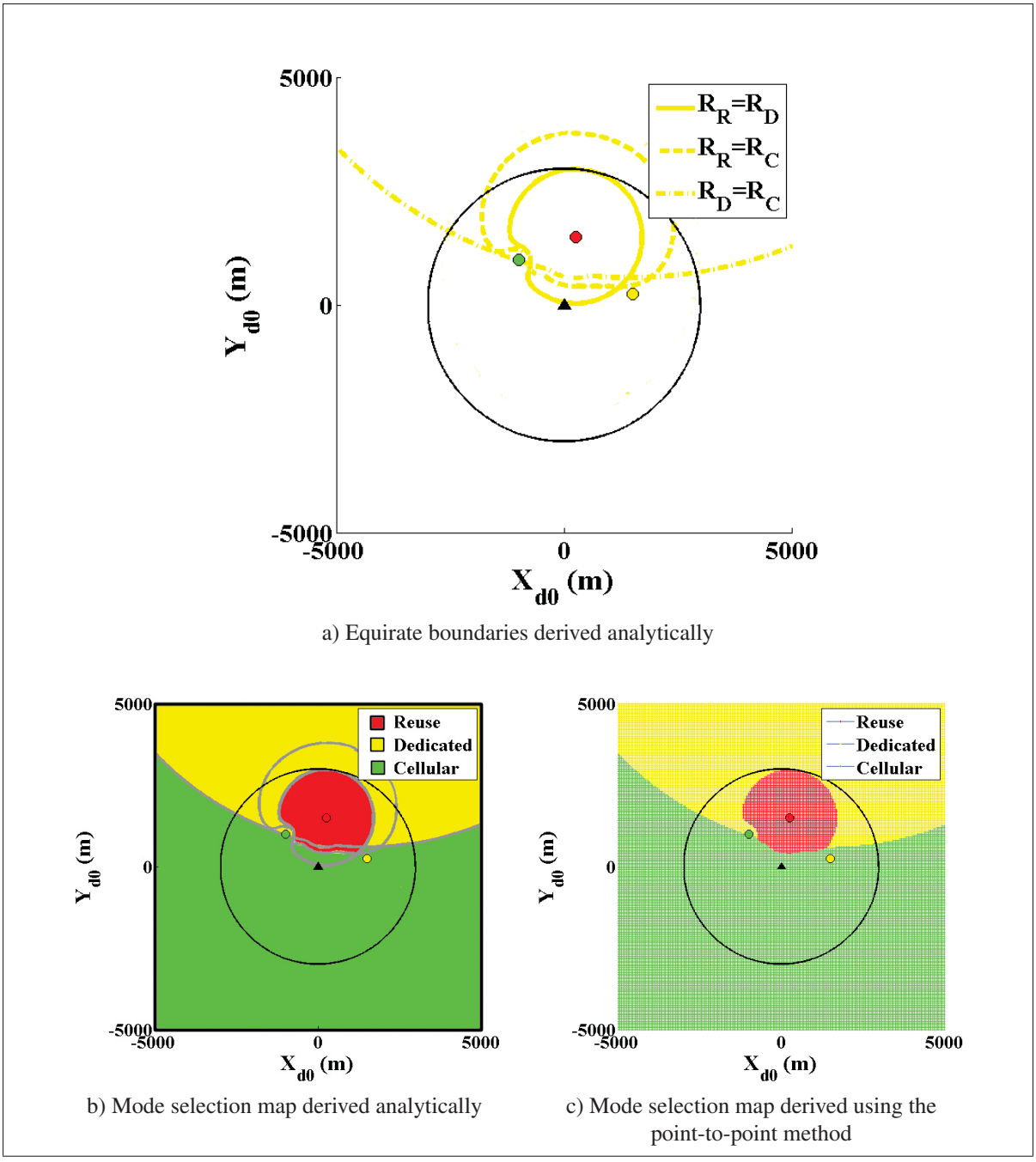

a) Equirate boundaries derived analytically

b) Mode selection map derived analytically

c) Mode selection map derived using the point-to-point method

Figure 1.6 Mode selection map and its boundaries when UE_d moves in the network and the communication channels are modeled as LoS pathloss

throughput for the network. We show that for fixed transmission and noise powers in an LoS channel, the optimal mode for communication between D2D UEs, depends on each UE's location. Moreover, we find that there are disjoint regions in the network where if a moving UE

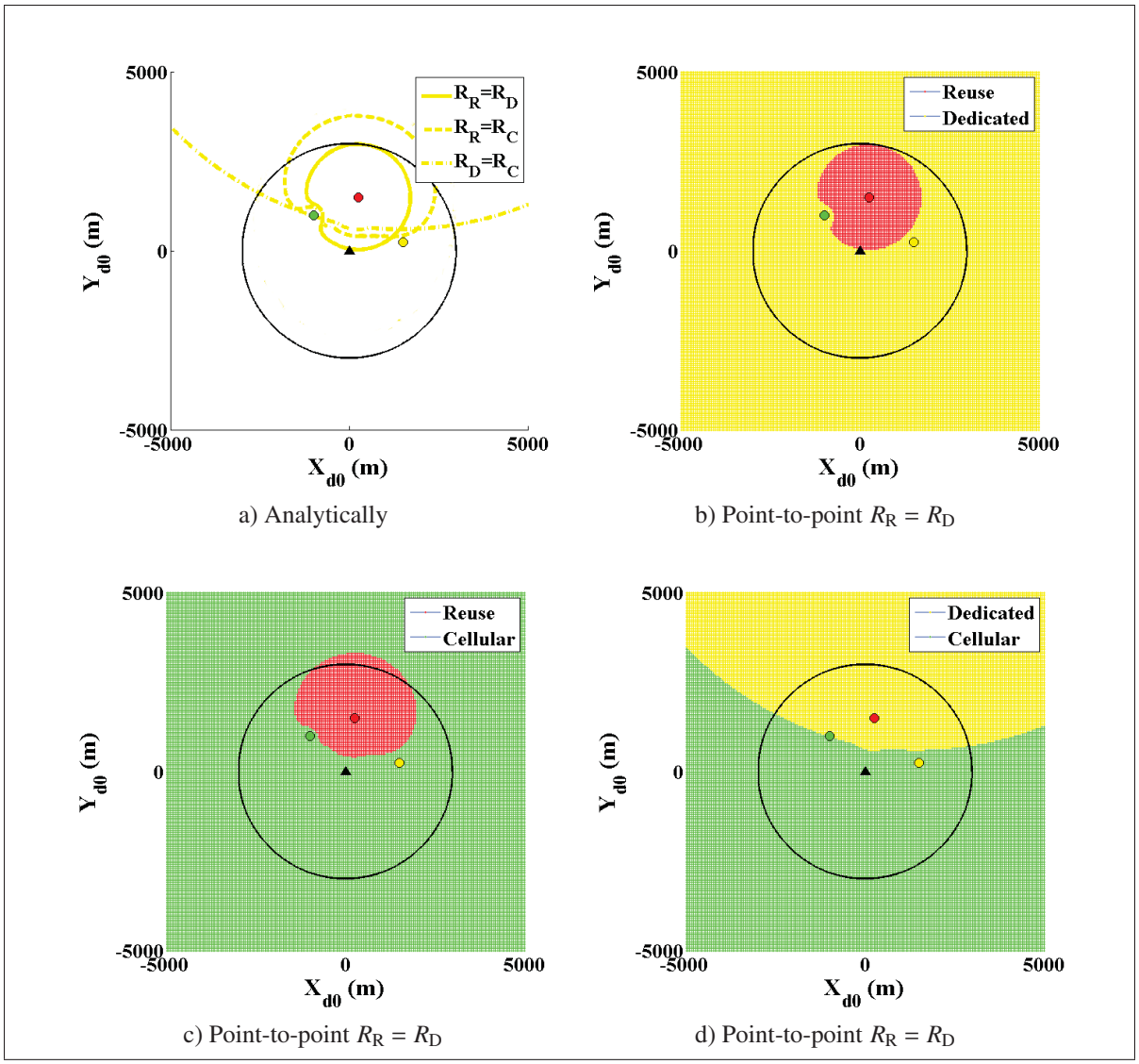

a) Analytically

b) Point-to-point $R_R = R_D$

c) Point-to-point $R_R = R_D$

d) Point-to-point $R_R = R_D$

Figure 1.7 Comparison of equirate boundaries derived analytically and from point-to-point simulation approaches, when UE_d moves in the network and the communication channels are modeled as LoS pathloss

stays inside that region, the TM mode between D2D UEs will not change. We realized that depending on which UE moves in the network there are three different cases to formulate the mode selection map problem where two of them have been discussed in this paper. Using analytical approaches for each case, we find a set of geometrical functions which explicitly define the mode selection map. Using the results from the analysis we develop simulation scenarios for each case and we realize that there are certain regions defined by equirate boundaries where

if UE_s or UE_d is located within those boundaries, there would be an optimal mode for communications. To verify our proposed our analytical map derivation, we propose a point-to-point mode selection map derivation to find the map of the network. We realized that the boundaries defined by these maps matches the boundaries derived analytically.

CHAPTER 2

MODE SELECTION MAP IN D2D ENABLED CELLULAR NETWORKS OVER FADING CHANNELS

Armin Morattab[1], Zbigniew Dziong[1], Kazem Sohraby[2]

[1] Department of Electrical Engineering, École de Technologie Supérieure,
1100 Notre-Dame Ouest, Montreal, Quebec, Canada, H3C 1K3
[2] Department of Electrical and Computer Engineering, South Dakota School of Mines & Technology, Rapid City, SD 57701, USA
& an Adjunct in Computer Science Department, Sand Diego State University, USA

Article submitted for review in January 2017.

Abstract

The number of mobile devices are increasing drastically each year and users demand for higher data rates grows exponentially. Device-to-Device (D2D) transmission is one of the promising features that is proposed for 5G networks to provide users with higher data rate and better Quality of Service (QoS). This technique enables direct transmission between User Equipment (UE) in addition to the traditional cellular transmission. Paired UEs select among the reuse, dedicated, and cellular modes taking into account the overall network throughput as selection criteria. In this work, we extend our finding to derive the mode selection map while the communication channel between each two entity is modeled using a line of sight (LoS) path loss model, to the case where the communication channel is experiencing both shadowing and fast fading. A simple network with two D2D UEs and one cellular UE in transmission with an evolved Node-B (eNB) is considered. It is assumed that the cellular UE could move in the network and it is in uplink transmission with eNB while the D2D UEs are static. Our approach leads to finding the boundaries which define the mode selection map of the network. The shape of these boundaries are dependent upon the transmission power of UEs and eNB, the location of static UEs, and the standard deviation of fading and shadowing variables. Our simulations verify the results of the mode selection map derivation using the proposed approach.

Introduction

The ever-increasing mobile traffic in recent years has induced service providers and telecommunications industries to find and develop new techniques and designs to provide higher data rates with guaranteed Quality-of-Service (QoS) at lower prices (CISCO, 2015) for their customers in their everyday cellular communications. This has provoked the introduction of the fifth generation (5G) networks which are expected to provide much higher data rates with less latency (Andrews *et al.*, 2014). Device-to-Device (D2D) transmission is one of the features proposed for the 5G and beyond networks that enables D2D User Equipment (UE) communicate directly with each other without unnecessary routing of traffic through the network infrastructure (Doppler *et al.*, 2009, 2011, 2010; Janis *et al.*, 2009), and which results in higher data rates, less power consumption, and less latency (Asadi *et al.*, 2014; Mumtaz and Rodriguez, 2014; Song *et al.*, 2015; Panagopoulos, 2015).

In addition to the traditional cellular mode, potential D2D UEs are free to select two additional transmission modes (TMs) which enables direct communication between them, the dedicated mode and the reuse mode (Song *et al.*, 2015; Feng *et al.*, 2015; Panagopoulos, 2015; Wang and Tang, 2016). In the reuse mode, D2D UEs reuse the same resources as cellular transmission, while in the dedicated mode, D2D UEs transmit data by the orthogonal resource to the regular cellular UE. Thus in the reuse mode interference is arising and in the dedicated mode interference is avoided. In the cellular mode, D2D UEs are treated as cellular UEs where the transmission between them is through the eNB. In order to start communication, D2D UEs should decide among the three different TMs (Doppler *et al.*, 2010; Liu *et al.*, 2012c; Song *et al.*, 2015; Feng *et al.*, 2015; Panagopoulos, 2015; Wang and Tang, 2016; Huang *et al.*, 2016), or they could also apply a mixed mode mechanism in which each D2D link can utilize multiple modes through mode switching or resource multiplexing (Feng *et al.*, 2015; Tang and Ding, 2016). Such a decision process is called mode selection.

The TM selection, is made periodically based on a specific criterion, such as the overall throughput of the network. In other words, the TM which results in the highest throughput

is selected. It has been shown that for a fixed transmission power, fading conditions, and noise power, the TM to be selected depends on the location of entities in the network (Morattab *et al.*, 2015, 2016), that is to say there are certain network geographical regions in which the best TM for D2D UEs' communication is the same, in spite of movement of one entity inside any particular region, while other entities are static. The set of these regions and the borders between them form the mode selection map of the D2D enabled network. This map can be used by eNB to assign the best TM for the communication between D2D UEs without applying the mode selection algorithm periodically. As long as the moving entity does not leave its region, the selected mode remains the same (Morattab *et al.*, 2016). Furthermore, the Mobility Management Entity (MME) can use the mode selection map to find the best policy for vertical handover when the moving entity leaves its first region and enters its neighboring regions where a different TM may be assigned. Such applications is left for future works and it is not discussed here.

Due to multi-path propagation and shadowing from obstacles affecting the wave propagation, the communication channels in wireless networks usually experience fading effects (Rappaport *et al.*, 1996; Tse and Viswanath, 2005). Being wireless, D2D transmission is not an exception to fading, therefore to have a reliable modeling and solid results, the fading effect should be taken into account (Li *et al.*, 2013; Feng *et al.*, 2013; Peng *et al.*, 2014; Cotton, 2015, 2016) whether for mode selection (Li *et al.*, 2013), performance analysis (Li *et al.*, 2013; Peng *et al.*, 2014), channel modeling (Cotton, 2015, 2016), or resource allocation (Wang *et al.*, 2011; Feng *et al.*, 2013). Likewise a new approach to derive the mode selection map considering the presence of fading effect, for the communication channels between each two entities, is required. Since the statistics of random variables which represent fading would not change for a long time, the resulting map could be used in applications such as mode selection, resource allocation, mobility management and handover. Such approach is the subject of this work where we provide a framework to derive the mode selection map of the network when fading is present.

2.1 Related Works

The idea of having a mode selection map have been implicitly discussed for the first time in (Doppler *et al.*, 2010) where a mode selection procedure in a single cell and then multi-cell environments is proposed. The map is derived numerically by optimizing for all possible TMs and selecting the one that gives the highest throughput for a given location of the cellular UE. In our previous work, (Morattab *et al.*, 2015), we extended the mode selection procedure in (Doppler *et al.*, 2010) assuming the UEs and eNB can use Multiple-Input-Multiple-Output (MIMO) precoding. We present a method to optimally design MIMO precoders and decoders at each transmitter and receiver respectively, to reach the highest possible overall throughput for different TMs. Our results in that work shows higher gain and efficiency compared to (Doppler *et al.*, 2010). Derivation of the mode selection map of the network numerically using the same point-to-point technique shows that using MIMO, the area where the dedicated and reuse modes reach the highest throughput is larger than in SISO scenarios.

The mode selection maps in (Doppler *et al.*, 2010; Morattab *et al.*, 2015) are derived numerically by applying a point-to-point procedure which is imprecise, complex, time consuming, and inefficient. Using such methods consumes a lot of execution time and systems memory. Since, such methods are point based, the precision of resulting map is a function of the distance between two consecutive points where mode selection algorithm is applied. To deal with these issues we presented in (Morattab *et al.*, 2016), an analytical approach to find the mode selection map for the case where the cellular UE moves in the network and the D2D UEs are static. For simplicity a line of sight (LoS) path-loss model is considered for the communication channel between each two entities with no fading presence. We showed that the resulting geometrical functions presented in the paper could trace the mode selection map precisely for each arbitrary position of the UEs in the network.

In a recent work in (Xu *et al.*, 2016), the authors provide theoretical analysis of D2D mode selection with user mobility. Although the authors do not explicitly present a mode selection map derivation method, they define a region where its border is computed by equating the

Received Signal Strength (RSS) of the cellular and reuse modes. In that work TM between the D2D UEs is changed whenever one of the UEs exits a specific region. Although the authors presented an analytical method to reach the equi-RSS boundaries, no solution was proposed to derive the mode selection map. Except presenting a circular region as the approximation of the analysis. Moreover the fading effect is missing in their problem modeling and calculations.

2.2 Contributions

In this work, we present a comprehensive approach to find the mode selection map for a network over fading channel. Then this approach is used to find the detailed mode selection maps for the case where cellular UE moves and the D2D UEs are static. The main contributions of this paper are summarized as follows:

- In this paper, to the best of our knowledge, the problem of calculating mode selection map over a fading channel is presented for the first time;
- We provide an algorithm which uses probabilistic functions to capture shadowing and fast fading to determine the geographical boundaries between disjoint regions where a specific mode is selected.

The remainder of the work is organized as follows. In Section 2.3, the mathematical model of the network is presented assuming three different TMs between the D2D UEs. The model for calculation of the overall network throughput is derived in Section 2.4. In Section 2.5, we present the construction of the mode selection maps as well as the solution approach for the case when cellular UE moves in the network while the D2D UEs are static. In Section 2.6, the simulation and validation results for the case presented in Section 2.5 is provided. Finally, the conclusions are formulated in Section 2.7.

2.3 System Model

We consider a single cell D2D enabled cellular network consisting of two D2D UEs, a cellular UE, and an evolved Node-B (eNB). D2D UEs are either communicating with each other or

they are about to start their communication. While the D2D UEs could operate in the reuse, dedicated, and cellular modes, the cellular UE transmission is limited to the cellular mode in Uplink (UL). As it is shown in Fig. 2.1, the transmission for D2D UEs is from source UE (UE_s) to destination UE (UE_d), while the cellular UE (UE_c) transmits data to eNB. It is also assumed that all entities in the network are equipped with a single antenna.

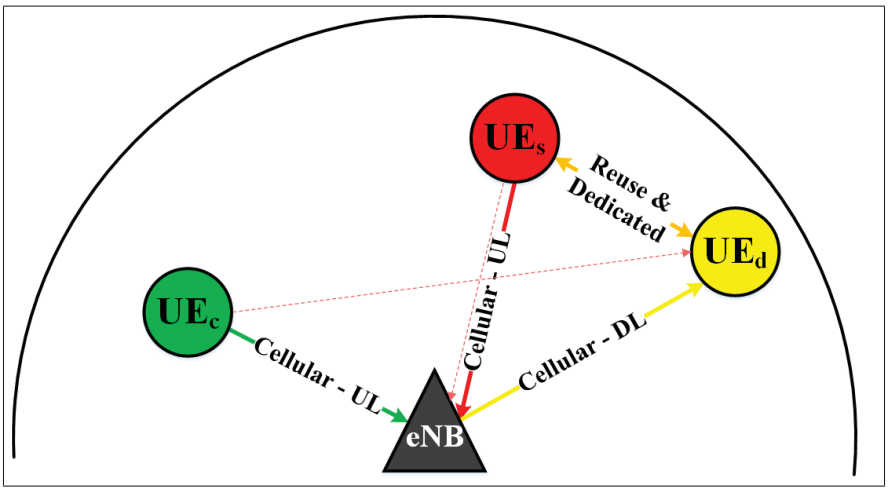

Figure 2.1 D2D enabled 5G network – fading channels

The communication channel between each two entities in the network, is modeled as a quasi-static Rayleigh frequency-flat fading channel as in (Sklar, 1997):

$$h_{ij} = \sqrt{c/d_{ij}^{\alpha}}\sqrt{S_{ij}}z_{ij} \tag{2.1}$$

where, h_{ij} is the channel gain between transmitter i and receiver j, where i is either s, c, or e, and j is either e or d. The subscripts s, c, d, and e stand for UE_s, UE_c, and UE_d, and eNB respectively. d_{ij} is the distance between the same transmitter and receiver as for h_{ij}, α is the pathloss exponent, and c is the propagation constant. $S_{ij} = 10^{s_{ij}/10}$ is a log-normal shadow fading variable, where s_{ij} is a zero mean Gaussian random variable with standard deviation

σ_s. z_{ij} represents the fast fading characteristic of the channel and it is modeled as a complex Gaussian random variable with standard deviation σ_z.

For simplicity, we define the following random variable:

$$K_{\mathrm{ij}} = c.S_{\mathrm{ij}}.\left|z_{\mathrm{ij}}\right|^2 \tag{2.2}$$

We assume that, in the reuse mode, the resources for $\mathrm{UE_s}$-$\mathrm{UE_d}$ transmission are shared with the $\mathrm{UE_c}$-eNB transmission. Therefore, each of the receivers in the network will be affected by the interference from the undesired transmitter as well as the background noise. The interference channel is shown in Fig. 2.1 as red dotted lines. However, when the D2D UEs' communication is in the dedicated or cellular modes, half of the resources are assigned to the D2D UEs' transmission, and the rest is assigned to $\mathrm{UE_c}$-eNB transmission, and hence there is no interference at receivers.

Based on the above assumptions, the received signal, y, at receivers for three different TMs between D2D UEs is as follows:

$$y_{\mathrm{d}}^{\mathrm{R}} = \sqrt{P_{\mathrm{s}}}h_{\mathrm{sd}}x_{\mathrm{s}}^{\mathrm{R}} + \sqrt{P_{\mathrm{c}}}h_{\mathrm{cd}}x_{\mathrm{c}}^{\mathrm{R}} + n_{\mathrm{d}}^{\mathrm{R}} \tag{2.3}$$

$$y_{\mathrm{e}}^{\mathrm{R}} = \sqrt{P_{\mathrm{c}}}h_{\mathrm{ce}}x_{\mathrm{c}}^{\mathrm{R}} + \sqrt{P_{\mathrm{s}}}h_{\mathrm{se}}x_{\mathrm{s}}^{\mathrm{R}} + n_{\mathrm{e}}^{\mathrm{R}} \tag{2.4}$$

$$y_{\mathrm{d}}^{\mathrm{D}} = \sqrt{P_{\mathrm{s}}}h_{\mathrm{sd}}x_{\mathrm{s}}^{\mathrm{D}} + n_{\mathrm{d}}^{\mathrm{D}} \tag{2.5}$$

$$y_{\mathrm{e}}^{\mathrm{D}} = \sqrt{P_{\mathrm{c}}}h_{\mathrm{ce}}x_{\mathrm{c}}^{\mathrm{D}} + n_{\mathrm{e}}^{\mathrm{D}} \tag{2.6}$$

$$y_{e1}^{C} = \sqrt{P_{\mathrm{s}}}h_{\mathrm{se}}x_{\mathrm{s}}^{\mathrm{C}} + n_{\mathrm{e1}}^{\mathrm{C}} \tag{2.7}$$

$$y_{\mathrm{d}}^{\mathrm{C}} = \sqrt{P_{\mathrm{e}}}h_{\mathrm{ed}}x_{\mathrm{e}}^{\mathrm{C}} + n_{\mathrm{d}}^{\mathrm{C}} \tag{2.8}$$

$$y_{\mathrm{e2}}^{\mathrm{C}} = \sqrt{P_{\mathrm{c}}}h_{\mathrm{ce}}x_{\mathrm{c}}^{\mathrm{C}} + n_{\mathrm{e2}}^{\mathrm{C}} \tag{2.9}$$

where x is the transmitted signal, n is the white Gaussian noise with spectral density of N_0, and P is the transmitter's power. For these variables the subscripts s, d, c, e represent UE_s, UE_d, UE_c, and eNB respectively, and R, D, and C superscripts represent the reuse, dedicated, and cellular modes respectively. It should be noted that when the TM of D2D UEs is cellular, the UE_s-UE_d transmission breaks into two cascade transmission, i.e. UE_s-eNB and eNB-UE_d. In this mode the eNB receives two signals, one from the UE_s which is y^{C}_{e1} and the other from UE_c which is y^{C}_{e2}.

The received signals in the reuse mode include three terms as presented in (2.3) and (2.4). The first term represents the desired signal from the paired entity, the second term is interference from other entity, and the last term is noise. However, the received signals in the dedicated and cellular modes do not include interference, as presented in (2.5)–(2.9) since the resources are not shared.

In the following section, we formulate the problem for overall throughput of the network, which is used later to derive the mode selection map of the network.

2.4 Problem Formulation

We assume that near capacity channel codes are used at transmitters, hence the overall throughput of the network in the reuse, dedicated, and cellular modes would be almost equal to the overall capacity of the network for each mode.

$$R_{\mathrm{R}} = R_{R1} + R_{R2} \tag{2.10}$$

$$R_{\mathrm{D}} = R_{D1} + R_{D2} \tag{2.11}$$

$$R_{\mathrm{C}} = R_{C1} + R_{C2} \tag{2.12}$$

where R_{R1}, R_{R2}, R_{D1}, R_{D2}, R_{C1}, and R_{C2} are the UE_s-UE_d throughput in reuse mode, UE_c-eNB throughput in reuse mode, UE_s-UE_d throughput in dedicated mode, UE_c-eNB in dedicated mode, UE_s-eNB-UE_d throughput in cellular mode, and UE_c-eNB in cellular mode, respectively. These throughput functions are defined as:

$$R_{R1} = \log\left(1 + \frac{|h_{sd}|^2 P_s}{|h_{cd}|^2 P_c + N_0}\right) \tag{2.13}$$

$$R_{R1} = \log\left(1 + \frac{|h_{ce}|^2 P_c}{|h_{se}|^2 P_s + N_0}\right) \tag{2.14}$$

$$R_{D1} = \frac{1}{2}\log\left(1 + \frac{|h_{sd}|^2 P_s}{N_0}\right) \tag{2.15}$$

$$R_{D2} = \frac{1}{2}\log\left(1 + \frac{|h_{ce}|^2 P_c}{N_0}\right) \tag{2.16}$$

$$R_{C1} = \frac{1}{4}\min\left(\log\left(1 + \frac{|h_{se}|^2 P_s}{N_0}\right), \log\left(1 + \frac{|h_{ed}|^2 P_e}{N_0}\right)\right) \tag{2.17}$$

$$R_{C2} = \frac{1}{2}\log\left(1 + \frac{|h_{ce}|^2 P_c}{N_0}\right) \tag{2.18}$$

In the above equations we assumed that the bandwidth is normalized to one, so it is not shown in the formulations.

Assuming shadowing and fast-fading in the channel, the mode selection map boundaries could be found by equating the expected value of overall throughput formulations in (2.10)–(2.12), one by one as follows:

$$\mathbb{E}[R_R] = \mathbb{E}[R_D] \tag{2.19}$$

$$\mathbb{E}[R_R] = \mathbb{E}[R_C] \tag{2.20}$$

$$\mathbb{E}[R_D] = \mathbb{E}[R_C] \tag{2.21}$$

where $\mathbb{E}[Z]$ is the expected value of the random variable Z. Moreover, since $\mathbb{E}[U+Z] = \mathbb{E}[U]+\mathbb{E}[Z]$, using (2.10)–(2.12):

$$\mathbb{E}[R_{\mathrm{R}}] = \mathbb{E}[R_{\mathrm{R1}}]+\mathbb{E}[R_{\mathrm{R2}}] \tag{2.22}$$

$$\mathbb{E}[R_{\mathrm{D}}] = \mathbb{E}[R_{\mathrm{D1}}]+\mathbb{E}[R_{\mathrm{D2}}] \tag{2.23}$$

$$\mathbb{E}[R_{\mathrm{C}}] = \mathbb{E}[R_{\mathrm{C1}}]+\mathbb{E}[R_{\mathrm{C2}}] \tag{2.24}$$

In the following section we use (2.19)–(2.21) and (2.22)–(2.24) to find the mode selection map.

2.5 Mode Selection Map

In this section we propose a solution approach for the case where $\mathrm{UE_c}$ moves in the network, while $\mathrm{UE_s}$ and $\mathrm{UE_d}$ are static. In this case, the network variables would be $X = d_{\mathrm{cd}}$ and $Y = d_{\mathrm{ce}}$ as shown in Fig.2.2. Using these variables, we can rewrite (2.13)–(2.18) as follows:

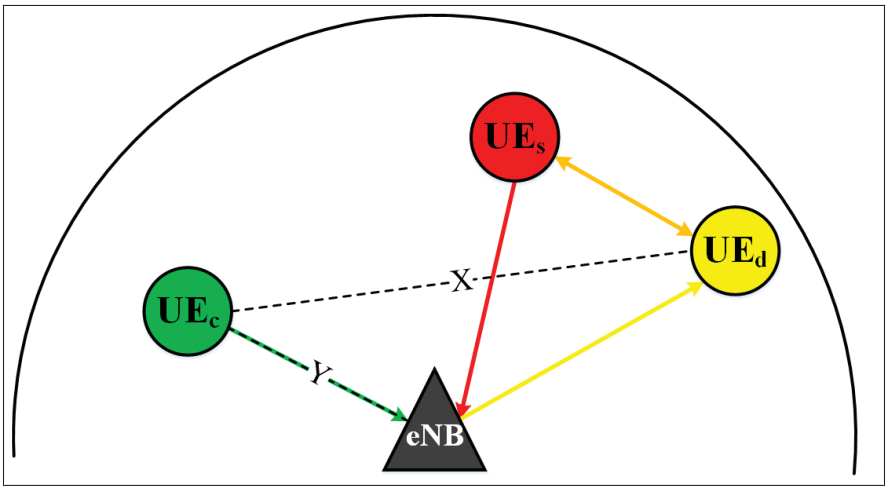

Figure 2.2 Tuple model and distance variables when $\mathrm{UE_c}$ moves in the network and the communication channels are modeled using fading model

$$R_{R1} = \log\left(1 + \frac{a_1}{1 + a_2 x}\right) \tag{2.25}$$

$$R_{R2} = \log(1 + a_3 y) \tag{2.26}$$

$$R_{D1} = \frac{1}{2}\log(1 + a_1) \tag{2.27}$$

$$R_{D2} = \frac{1}{2}\log(1 + a_4 y) \tag{2.28}$$

$$R_{C1} = \frac{1}{4}\log(1 + a_5) \tag{2.29}$$

$$R_{C2} = \frac{1}{2}\log(1 + a_4 y) \tag{2.30}$$

and:

$$a_1 = \frac{K_{sd} P_s}{d_{sd}^{\alpha} N_0} \tag{2.31a}$$

$$a_2 = \frac{K_{cd} P_c}{N_0} \tag{2.31b}$$

$$a_3 = \frac{K_{ce} P_c}{d_{ce}^{\alpha}\left(\frac{K_{se} P_s}{d_{se}^{\alpha}} + N_0\right)} \tag{2.31c}$$

$$a_4 = \frac{K_{ce} P_c}{N_0} \tag{2.31d}$$

$$a_5 = \min\left(\frac{K_{se} P_s}{d_{se}^{\alpha} N_0}, \frac{K_{ed} P_e}{d_{ed}^{\alpha} N_0}\right) \tag{2.31e}$$

where a_1 to a_5 are random variables that their value varies in the network because of the shadowing and fast fading effects of the communication channels.

To simplify our solution approach the following conversions are used in (2.25)–(2.30):

$$x = \frac{1}{X^{\alpha}} \quad or \quad X = \sqrt[\alpha]{\frac{1}{x}} \tag{2.32a}$$

$$y = \frac{1}{Y^{\alpha}} \quad or \quad Y = \sqrt[\alpha]{\frac{1}{y}} \tag{2.32b}$$

From (2.11), (2.12), and (2.27)–(2.30), it can be seen that R_{D} is a specific form of R_{C} where a_5 is substituted by $(1+a_1)^2 - 1$. Therefore the solution to (2.19) would follow the same steps as for (2.20) that is more general. It is also important to notice that equation (2.21) never leads to a solution unless $\mathbb{E}[\log(1+a_1)] = \mathbb{E}[\frac{1}{2}\log(1+a_5)]$, and if it happens, equation (2.21) is valid for all values of X and Y. Besides, if $\mathbb{E}[\log(1+a_1)] > \mathbb{E}[\frac{1}{2}\log(1+a_5)]$, then $\mathbb{E}[R_{\mathrm{D}}] > \mathbb{E}[R_{\mathrm{C}}]$ and if $\mathbb{E}[\log(1+a_1)] < \mathbb{E}[\frac{1}{2}\log(1+a_5)]$, then $\mathbb{E}[R_{\mathrm{D}}] < \mathbb{E}[R_{\mathrm{C}}]$.

As discussed above, if we assume $\mathbb{E}[\log(1+a_1)] \neq \mathbb{E}[\frac{1}{2}\log(1+a_5)]$, only (2.19) and (2.20) possibly have solutions. We also know that (2.20) has more general form than (2.19). Therefore in this section we develop our method only for (2.20).

For the (X,Y) pair which satisfies (2.19) and (2.20), we apply the following conversion to find their geometrical representation as Cartesian coordinates (Xc,Yc):

$$X_c = -\frac{X^2 - Y^2 - d_{ed}^2}{2d_{ed}}\frac{X_d}{d_{ed}} \mp \sqrt{Y^2 - \left(\frac{X^2 - Y^2 - d_{ed}^2}{2d_{ed}}\right)^2}\frac{Y_d}{d_{ed}} \tag{2.33a}$$

$$Y_c = \pm\sqrt{Y^2 - \left(\frac{X^2 - Y^2 - d_{ed}^2}{2d_{ed}}\right)^2}\frac{X_d}{d_{ed}} + \frac{X^2 - Y^2 - d_{ed}^2}{2d_{ed}}\frac{Y_d}{d_{ed}} \tag{2.33b}$$

where (X_d,Y_d) are the coordinates of $\mathrm{UE_d}$ in the network.

To solve (2.19) and (2.20), we need to find $\mathbb{E}[R_{\mathrm{R1}}]$, $\mathbb{E}[R_{\mathrm{R2}}]$, $\mathbb{E}[R_{\mathrm{D1}}]$, $\mathbb{E}[R_{\mathrm{D2}}]$, $\mathbb{E}[R_{\mathrm{C1}}]$, and $\mathbb{E}[R_{\mathrm{C2}}]$ functions numerically. The results for these functions are summarized in Fig. 2.3.

As discussed earlier here we only present our approach to solve (2.20) since it has more general form. This approach is summarized in the following algorithm:

Input: X_{d}, Y_{d}, $\mathbb{E}[R_{R1}]$, $\mathbb{E}[R_{R2}]$, $\mathbb{E}[R_{C1}]$, and $\mathbb{E}[R_{C2}]$

Output: X_{c}, Y_{c}

Initialization :

$d_{\mathrm{ed}} = \sqrt{X_{\mathrm{d}}^2 + Y_{\mathrm{d}}^2}$

for $X = 0$ to 3500 **do**

Find $\mathbb{E}[R_{R1}]$ for X using Fig. 2.3a.

Find $\mathbb{E}[R_{R2}]$, $\mathbb{E}[R_{C1}]$, and $\mathbb{E}[R_{C2}]$ for $Y = |X - d_{\mathrm{ed}}|$ using Fig. 2.3b, 2.3e, and 2.3f respectively.

Calculate $\mathbb{E}[R_R]$ and $\mathbb{E}[R_C]$ functions using (2.22) and (2.24) respectively.

Find the intersection of $\mathbb{E}[R_R]$ and $\mathbb{E}[R_C]$ numerically, as $(X_{\mathrm{i}} = X, Y_{\mathrm{i}})$.

Convert $(X_{\mathrm{i}}, Y_{\mathrm{i}})$ to $(X_{\mathrm{c}}, Y_{\mathrm{c}})$ using (2.33a) and (2.33b) respectively.

end for

return $(X_{\mathrm{c}}, Y_{\mathrm{c}})$

The $(X_{\mathrm{c}}, Y_{\mathrm{c}})$ coordinates determine the equi-average-rate boundaries for (2.20). In the following section we present the simulation results for the presented algorithm for both (2.19) and (2.20), as well as the validation of our approach by applying a point-to-point mode selection in the area of the network.

2.6 Numerical Results

In this section first we present the mode selection map of the D2D enabled network presented in Fig. 2.1 using our solution in Section 2.5. Then to validate the results from that approach, we apply a point-to-point mode selection map derivation and compare both results. We assume that UEs and eNB have fixed power and use a single antenna for their communication. Moreover we assume that all communication channels between the involved entities experience shadowing and fast fading.

The parameters of our simulation are summarized in Table 2.1.

Table 2.1 Simulation parameters for mode selection map derivation in fading channel

Parameter	**Value**
Cell radius (r_C)	3 km
UE_s's position ((X_s,Y_s))	(250,1500)
UE_d's position ((X_d,Y_d))	(300,1000)
UE's maximum power (P_c, P_s, P_d)	23dBm
eNB's maximum power (P_e)	46dBm
Pathloss exponent (α)	3 (for urban areas)
Shadowing variance (σ_s^2)	7
Fast fading variance (σ_z^2)	1

Using the algorithm presented in Section 2.5, the results are shown in Fig. 2.4. As can be seen, the network area is divided into disjoint regions by equi-average-rate boundaries. These curves show the set of points for which equations (2.19) and (2.20) are satisfied respectively. If UE_c moves outside the solid curve the reuse mode will give higher throughput than the dedicated mode for transmission between D2D UEs. If UE_c moves inside the solid curve, the dedicated mode would have higher throughput than the reuse mode. If UE_c moves outside the dashed curve, the reuse mode will give higher throughput than the cellular mode. However, if it moves inside the dashed curve, the cellular mode will have higher throughput than the reuse mode.

To verify the results achieved from the algorithm presented in the previous section, we use a point-to-point mode selection map derivation method. We divide the area of the network into a matrix of points where the vertical and horizontal distances between two neighbor points is 25m. We place the UE_c at each point and generate S_{ij} and z_{ij} randomly based on their probability density function (pdf) which determined by their variance presented in Table 2.1. Then we use (2.1) to calculate h_{ij}s. Then using (2.10)–(2.12) and (2.25)–(2.30) we calculate the overall throughput of the network for different modes. This procedure is executed 10^6 times and for each mode we average over all resulted throughputs. Finally, the mode that gives the

highest average overall throughput is assigned to that specific point. For simplicity we assign red, yellow, and green for reuse, dedicated, and cellular modes respectively. We apply this procedure for all the points in the area of the network. The results of this point-to-point mode selection map derivation method are shown in Fig. 2.5.

Comparing the results achieved from the point-to-point map derivation in Fig. 2.5a and 2.5b with the simulation results of the proposed map derivation in Fig. 2.4, we realize that the boundaries between the disjoint regions in 2.5a and 2.5b, matches the solid and dashed curves respectively which represent $\mathbb{E}[R_{\mathrm{R}}] = \mathbb{E}[R_{\mathrm{D}}]$ and $\mathbb{E}[R_{\mathrm{R}}] = \mathbb{E}[R_{\mathrm{C}}]$ respectively. This confirms that our presented algorithm in Section 2.5 generates valid mode selection map boundaries.

2.7 Conclusion

In this paper, we propose a solution approach to find the mode selection map of a single cell D2D enabled 5G network over fading channels consisting of two D2D UEs, one cellular UE, and one eNB. While D2D UEs can select their TM among the reuse, dedicated, and cellular modes, the cellular UE communicates with eNB in UL. We show that there are disjoint regions in the network where if a moving UE stays inside that region, the TM mode between D2D UEs will not change. First we find average throughput of communication channels for all three modes. These functions are dependent on the transmission power and location of entities, noise power, and standard deviation of fading and shadowing variables. Our solution to derive the mode selection map boundaries using these functions is summarized as an algorithm. We use the results from this solution to find the map boundaries for a specific network presented in this work. To verify the operation of the proposed algorithm, we propose a point-to-point mode selection map derivation to find the map of the network. We realized that the boundaries defined by these maps matches the boundaries derived using the proposed algorithm. Although the fast fading and shadowing effect causes changes in communication channels, their statistics remains unchanged. Therefore, the resulting map is constant, in spite of channel fluctuations and it can be a reliable source for applications such as mode selection, resource allocation, mobility management and handover.

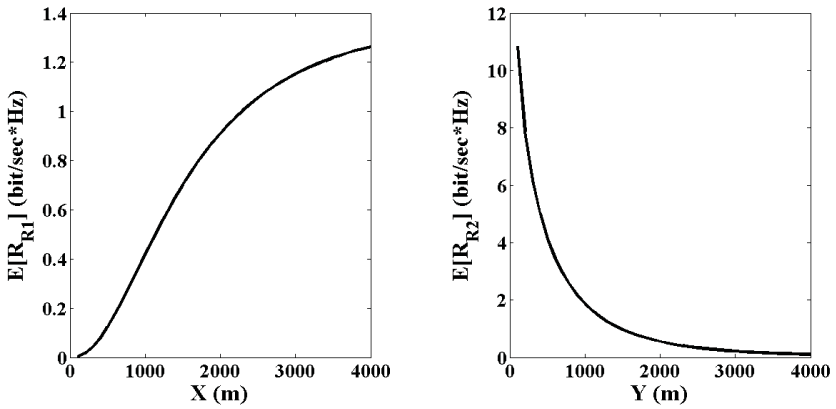

a) UE_s-UE_d throughput in reuse mode

b) UE_c-eNB throughput in reuse mode

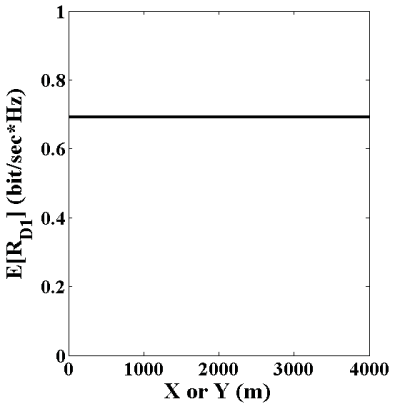

c) UE_s-UE_d throughput in dedicated mode

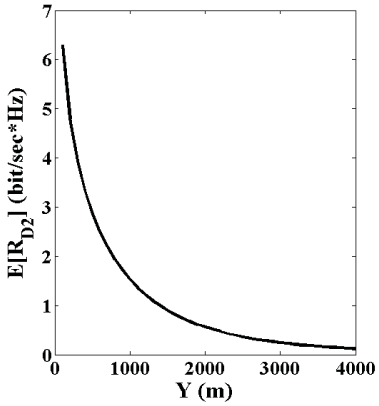

d) UE_c-eNB throughput in dedicated mode

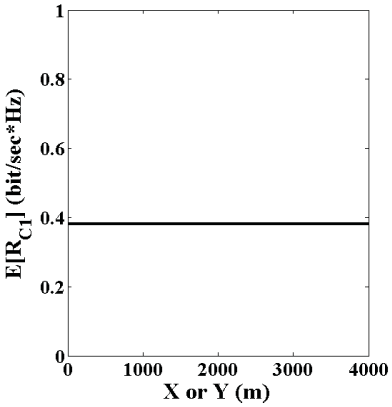

e) UE_s-eNB-UE_d throughput in cellular mode

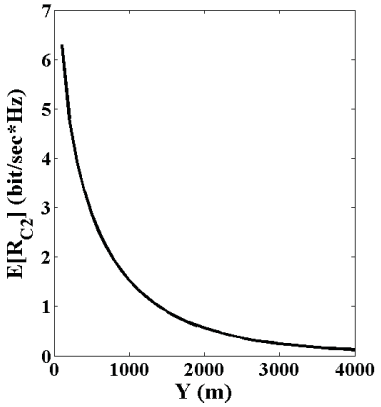

f) UE_c-eNB throughput in cellular mode

Figure 2.3 Different channels' throughput for reuse, dedicated, and cellular modes.

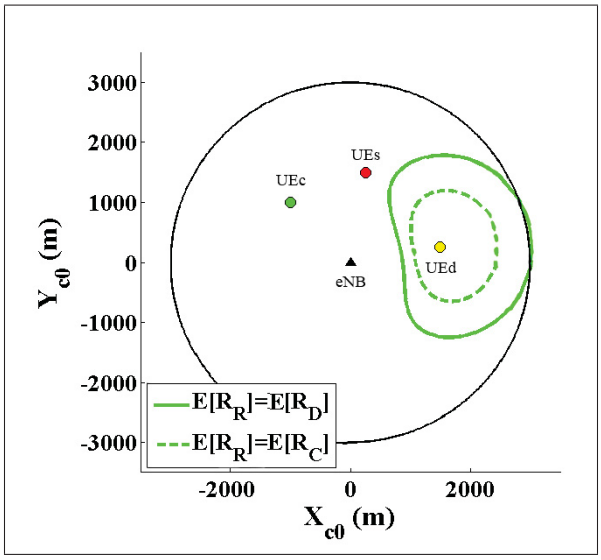

Figure 2.4 Mode selection map boundaries derived from the algorithm presented in Section 2.5 when UE_c moves and the communication channels experience fast fading and shadowing.

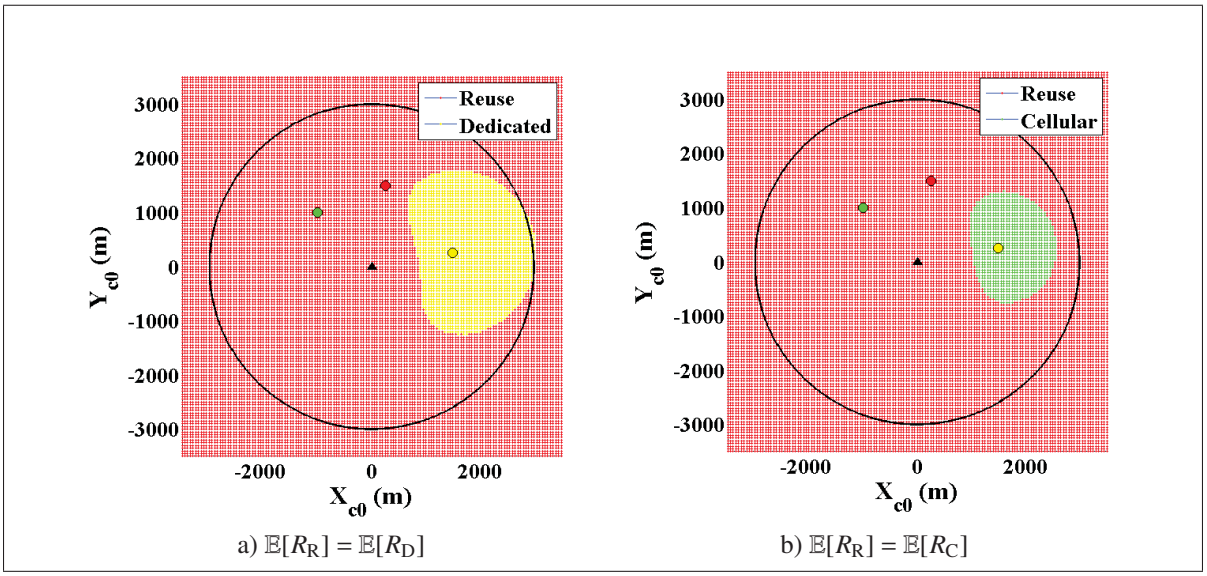

a) $\mathbb{E}[R_R] = \mathbb{E}[R_D]$ b) $\mathbb{E}[R_R] = \mathbb{E}[R_C]$

Figure 2.5 Mode selection map derived from point-to-point mode selection when UE_c moves and the communication channels experience fast fading and shadowing.

CHAPTER 3

VERTICAL HANDOVER IN D2D ENABLED 5G NETWORKS BASED ON MODE SELECTION MAP

Armin Morattab[1], Zbigniew Dziong[1], Kazem Sohraby[2]

[1] Department of Electrical Engineering, École de Technologie Supérieure,
1100 Notre-Dame Ouest, Montreal, Quebec, Canada, H3C 1K3
[2] Department of Electrical and Computer Engineering, South Dakota School of Mines & Technology, Rapid City, SD 57701, USA
& an Adjunct in Computer Science Department, Sand Diego State University, USA

Article submitted for review in January 2017.

Abstract

As one of the promising features of 5G networks, Device-to-Device (D2D) communication, enables direct transmission between D2D User Equipment (UE). In addition to the traditional cellular transmission mode (TM), using D2D, UEs can select also between the reuse and dedicated modes. The selection criterion which is used most of the time is the overall throughput of the network. That is the mode which results in the highest overall throughput is selected. In this paper, a simple network with two D2D enabled UEs and one cellular UE in transmission with an evolved Node-B (eNB) in uplink (UL) is considered. It is assumed that the cellular UE can move in the network while the D2D UEs are static. For such a network, using our previous results to derive the mode selection map, we analytically determine mobility measurement variables to be used by our proposed vertical handover algorithm. We also analytically calculate handover rate and sojourn time in order to analyze the performance of the handover algorithm.

Introduction

The recent huge growth in the number of mobile devices and their demand for data has created scarcity for bandwidth on the available frequency spectrum. Relying solely on the traditional cellular networking cannot provide the ever increasing number of users with an acceptable

Quality-of-Service (QoS). Therefore in the last decade providers and industrial telecommunication companies have developed new techniques and designs, such as cognitive radio (Mitola and Maguire, 1999; Liang *et al.*, 2008), Femtocells (Chandrasekhar *et al.*, 2008; Claussen *et al.*, 2008), Device-to-Device (D2D) communications (Doppler *et al.*, 2009; Janis *et al.*, 2009; Doppler *et al.*, 2011, 2010), etc., to satisfy their costumers' demand.

D2D communication has recently attracted significant attention from both industry and academia, mainly due to its unique advantages to offload cellular traffic, improved system throughput, higher energy efficiency and robustness to infrastructure failures (Asadi *et al.*, 2014; Mumtaz and Rodriguez, 2014; Song *et al.*, 2015; Panagopoulos, 2015).

In D2D communication, UEs are enabled to communicate with each other using three different modes: the reuse, dedicated , and cellular modes. In the reuse and dedicated modes, the UEs directly connect to each other while in the cellular mode the transmission between two UEs is through the evolved Node-B (eNB). In the reuse mode the same frequency resource is reused by both D2D UEs and other cellular transmission in the network, which causes interference at the receivers. However, in the dedicated and cellular modes different resources are dedicated to each D2D and cellular transmission, hence no interference appears at receivers. At the beginning of transmission, D2D UEs would select a single mode (Doppler *et al.*, 2010; Liu *et al.*, 2012c; Song *et al.*, 2015; Feng *et al.*, 2015; Panagopoulos, 2015; Wang and Tang, 2016; Huang *et al.*, 2016) or mixed modes (Feng *et al.*, 2015; Tang and Ding, 2016) to find the best policy for their transmission.

The UEs report their measurements to the eNB periodically, on time based, movement based, or distance based (Akyildiz *et al.*, 1999) options. Relying on this information a specific mode is selected. Based on the throughput maximization objective and due to mobility of UEs, the TM might have to change. Switching from one TM to another, when the moving UE remains inside one cell, is called vertical handover (Lin *et al.*, 2013; Raghothaman *et al.*, 2013; Chen *et al.*, 2015).

It has been shown that in the traditional cellular networks, the distance based method which performs a location update by reporting the UEs' locations when distance from the cell where it performed the last location update, exceeds a predefined value, results in the best performance for the handover mechanism comparing to the time based and movement based methods (Bar-Noy *et al.*, 1994). Without loss of generality the results of this work will be applied to the vertical mobility management mechanism for D2D enabled 5G networks. Thus we adopt the distance based location update as the candidate for our application.

We presented an analytical approach in (Morattab *et al.*, 2016) that defines the regions in the network that if the moving UE remains in those regions, its current TM can be kept. The set collection of such regions together with the border between them is defined as the mode selection map of the network. We further propose a handover algorithm based on this map and an analytical framework to find the tangent points, perpendicular points, and intersection points to the map. The results are applied to find the distance from the map and critical direction set which is defined as the set of all possible directions that if the moving UE takes, it will intersect with the boundaries of the map. Our proposed algorithm, uses this distance variable together with the direction of movement, to decide the best time to start the vertical handover procedure. The critical direction set is introduced as a useful variable used to analytically determine two performance metrics in order to analyze the efficiency of the proposed algorithm.

3.1 Related Works

The idea of having a mode selection map was implicitly discussed for the first time in (Doppler *et al.*, 2010). There a mode selection procedure in a single cell and multi-cell environments was proposed. The map is derived numerically by optimizing all possible TMs and selecting the one that results in the highest throughput for the locations of the cellular UE. In our previous work, (Morattab *et al.*, 2015), we extended the mode selection procedure in (Doppler *et al.*, 2010) assuming the UEs and eNB utilize Multiple-Input-Multiple-Output (MIMO) precoding. We presented a method to optimally design MIMO precoders and decoders at each transmitter and receiver respectively, to maximize overall throughput for different TMs. Our results in that

work shows higher gain and efficiency compared to (Doppler *et al.*, 2010). Derivation of the mode selection map of the network using the same point-to-point techniques shows that using MIMO, a larger area than SISO can be covered using dedicated and reuse modes.

The mode selection maps in (Doppler *et al.*, 2010; Morattab *et al.*, 2015) are derived numerically by applying a point-to-point procedure which is generally imprecise, complex, time consuming, and inefficient. Using such methods consumes large execution time and systems memory. Since, such methods are point based, the precision of the resulting map is a function of the distance between two consecutive points where mode selection algorithm is applied.

The derivation of the mode selection map in this work is based on methods in (Morattab *et al.*, 2016) where for the case of moving cellular UEs with fixed D2D UEs an analytical approach to find the mode selection map is developed. The methods in this paper provide implicit functions for the derivation of the mode selection map. Therefore, it draws precise borders of different regions that a specific mode is dedicated, with smaller execution time.

One of the main issues in D2D enabled networks, is how to design a handover scheme that could maintain the QoS of a connection between two D2D UEs and execute TM change in a seamless way. Previous research was done in recent years to study this issue in different applications and scenarios (Raghothaman *et al.*, 2013; Yilmaz *et al.*, 2014; Chen *et al.*, 2015; Orsino *et al.*, 2015; Jarray and Giovanidis, 2016; Xu *et al.*, 2016).

In (Raghothaman *et al.*, 2013), the authors present protocols to extend the 3GPP LTE-Advanced (LTE-A) system to incorporate D2D communication, including establishing and maintaining a D2D call and procedures for efficient mobility between a traditional the cellular mode and a D2D mode of operation within one cell. This work only provides a time sequence procedure for the handover mechanism without presenting a specific decision criteria. Moreover it is not clear whether the direct D2D is for the reuse or the dedicated mode.

In (Yilmaz *et al.*, 2014), a handover mechanism based on the received signal strength (RSS) which is able to minimize the end-to-end latency and signaling overhead for the communicating

D2D UEs is developed. The authors in (Chen *et al.*, 2015), provide the same handover scenario as in (Yilmaz *et al.*, 2014), however unlike the previous work, several decision criteria were taken into account to find the best time to start the handover. The proposed handover scheme in (Yilmaz *et al.*, 2014; Chen *et al.*, 2015) do not provide performance metrics for their algorithm. In (Orsino *et al.*, 2015) a handover scheme, where D2D connectivity helps to improve the migration of users across different BSs to enhance the overall link quality experienced by the UEs is presented. Like (Yilmaz *et al.*, 2014; Chen *et al.*, 2015) the handover is for the case when D2D UEs move from one cell to other cells. The mechanism presented in this work is able to efficiently offer the attractive energy efficiency, data rate, and packet delivery ratio benefits. Moreover performance metrics of their solution by utilizing the tools from stochastic geometry are derived which is an advantage over (Yilmaz *et al.*, 2014; Chen *et al.*, 2015).

In (Jarray and Giovanidis, 2016), the performance of caching in D2D networks for different degrees of node mobility is studied. Devices establish connection with transmitters that have the desired content cached, however due to the mobility the link quality between receivers and transmitters is affected which may result in a connection drop. This work does not propose a handover mechanism and only studies the performance of the network while UEs move.

This paper is based on the recent work in (Xu *et al.*, 2016), that is the theoretical analysis of D2D mode selection with user mobility. Although (Xu *et al.*, 2016) a mode selection map is not derived, the authors define a region where its border is computed by equating the RSS of the cellular and reuse modes. In that paper TM between the D2D UEs is changed whenever one of the D2D UEs exits a specific region which has been defined by RSS. Although the authors presented an equation to reach the equi-RSS boundaries, no solution is proposed to derive the mode selection map. Only a circular approximation of the equation is applied. Also, the dedicated mode is not considered in problem modeling and calculations.

3.2 Contributions

When the cellular UE moves, depending on the objective function to be maximized, the selected TM between the D2D UEs might not remain the optimal TM. The reason is usually due to the change in the amount of interference that cellular UE can cause to the receiving D2D UE, and vice versa, or change in transmission power, noise, or channel characteristics. To ensure that the UEs continue in an appropriate mode, a vertical handover needs to be applied. Relying on the mode selection map derived in (Morattab *et al.*, 2016), in this work, we develop a distance based vertical handover mechanism that takes into account the direction of the movement. To evaluate the performance of our algorithm we analytically determine the handover rate and sojourn time using the methods proposed in (Lin *et al.*, 2013; Xu *et al.*, 2016).

The contributions of this paper are summarized as follows:

- A new mobility management and vertical handover technique is proposed based on the distance from the mode selection map and the direction of the moving cellular UE;
- The proposed vertical handover handles mode transition to the reuse, dedicated, and cellular modes for the transmission between the D2D UEs;
- The moving cellular UE may cause the mode change for the D2D UEs;
- An analytical approach for determining the distance from the map, as the decision variable of the handover algorithm, and critical direction set is presented;
- Analytical derivation of handover rate and sojourn time as the performance metrics of the handover mechanism.

The remainder of this paper is as follows: In Section 3.3 the models for transmission (Section 3.3.1) and also mobility of the cellular UE (Section 3.3.2) are introduced. The problem formulation is presented in Section 3.4. Section 3.4.1 presents mode selection map and formulation of perpendicular points, tangent points, and intersection points from the location of the moving cellular UE. Moreover in Section 3.4.2 two performance metrics of the handover scheme, i.e. handover rate (Section 3.4.2.1) and sojourn time (Section 3.4.2.2) are introduced. In Section 3.5 we present our analytical approach to reach the tangent points and perpendicular

points (Section 3.5.1) as well as the formulation of the handover rate (Section 3.5.2) and the sojourn time (Section 3.5.3) for our specific D2D network. Our vertical handover algorithm is presented in Section 3.6. Section 3.7 presents to our simulation results for mobility metrics and performance of the proposed handover algorithm. Finally, we give our conclusions in Section 3.8.

3.3 System Model

In this section we introduce a model for the data D2D enabled cellular network. Then we discuss the mobility model used to estimate the behavior of the moving cellular UE.

3.3.1 Network Model

In this paper, we use the single cell D2D enabled cellular network model first developed in (Morattab *et al.*, 2016). As shown in Fig. 3.1, the model consists of a pair of D2D enabled UEs, a cellular UE, and a base station in the center of the cell, which are denoted as UE_s, UE_d, UE_c, and eNB respectively. While the communication from UE_s to UE_d can be in the reuse, dedicated, and cellular modes, UE_c operates in cellular mode in UL. It is also assumed that all entities in the network are equipped with a single antenna.

For simplicity a simple path-loss channel model, with line of sight (LoS) communication between the entities is considered. That is, the fading effect is not taken into account.

We assume that, in the reuse mode, the resources for UE_s-UE_d transmission are shared with the UE_c-eNB transmission. Therefore, each of the receivers in the network will be affected by the interference from the transmitters as well as the background noise. The interference channel is shown in Fig. 3.1 as red dotted lines. However, when the D2D UE are in the dedicated or cellular modes, half of the resources are assigned to the D2D UE, and the rest is assigned to UE_c-eNB transmission, and hence there will be no interference at the receivers.

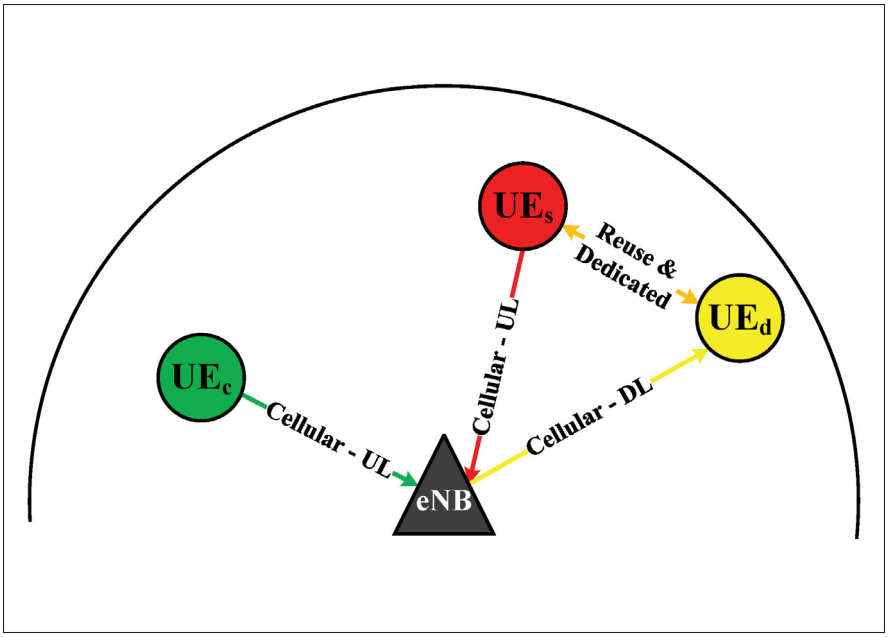

Figure 3.1 Simulation results for the network.

Interested readers refer to our previous paper in (Morattab *et al.*, 2016), to study the details of the transmit and receive models we used here.

3.3.2 Mobility Model

The mobility model we use in this paper is based on the Random Way Point (RWP) model in (Lin *et al.*, 2013) in which the moving entity randomly shifts between two points called waypoints. At each waypoint the mobile node chooses 1) a random direction uniformly distributed in the range [0,2π], 2) a transition length from some distribution, and 3) velocity from some distribution. The node may have a random pause time at each waypoint.

3.4 Problem Formulation

As discussed earlier, in order for a handover process to start, it relies on the value of specific decision variables that are computed based on the measurements in the network. In this section we formulate the decision variables to be used by the handover mechanism. These decision variables are: 1) distance form the mode selection map, 2) the critical direction set.

The distance variable, is the distance of the moving UE_c from the mode selection map and it is computed as the minimum of the set of all perpendicular distances from UE_c's location to the map as it is shown in Fig. 3.2a. This variable can be calculated by determining the tangent lines to the boundaries of the map from the location of the UE_c as is discussed later in this work. Such tangent lines are shown in Fig. 3.2b for the sample network.

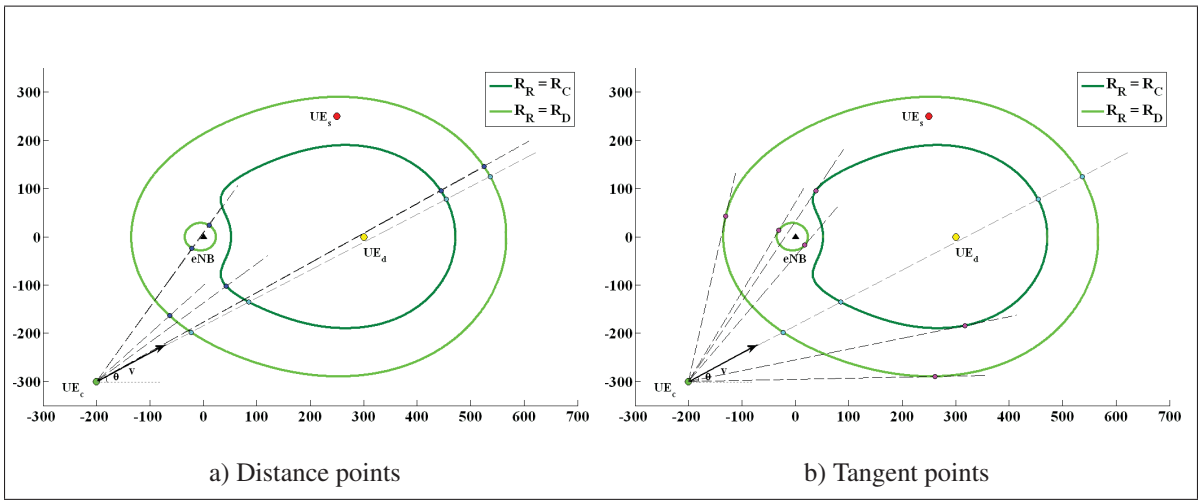

a) Distance points b) Tangent points

Figure 3.2 Distance and tangent points from the moving UE_c to the mode selection map boundaries

Moreover, as performance metrics of the handover for the purpose of analysis, we introduce handover rate and sojourn time.

3.4.1 Decision Variables

In this paper, it is assumed that UE_c moves, while UE_s and UE_d are static as discussed in (Morattab *et al.*, 2016). In this case the network is as shown in Fig. 3.3 where X and Y are distance variables that their value changes by UE_c's movement.

The relationship that define the mode selection map of the network, are derived from the overall throughput of the network as the total throughput in for the reuse, dedicated, and cellular modes, denoted as R_C, R_D, and R_C respectively, where:

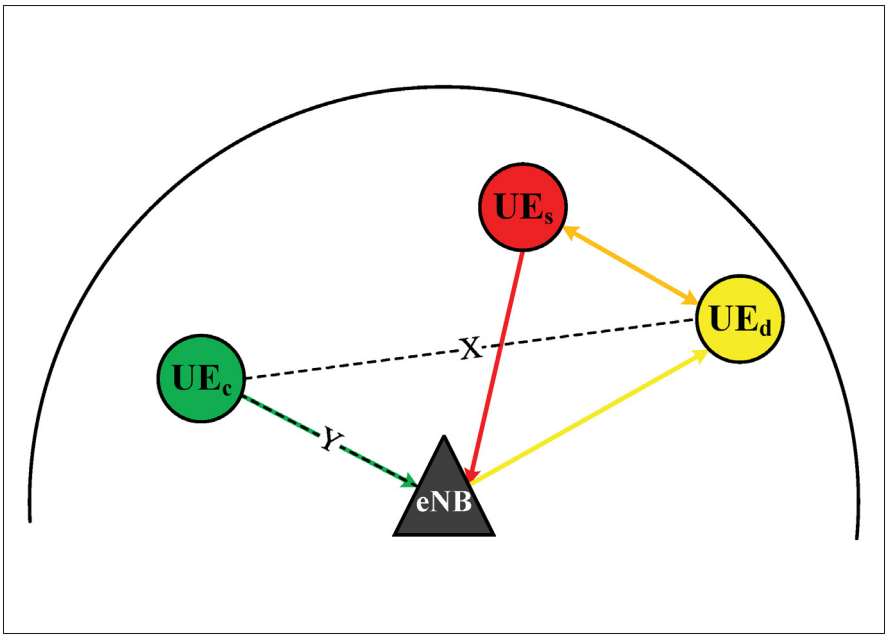

Figure 3.3 UE$_c$ moves in the network

$$R_R = \log_2\left(\left(1+\frac{a_1}{1+a_2 x}\right)(1+a_3 y)\right) \tag{3.1}$$

$$R_D = \frac{1}{2}\log_2\left(a_1'(1+a_4 y)\right) \tag{3.2}$$

$$R_C = \frac{1}{4}\log_2(a_5) + \frac{1}{2}\log_2(1+a_4 y) \tag{3.3}$$

and:

$$a_1 = \frac{KP_s}{d_{sd}^{\alpha} N_0} \tag{3.4a}$$

$$a_1' = 1 + a_1 \tag{3.4b}$$

$$a_2 = \frac{KP_c}{N_0} \tag{3.4c}$$

$$a_3 = \frac{KP_c}{d_{ce}\left(\frac{KP_s}{d_{se}^{\alpha}} + N_0\right)} \tag{3.4d}$$

$$a_4 = \frac{KP_c}{N_0} \tag{3.4e}$$

$$a_5 = \min\left(1 + \frac{KP_s}{d_{se}^{\alpha} N_0}, 1 + \frac{KP_e}{d_{ed}^{\alpha} N_0}\right) \tag{3.4f}$$

and x and y are defined as follows:

$$x = \frac{1}{X^{\alpha}} \tag{3.5a}$$

$$y = \frac{1}{Y^{\alpha}} \tag{3.5b}$$

In the above equations, d_{ij} is the distance between transmitter i and receiver j and P_{i} is the transmitter i's power, where i = s, c, e, and j = e, d. The subscripts s, c, d, and e describe the type of entity, such as $\mathrm{UE_s}$, $\mathrm{UE_c}$, and $\mathrm{UE_d}$, and eNB respectively. N_0 denotes the spectral density of the Gaussian noise, K is a unitless constant that depends on the antennas characteristics, and α is the path loss exponent.

It is shown in (Morattab *et al.*, 2016), that when $R_D = R_C$ there is no solution. Moreover, the $R_R = R_C$ equation is the general form of $R_R = R_D$ that the solution to the latter can be obtained by a simple substitution of the constants. Therefore, in the subsequent discussion we only develop results for the case $R_R = R_C$. Referring to (Morattab *et al.*, 2016), this relation is simplified as follows:

$$f(x,y) = a(x)\, y^2 + b(x)\, y + c(x) = 0 \tag{3.6}$$

where:

$$a(x) = a_3^2 \left(a_1' + a_2 x\right)^2 \tag{3.7a}$$

$$b(x) = 2a_3\left(a_1' + a_2x\right)^2 - a_4\sqrt{a_5}\,(1+a_2x)^2 \tag{3.7b}$$

$$c(x) = \left(a_1' + a_2x\right)^2 - \sqrt{a_5}\,(1+a_2x)^2 \tag{3.7c}$$

For each solution pair (x,y) of (3.6), we use (3.5a) and (3.5b) to find corresponding X and y distance variables. Then the following equations are used to convert X and Y to (X_c,Y_c) coordinates and obtain the mode selection map:

$$X^2 = (X_c - X_d)^2 + (Y_c - Y_d)^2 \tag{3.8a}$$

$$Y^2 = X_c^2 + Y_c^2; \tag{3.8b}$$

where (X_d,Y_d) are the coordinates of the static UE_d.

Since the mode selection map is derived using the above equations, we develop our formulations in order to find the distance from the map as well as the critical direction set. As shown in Fig. 3.2, both subfigures include a cellular user, i.e. UE_c, which moves in the network in direction of θ with velocity of v as well as the mode selection map of a sample network. The map consists of two equi-rate borders resulted by solving $R_R = R_C$ and $R_R = R_D$ equations respectively. If UE_c moves and specific conditions are satisfied, a vertical handover is needed for transmission between UE_s and UE_d in order to guarantee the maximum overall throughput. To determine these conditions, the distance from map boundaries and the direction of the movement are considered as the decision variables. The handover process is executed only if the distance from the map is less than a specified threshold and if the moving direction of UE_c belongs to the set of critical directions.

For both distance variable and critical direction set, we need to determine the slope of the tangent line to the map, $\frac{dY_c}{dX_c}$, where (X_c,Y_c) are the coordinates of a point on the map's boundary.

If (X_i, Y_i) is the coordinate of the moving UE_c, then the tangent line from this point to the map boundary is:

$$Y_c = \frac{dY_c}{dX_c}(X_c - X_i) + Y_i \tag{3.9}$$

and the perpendicular line from is:

$$Y_c = \frac{-1}{\frac{dY_c}{dX_c}}(X_c - X_i) + Y_i \tag{3.10}$$

(3.9) and (3.10) are used to find the critical direction set and distance from map. The solution to the above equations determines tangent points $\{(X_{tn}, Y_{tn}) | n = 1, \cdots, N_t\}$ and perpendicular points $\{(X_{pn}, Y_{pn}) | n = 1, \cdots, N_p\}$ respectively, where N_t and N_p denote the maximum number of possible tangent and perpendicular points from (X_i, Y_i) to the mode selection map respectively. The perpendicular points are shown in Fig. 3.2a as blue dots. The magenta points in Fig. 3.2b denote the tangent points to the mode selection map, and the cyan points represent the intersection points of the moving UE_c with the map, if it goes in the direction of θ.

The set of perpendicular distance variables are denoted as $H = \{d_{pn} | n = 1, \cdots, N_p\}$ where d_{pn} is computed as follows:

$$d_{pn} = \sqrt{\left(X_{pn} - X_i\right)^2 + \left(Y_{pn} - Y_i\right)^2} \tag{3.11}$$

The distance of the moving UE_c from the map is as follows:

$$d_p = \min(H) \tag{3.12}$$

Now that we calculated the distance from the map, as the decision variable for the handover algorithm, we follow our calculations to present some useful variables which will be used in the next section to derive the performance metrics of the handover algorithm.

We find the set of tangent directions denoted as $\{\theta_{tn} | n = 1, \cdots, N_t\}$ as follows:

$$\theta_{tn} = \begin{cases} \tan^{-1}(\frac{Y_{tn} - Y_i}{X_{tn} - X_i}) + \pi, \text{if } X_{tn} < X_i, Y_{tn} > Y_i & \text{(3.13a)} \\ \tan^{-1}(\frac{Y_{tn} - Y_i}{X_{tn} - X_i}) \quad , \text{if } X_{tn} > X_i & \text{(3.13b)} \\ \tan^{-1}(\frac{Y_{tn} - Y_i}{X_{tn} - X_i}) - \pi, \text{if } X_{tn} < X_i, Y_{tn} < Y_i & \text{(3.13c)} \end{cases}$$

We define the following extended set:

$$\Phi = \{-\pi, \pi\} \cup \{\theta_{tn} | n = 1, \cdots, N_t\} \tag{3.14}$$

We denote the elements of the ordered set Φ as ϕ_n where $n = 1, \cdots, N_t + 2$. Then the set of critical directions, which is also assumed to be an ordered set, is computed as follows:

$$\begin{aligned} \Psi = \{\psi_n = [\phi_k, \phi_{k+1}] \text{ for } k = 1, \cdots, N_t + 1 | \text{ if } \theta \in \psi_n, \\ \Rightarrow \text{ UE}_\text{c} \text{ intersects whith the map}\} \end{aligned} \tag{3.15}$$

The elements of Ψ are denoted as ψ_n for $n = 1, \cdots, N_d = |\Psi|$ as follows:

$$\psi_n = [\alpha_n, \beta_n] \tag{3.16}$$

Next, we need to find the intersection points from (X_i,Y_i) and the mode selection map in the direction of movement. This will be used later in the next section in order to compute performance metrics of the mobility management method.

If we assume that $\mathrm{UE_c}$ moves in the direction of θ, the following equation leads to the intersection points:

$$Y_c = \tan(\theta)(X_c - X_i) + Y_i \tag{3.17}$$

Where (Xc,Y_c) are coordinates of a point on the mode selection map. Solution of this equation is obtained by substituting the above Y_c, as a function of X_c, with the Y_c in the mode selection map function derived earlier, and then solving the resulting single variable nonlinear equation. The intersection points are denoted as $\{(X_{cn},Y_{cn})|n = 1,\cdots,N_c\}$, where N_c is the maximum number of intersections. The set of distance values is $\{r_{cn}|n = 1,\cdots,N_c\}$, which r_{cn} is the distance between (X_i,Y_i) to (X_{cn},Y_{cn}):

$$r_{cn} = \sqrt{(X_{cn} - X_i)^2 + (Y_{cn} - Y_i)^2} \tag{3.18}$$

3.4.2 Performance Metrics

Using the RWP mobility model in (Lin *et al.*, 2013), the movement trace of the $\mathrm{UE_c}$ can be described by an infinite sequence of quadruples: $\{((X_i,Y_i),(X_{i+1},Y_{i+1}),V_i,S_i)\}_{i=\mathcal{N}}$, where i is the i-th movement period. During the i-th movement period, (X_i,Y_i) represents the starting waypoint, (X_{i+1},Y_{i+1}) the target waypoint, V_i the velocity, and S_i the pause time at waypoint (X_{i+1},Y_{i+1}). Given the current waypoint (X_i,Y_i), the next waypoint (X_{i+1},Y_{i+1}) is such that the angle between the vector $(X_{i+1},Y_{i+1}) - (X_i,Y_i)$ and the abscissa, i.e. θ_i, is uniformly distributed

in $[0,2\pi]$ and the transition length $L_i = ||(X_{i+1},Y_{i+1}) - (X_i,Y_i)||$ is nonnegative. The selection of waypoint is independent and identical for each movement period.

The transition lengths $\{L_1,L_2,...\}$ are chosen to be independent and identically distributed (i.i.d.) with Cumulative Distribution Function (CDF):

$$P(L <= l) = 1 - exp\left(-\lambda\pi l^2\right) \tag{3.19}$$

The transition lengths are Rayleigh distributed with density λ. Velocities V_i are i.i.d. with distribution $P_V(.)$. Pause times S_i are also i.i.d. with distribution $P_S(.)$. It can be shown that the expected value of the transition length is:

$$\mathbb{E}[L] = \frac{1}{2\sqrt{\lambda}} \tag{3.20}$$

The period time, i.e. T_p, is defined as the sum of transition time, i.e. T, and the pause time, i.e. S as follows:

$$T_p = T + S \tag{3.21}$$

The transition time denotes the time a node spends during the movement between two successive waypoints that is formulated as follows:

$$T = L/V \tag{3.22}$$

where L and V denote transition length and velocity random variables respectively.

Two important metrics to evaluate the performance of a mobility management technique are handover rate and the sojourn time which are described as follows:

3.4.2.1 Handover Rate

The handover rate is defined as the ratio of the expected number of required handovers for the D2D UEs when UE_c moves between two waypoints during one movement period, over the expected value of the period time. That is:

$$R_H = \frac{\mathbb{E}[N]}{\mathbb{E}[T_p]} \tag{3.23}$$

Where random variable N is the number of handovers, and T_p represents the period time random variable.

The expected number of handovers during a one movement period could be calculated as:

$$\mathbb{E}[N] = \sum_{n=1}^{\infty} n \int_{C_n} P\left(dA(r,\theta)\right) \tag{3.24}$$

where C_n is the area such that if UE_c enters and moves within one movement period, the D2D UEs will experience n handovers. $P\left(dA(r,\theta)\right)$ is the probability of the moving entity being in the area $dA(r,\theta)$ after one movement from the origin.

The expected value of period time can be computed by first determining $\mathbb{E}[T]$ and $\mathbb{E}[S]$.

3.4.2.2 Sojourn Time

Sojourn time is defined as the expected time duration that the mobile UE_c movement would not result in a TM change for the D2D UEs. Assuming that the mobile node does not have the

pause time with a constant velocity, i.e., $V \equiv v$, the sojourn time in any coverage area C_0 can be determined as:

$$S_T = \mathbb{E}[T]. \int_{C_0} P\left(dA(r,\theta)\right) \tag{3.25}$$

3.5 Solution

In this section we provide analytical solutions for the tangent and perpendicular points as well as the relationship for the handover rate and sojourn time as performance metrics.

3.5.1 Tangent and Perpendicular Points

As discussed earlier in Section 3.4.1, the mobility management technique is relying on the direction of the $\mathrm{UE_c}$'s movement and its distance from the mode selection map. We found the critical direction set in (3.15) as well as the perpendicular distance using (3.12). We computed these variables with the assumption that the tangent and perpendicular points are given. These can be be found using (3.9) and (3.10).

First we compute the derivatives of (3.8a) and (3.8b) with respect to X_c and simplify them as follows:

$$X\frac{dX}{dX_c} = (X_c - X_d) + (Y_c - Y_d)\frac{dY_c}{dX_c} \tag{3.26a}$$

$$Y\frac{dY}{dX_c} = X_c + Y_c\frac{dY_c}{dX_c} \tag{3.26b}$$

Dividing the equation (3.26b) by (3.26a) and simplifying:

Clicours.COM

$$\frac{\frac{dY}{dX_c}}{\frac{dX}{dX_c}} = \frac{X}{Y} \cdot \frac{X_c + Y_c \frac{dY_c}{dX_c}}{(X_c - X_d) + (Y_c - Y_d) \frac{dY_c}{dX_c}} \tag{3.27}$$

On the other hand:

$$\frac{dY}{dX_c} = \frac{dY}{dy} \cdot \frac{dy}{dx} \cdot \frac{dx}{dX} \cdot \frac{dX}{dX_c} \tag{3.28}$$

therefore:

$$\begin{aligned} \frac{\frac{dY}{dX_c}}{\frac{dX}{dX_c}} &= \frac{dY}{dy} \cdot \frac{dy}{dx} \cdot \frac{dx}{dX} \\ &= \frac{\frac{dY}{dy}}{\frac{dX}{dx}} \cdot \frac{dy}{dx} \end{aligned} \tag{3.29}$$

Differentiating (3.5a), (3.5b), and (3.6), we find $\frac{dY}{dy}$, $\frac{dX}{dx}$, and $\frac{dy}{dx}$ as follows:

$$\frac{dY}{dy} = -\frac{Y^{\alpha+1}}{\alpha} \tag{3.30a}$$

$$\frac{dX}{dx} = -\frac{X^{\alpha+1}}{\alpha} \tag{3.30b}$$

$$\frac{dy}{dx} = -\frac{a'(x)y^2 + b'(x)y + c'(x)}{2a(x)y + b(x)} \tag{3.30c}$$

where:

$$a'(x) = \frac{da(x)}{dx} = 2a_2 a_3^2 (a_1' + a_2 x) \tag{3.31a}$$

$$b'(x) = \frac{da(x)}{dx} = 4a_2a_3(a'_1 + a_2x) - 2a_2a_4\sqrt{a_5}(1 + a_2x) \tag{3.31b}$$

$$b'(x) = \frac{da(x)}{dx} = 2a_2(a'_1 + a_2x) - 2a_2\sqrt{a_5}(1 + a_2x) \tag{3.31c}$$

We simplify (3.29) using (3.30a) and (3.30b) as follows:

$$\begin{aligned} \frac{\frac{dY}{dX_c}}{\frac{dX}{dX_c}} &= \frac{Y^{\alpha+1}}{X^{\alpha+1}} \cdot \frac{dy}{dx} \\ &= \frac{Y}{X} \cdot \frac{x}{y} \cdot \frac{dy}{dx} \end{aligned} \tag{3.32}$$

For simplicity of presentation, in (3.32) and the subsequent calculations $\frac{dy}{dx}$ is not substitute with (3.30c).

Equating (3.27) and (3.32) results in:

$$\frac{X}{Y} \cdot \frac{X_c + Y_c \frac{dY_c}{dX_c}}{(X_c - X_d) + (Y_c - Y_d)\frac{dY_c}{dX_c}} = \frac{Y}{X} \cdot \frac{x}{y} \cdot \frac{dy}{dx} \tag{3.33}$$

$\frac{dY_c}{dX_c}$ can be determined using the above equation as follows:

$$\frac{dY_c}{dX_c} = -\frac{X_c - \frac{Y^2}{X^2} \cdot \frac{x}{y} \cdot \frac{dy}{dx} \cdot (X_c - X_d)}{Y_c - \frac{Y^2}{X^2} \cdot \frac{x}{y} \cdot \frac{dy}{dx} \cdot (Y_c - Y_d)} \tag{3.34}$$

Substituting $\frac{dY_c}{dX_c}$ from (3.34) in (3.9) and (3.10), results in the tangent and perpendicular points relationships respectively, as follows:

$$\frac{Y_c - Y_i}{X_c - X_i} = -\frac{X_c - \frac{Y^2}{X^2} \cdot \frac{x}{y} \cdot \frac{dy}{dx} \cdot (X_c - X_d)}{Y_c - \frac{Y^2}{X^2} \cdot \frac{x}{y} \cdot \frac{dy}{dx} \cdot (Y_c - Y_d)} \tag{3.35a}$$

$$\frac{Y_c - Y_i}{X_c - X_i} = \frac{Y_c - \frac{Y^2}{X^2}\cdot\frac{x}{y}\cdot\frac{dy}{dx}\cdot(Y_c - Y_d)}{X_c - \frac{Y^2}{X^2}\cdot\frac{x}{y}\cdot\frac{dy}{dx}\cdot(X_c - X_d)} \tag{3.35b}$$

Because of the non-linearity and irreversibility of the equations in (3.35a) and (3.35b) , we use a numerical method to find the tangent and perpendicular points, denoted as $\{(X_{tn},Y_{tn})|n = 1,\cdots,N_t\}$ and $\{(X_{pn},Y_{pn})|n = 1,\cdots,N_p\}$ respectively.

Having the tangent and perpendicular points, the distance from the map and critical direction variables can easily be determined using the formulas presented in Section 3.4.1.

3.5.2 Handover Rate

The general procedure to find the handover rate was presented in 3.4.2.1. In this part we present an analytical approach for finding the handover rate for D2D enabled network. As shown in (3.23), to calculate R_H, $\mathbb{E}[N]$ and $\mathbb{E}[T_p]$ should be determined first.

Based on mode selection map derived from $R_R = R_D$ and $R_R = R_C$, Fig. 3.4 shows the C_n zones with different colors. C_n defines the region where if $\mathrm{UE_c}$ moves from its current location to C_n, then TM for communication between the D2D UEs changes n times. We note that depending on the $\mathrm{UE_c}$'s location, the direction of movement, the transition length, and the mode selection map's shape, the number of handovers for D2D caused by $\mathrm{UE_c}$'s movement, is different. Fig. 3.4a and 3.4b show the map derived from $R_R = R_D$ and $R_R = R_C$ respectively, that the modes to be selected by D2D UEs in the former case is only between the reuse and dedicated modes while in the latter D2D UEs could select between the reuse and cellular modes.

As shown in Fig. 3.4a, as $\mathrm{UE_c}$, moves in the direction shown by the arrow, the number of handovers changes from one to four, depending on the transition length between two waypoints. However referring to Fig. 3.4b, the number of handovers changes from one to two. In order to determine C_n, we need to compute the intersection points of the moving $\mathrm{UE_c}$, as it moves from waypoint (X_i,Y_i) in the direction of θ, with the mode selection map shown for the two cases.

For example for Fig. 3.4a, the part of the line between the third and fourth intersection points, belongs to the C_3.

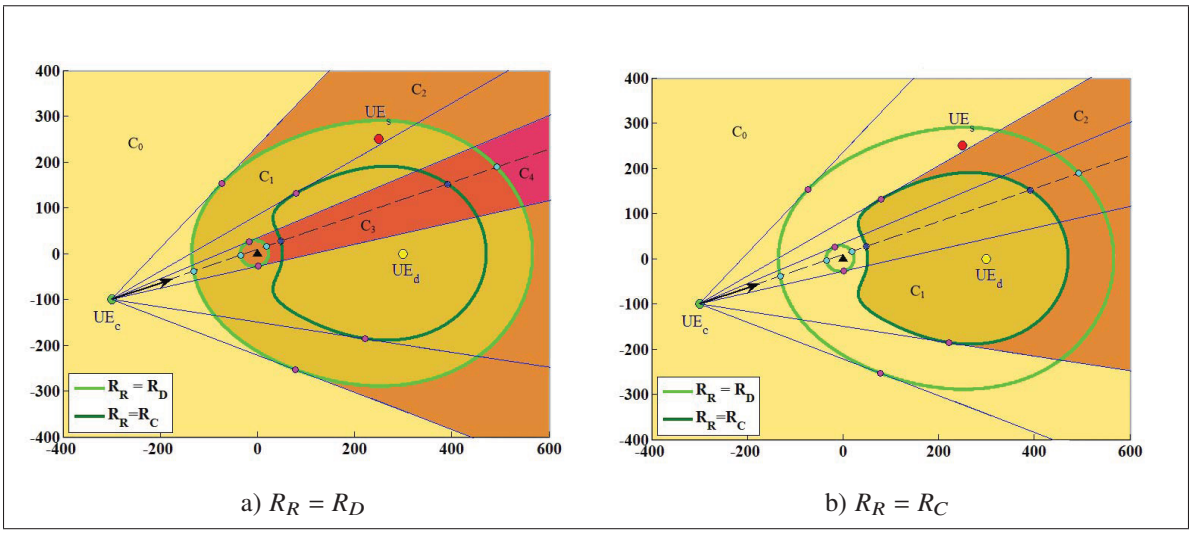

Figure 3.4 *n* handover regions

Determining the C_n zones analytically is complex, therefore we use the fact that for a specific direction of movement, i.e. θ, for UE_c located in waypoint (X_i,Y_i), depending on the transition length, l, in one movement period, the next waypoint could be located in any of C_ns. Knowing (X_i,Y_i) and θ, we can find the intersection points with the mode selection map using (3.17). The set of intersection points is $\{(X_{cn}(\theta),Y_{cn}(\theta))\}_{n=1,\cdots,N_c(\theta)}$, where $N_c(\theta)$ is the maximum number of intersections when UE_c moves in the direction of θ. Then using (3.18), we find $\{r_{cn}(\theta)\}_{n=1,\cdots,N_c(\theta)}$, i.e. the distance of intersection points from (X_i,Y_i). We assume that $r_{cn}(\theta)$s are ordered, that is for $n,m \in \{1,\cdots,N_c(\theta)\}$ if $n < m$ then $r_{cn}(\theta) < r_{cm}(\theta)$. The probability of UE_c, being in C_n, in one movement period in direction of θ is denoted as $P_{C_n}(\theta)$ and is calculated using (3.19) as follows:

$$P_{C_0}(\theta) = P(l < r_{c1}(\theta))$$

$$= 1 - exp\left(-\lambda\pi r_{c1}^2(\theta)\right) \tag{3.36a}$$

$$\underset{n=1,\cdots,N_c(\theta)-1}{P_{C_n}(\theta)} = P(r_{cn}(\theta) < l < r_{c(n+1)}(\theta))$$

$$= exp\left(-\lambda\pi r_{cn}^2(\theta)\right) - exp\left(-\lambda\pi r_{c(n+1)}^2(\theta)\right) \quad (3.36b)$$

$$P_{C_{N_c(\theta)}}(\theta) = P(r_{cN_c(\theta)}(\theta) < l)$$

$$= exp\left(-\lambda\pi r_{cN_c(\theta)}^2(\theta)\right) \quad (3.36c)$$

Using (3.36a)–(3.36c), the expected number of handovers for the movement from (X_i,Y_i) in the direction of θ, as shown in (3.24) is reformulated as:

$$\mathbb{E}[N_\theta] = \sum_{n=1}^{N_c(\theta)} n.P_{C_n}(\theta) \quad (3.37)$$

To compute the expected number of handovers for UE_c located in (X_i,Y_i) we determine $\mathbb{E}[N_\theta]$ over θ which is a random variable with uniform distribution over $[0,2\pi]$. Presenting a close form for $P_{C_0}(\theta)$, $P_{C_n}(\theta)$ for $n = 1,\cdots,N_c(\theta)-1$, and $P_{C_{N_c(\theta)}}(\theta)$ as a function of θ is very complex, since it first requires calculation of intersection points $\{(X_{tn}(\theta),Y_{tn}(\theta))|n = 1,\cdots,N_t(\theta)\}$, which can not be determined analytically. Therefore to find the expected number of handovers, we use discrete values of θ. We only apply the values of θ which if UE_c takes those values as the direction of movement, it will intersect with the mode selection map. In other words for $\theta \in \underset{n=1,\cdots,N_d}{\cup} \psi_n$, which ψ_n is defined in (3.16). The discrete value of θ is denoted as θ_{kl} and it is defined as:

$$\theta_{kl} = \alpha_l + k(\frac{\beta_l - \alpha_l}{K+1}), k = 1,\cdots,K \text{ and } l = 1,\cdots,N_d \quad (3.38)$$

where α_l and β_l are lower and upper bounds of ψ_n in (3.16), and K is denoted as the total number of discrete directions in each $\psi_l = [\alpha_l,\beta_l]$ interval.

It should be noted that for the values of $\theta \in \{[0,2\pi] \setminus \underset{n=1,\cdots,N_d}{\cup} \psi_n\}$, $\mathbb{E}[N_\theta] = 0$, since $\mathrm{UE_c}$ will not intersect with the mode selection map and $\underset{n=1,\cdots,N_c(\theta)}{P_{C_n}(\theta)} = 0$.

The following probabilities are used later for developing equations to find the expected number of hand-overs and sojourn time:

$$P(\theta \in \psi_n) = \frac{(\beta_n - \alpha_n)}{2\pi} \tag{3.39a}$$

$$\begin{aligned} P(\theta \in \{[0,2\pi] \setminus \underset{n=1,\cdots,N_d}{\cup} \psi_n\}) &= P(\theta \notin \underset{n=1,\cdots,N_d}{\cup} \psi_n\}) \\ &= 1 - \frac{\sum_{n=1}^{N_d} (\beta_n - \alpha_n)}{2\pi} \end{aligned} \tag{3.39b}$$

Finally the expected number of handovers for $\mathrm{UE_c}$ located in (X_i, Y_i) is determined as:

$$\begin{aligned} \mathbb{E}[N] &= \sum_{l=1}^{N_d} P(\theta \in \psi_l) . \sum_{k=1}^{K} P(\theta = \theta_{kl}) . \mathbb{E}[N_{\theta_{kl}}] \\ &= \sum_{l=1}^{N_d} \frac{(\beta_l - \alpha_l)}{2\pi} . \sum_{k=1}^{K} \frac{1}{K} . \sum_{n=1}^{N_c(\theta_{kl})} n . P_{C_n}(\theta_{kl}) \end{aligned} \tag{3.40}$$

where $\mathbb{E}[N_{\theta_{kl}}]$ is substituted by (3.37).

Another term that should be calculated to determine the handover rate, is the expected value of the time period as defined in (3.21). We assume that $S \equiv 0$. Using (3.20)–(3.22), we develop the following relations in order to find $\mathbb{E}[T_p]$:

$$\begin{aligned} \mathbb{E}[Tp] &= \mathbb{E}[T] \\ &= \mathbb{E}[L/V] \end{aligned}$$

$$= \mathbb{E}[L].\mathbb{E}[1/V]$$
$$= \frac{1}{2\sqrt{\lambda}} \int_{\mathcal{V}} \frac{1}{v} dP_V(v) \tag{3.41}$$

Assuming $\mathrm{UE_c}$, moves with a constant velocity, $V \equiv v_c$, (3.41) is simplified as follows:

$$\mathbb{E}[Tp] = \frac{1}{2v_c\sqrt{\lambda}} \tag{3.42}$$

Now using (3.40) and (3.41), we find the handover rate using (3.23).

We later perform a simulation for our test network presented in Fig. 3.3 to find the handover rate for specific locations of $\mathrm{UE_c}$.

3.5.3 Sojourn Time

To find the sojourn time as defined in Section 3.4.2.2, we use (3.25). The expected value of transition time, $\mathbb{E}[T]$ has already been determined in (3.41). However, the second term in (3.25) denotes the cumulative probability of $\mathrm{UE_c}$ moving from the first waypoint (X_i,Y_i) to the second waypoint without a handover. If we assume that $\mathrm{UE_c}$ moves in the direction of θ, this probability is equal to $P_{C_0}(\theta)$ as defined in (3.36a). The sojourn time in the direction of θ then is derived from (3.25) as follows:

$$S_{T\theta} = \mathbb{E}[T].P_{C_0}(\theta) \tag{3.43}$$

To compute the average sojourn time in (X_i,Y_i), we should find the expected value of $S_{T\theta}$ over all possible values of θ. For the direction of movement of $\theta \in \{[0,2\pi] \setminus \bigcup_{n=1,\cdots,N_d} \psi_n\}$, as ψ_n presented in (3.16), $\mathrm{UE_c}$ does not intersect with the mode selection map. Hence for these values of θ, we can substitute $r_{c1}(\theta) = \infty$ in (3.36a) for $P_{C_0}(\theta)$:

$$P_{C_0}(\theta|\theta \in \{[0,2\pi] \setminus \bigcup_{n=1,\cdots,N_d} \psi_n\}) = P(L < \infty)$$
$$= 1 \tag{3.44a}$$

For any θ that $\theta \in \bigcup_{n=1,\cdots,N_d} \psi_n$, there exists at least one intersection with the mode selection map. Again due to the complexity of finding a close form expression for $P_{C_0}(\theta)$ as a function of θ, discrete values of θ, i.e. θ_{kl} as defined in (3.38) are used. To determine $P_{C_0}(\theta_{kl})$, (3.36a) is used. Finally, the sojourn time for UE_c located in (X_i, Y_i) is as follows:

$$S_T = \mathbb{E}[T].\Bigg(P(\theta \in \{[0,2\pi] \setminus \bigcup_{n=1,\cdots,N_d} \psi_n\}).P_{C_0}(\theta|\theta \in \{[0,2\pi] \setminus \bigcup_{n=1,\cdots,N_d} \psi_n\})$$
$$+ \sum_{l=1}^{N_d} P(\theta \in \psi_l).\sum_{k=1}^{K} P(\theta = \theta_{kl}).P_{C_0}(\theta_{kl})\Bigg) \tag{3.45a}$$
$$= \mathbb{E}[T].\left(\left(1 - \frac{\sum_{n=1}^{N_d}(\beta_n - \alpha_n)}{2\pi}\right) + \sum_{l=1}^{N_d} \frac{(\beta_l - \alpha_l)}{2\pi}.\sum_{k=1}^{K} \frac{1}{K} P_{C_0}(\theta_{kl})\right) \tag{3.45b}$$

3.6 Handover Algorithm

In this section we present a distance based vertical handover algorithm relying on results in Section 3.4.1. As discussed earlier the mode selection map specifies the geometrical boundaries where the overall throughput of the network in two different transmission modes are equal. When UE_c moves in the network it might pass the boundaries of the mode selection map. This is equivalent to the change in the TM for the D2D UEs. Such a transition should be determined by a handover mechanism that could track the behavior of UE_c and when executes the handover process.

Our handover algorithm is summarized in Fig. 3.5. In this flowchart, there is a predefined process that calculates the mode selection map and periodically obtains the location updates,

and direction of movement, denoted as (X_i,Y_i) and θ, respectively. These parameters are used to calculate the perpendicular points and intersection points by the algorithm. Moreover, there is another process that estimates the processing time of handover as well as the velocity of UE_c which are denoted as μ and V, respectively. These two parameters are used to calculate the distance threshold from the map, i.e. $d_{pT} = \mu.V$, and the running delay of the algorithm, i.e. $T_d < \mu$.

The algorithm is executed periodically every T_d units of time. Provided the mode selection map and (X_i,Y_i), the algorithm starts by first finding the perpendicular points , i.e. $\{(X_{pn},Y_{pn})\}_{n=1,\cdots,N_p}$ by solving (3.35b). Then the resulting coordinates are substituted in (3.11) to determine the distance set, H. Then the distance of UE_c from the map, i.e. d_p, is computed using (3.12). The algorithm then checks if $d_p < d_{pT}$. This condition checks the proximity of the moving UE_c with respect to the borders of the mode selection map. If the condition is satisfied then, the Mobility Management Entity (MME) checks if the moving UE_c intersects with the map when it moves in the direction of θ by solving (3.17) and finding the solutions as $\{(X_{cn}(\theta),Y_{cn}(\theta))\}_{n=1,\cdots,N_c(\theta)}$. The handover starts only when this equation has at least one solution, i.e. $N_c(\theta) > 0$, meaning UE_c intersects with the map. The last condition ensures that even if the moving UE_c is close to the border of the map, the handover would not be applied until an intersection with map is seen. If any of the two conditions are not satisfied, the algorithm is repeated in T_d units of time.

3.7 Numerical Results

In this section we present our simulation results for running the handover algorithm in Section 3.6. Then we evaluate the performance of the algorithm using the performance metrics defined in Section 3.4.2.1 and 3.4.2.2. We assume that UE_s an UE_d are static. Moreover the transmission power of UE_s and eNB is considered to be constant.

First we apply the handover algorithm in two different cases where TM is selected between the 1) reuse or cellular modes, and 2) reuse or dedicated modes. For both cases we apply the parameters in Table 3.1.

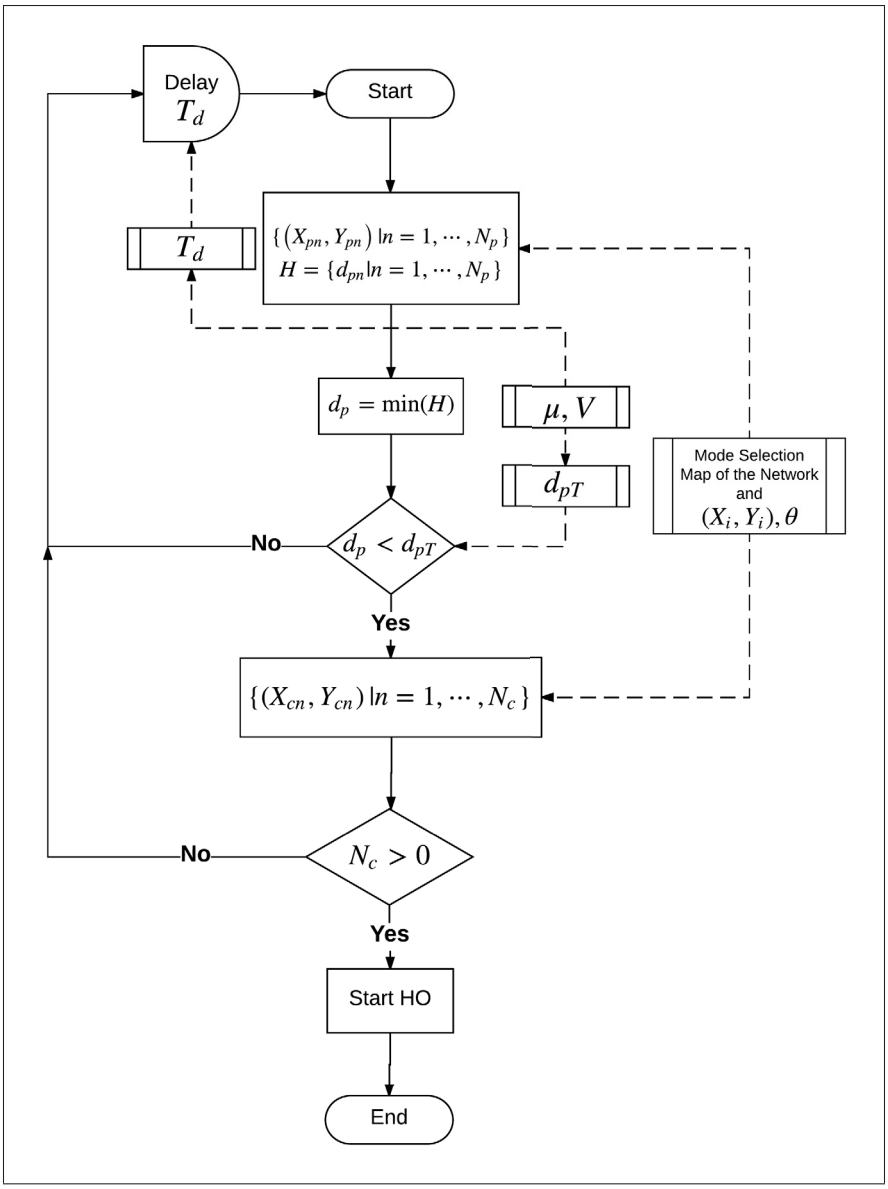

Figure 3.5 Distance based handover mechanism

We assume that UE_c starts moving from $(X_c,Y_c) = (1,1)$ and takes 10 steps using the RWP model as described in Section 3.3.2 and 3.4.2 with $\mathbb{E}[L] = 50$ m. We also assume that UE_c velocity is constant, $V = 5$ m/sec. The simulation results for case 1 and 2, are shown in Fig. 3.6 and Fig. 3.7 respectively. Based on the parameter values in Table 3.1, the distance threshold is calculated to be $d_{pT} = \mu.V = (1 \text{ sec}).(5 \text{ m/sec}) = 5$ m.

Table 3.1 Simulation parameters for vertical handover algorithm

Parameter	Value
Cell radius (r_C)	3 km
UE_s's position (X_s,Y_s)	(250,250)
UE_d's position (X_d,Y_d)	(0,300)
UE's maximum power (P_c, P_s, P_d)	23dBm
eNB's maximum power (P_e)	46dBm
Pathloss exponent (α)	3 (for urban areas)
Processing time (μ)	1 sec
Velocity (V)	5 m/sec
Average transition length ($\mathbb{E}[L]$)	50 m
Nomber of steps	10

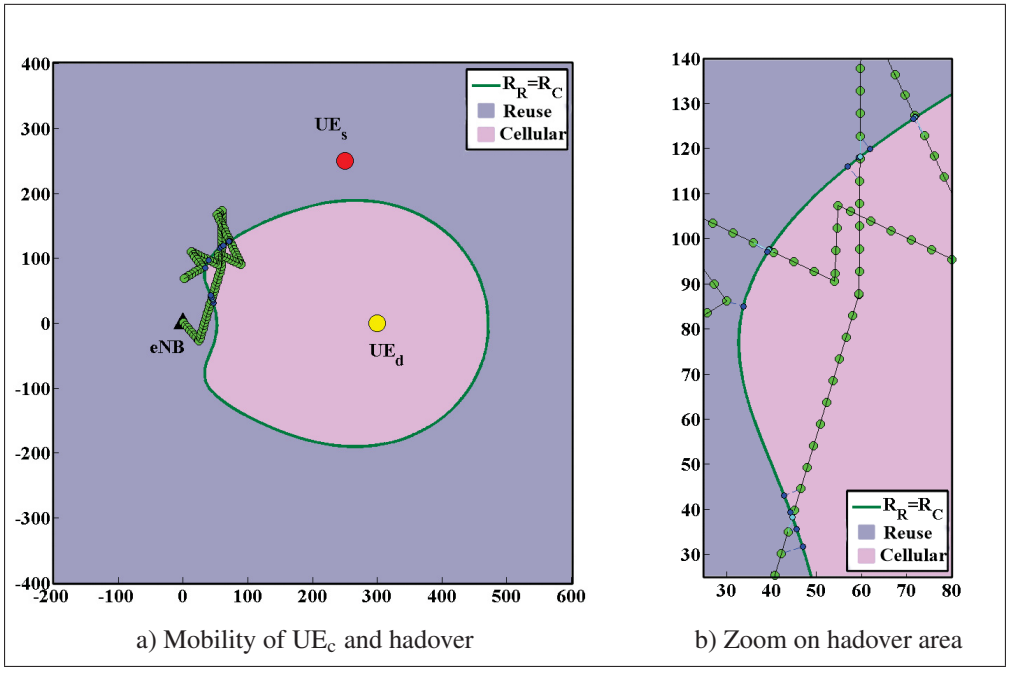

a) Mobility of UE_c and hadover b) Zoom on hadover area

Figure 3.6 Handover for the moving UE_c when the TM to be selected is either the reuse or cellular

Fig. 3.6a, shows simulation result of the handover algorithm when the movement of the UE_c causes mode changes between the reuse and cellular for the D2D UEs. As observed in this case

UE_c intersects with the mode selection map in several points. A larger view of the intersection part is shown in Fig. 3.6b. The perpendicular points shown in blue are when the distance from the map is less than the threshold ($d_p < d_{pT}$). It defines the distance of the moving UE_c from the map. Then for each of these points the algorithm checks if during the next T_d units of time, UEc intersects with the map. If there is at least one intersection the handover is applied. This is shown as cyan links and intersection points on the map. If the handover is not performed, the link color remains black in the figure.

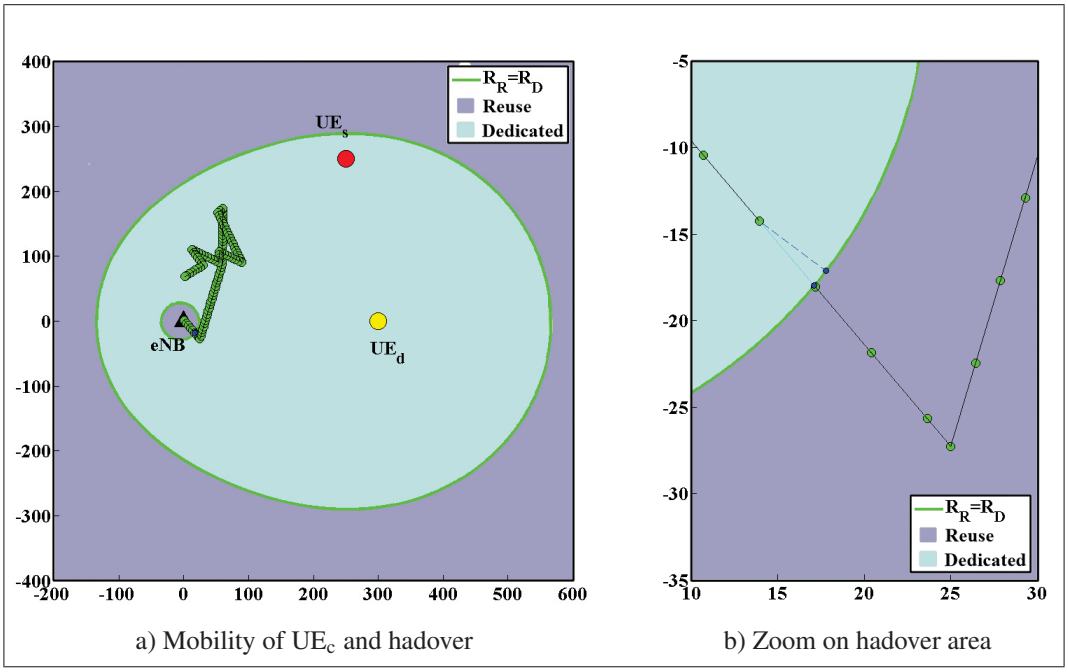

a) Mobility of UE_c and hadover b) Zoom on hadover area

Figure 3.7 Handover for the moving UE_c when the TM to be selected is either the reuse or dedicated

The same explanation stands for the simulation results presented in Fig. 3.7a and Fig. 3.7b. In this case the mode selection is between the reuse and dedicated modes. Considering the same movement pattern as applied in the previous case, the moving UEc causes only one handover, i.e. it intersects with the map in one point.

To evaluate the performance of our handover algorithm we use the metrics presented in Section 3.5.2 and 3.5.3. The handover rate and sojourn time are location based functions with values

dependent on the first waypoint. For simplicity we consider a simulation scenario where UE_c's first waypoint could be any point on y-axis between 0 and 250 meters. This is shown in Fig. 3.8a where the blue line represents the set of locations for first waypoint. Fig. 3.8b shows the distance of each waypoint from the map for the two cases where $R_R = R_C$ and $R_R = R_D$.

Having mode selection map defined by $R_R = R_C$ and $R_R = R_D$, for each waypoint on y-axis, denoted as Y_{c0}, with its value changing between 0 and 250, the handover rate and sojourn time is calculated using (3.40), (3.42), and (3.23) for handover rate, and (3.45b) for sojourn time. We take $K = 30$ discrete values of $\theta \in \psi_n$. All other initialization parameters remain the same as in Table 3.1. The simulation results corresponding to the performance metrics of the algorithm are shown in Fig. 3.9 and 3.10.

As can be seen from Fig. 3.9, for the curves related to $R_R = R_C$, the handover rate increases with a low slope until $Y_{c0} \approx 80$. Referring to Fig. 3.8b, we realize that this is the point that the distance from the map, d_p is minimum. For $Y_{c0} > 80$, the handover rate decreases, and $\lim_{Y_{c0}\to\infty} R_H = 0$. For the curves related to $R_R = R_D$, the handover rate increases slightly until $Y_{c0} \approx 25$. This is close to the first intersection point of the blue line in Fig. 3.8a with the map which corresponds to $d_p \approx 0$. After this point, the handover rate decreases sharply until it reaches a local minimum at $Y_{c0} \approx 100$. Then again the handover rate increases until $Y_{c0} \approx 210$ where $d_p \approx 0$ and the blue line intersects with the map. Between these two intersections, as it is seen from Fig. 3.8a, d_p's value starts from zero, reaches a maximum, and then at the other intersection reaches zero again. Finally when Y_{c0} exceeds 210, the handover rate declines sharply. One difference between the handover curves for $R_R = R_C$ and $R_R = R_D$, is that the latter comes with sharp changes and higher values for handover rate, however the former changes smoothly. This is due to the fact that the waypoint line in the latter intersects with the map, which causes to reach handover rate for close to border points.

Fig. 3.10 shows sojourn time as the other performance metric of the handover algorithm. The two mode selection maps are for Y_{c0} changes between 0 and 250. By comparing curves in Fig. 3.10 with the results in Fig. 3.9, it is seen that the changing in sojourn time follows the

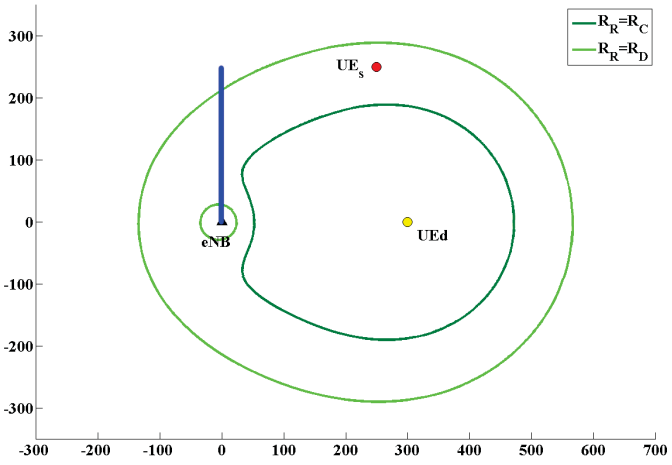

a) Mode selection map and the first waypoint of the moving UE_c

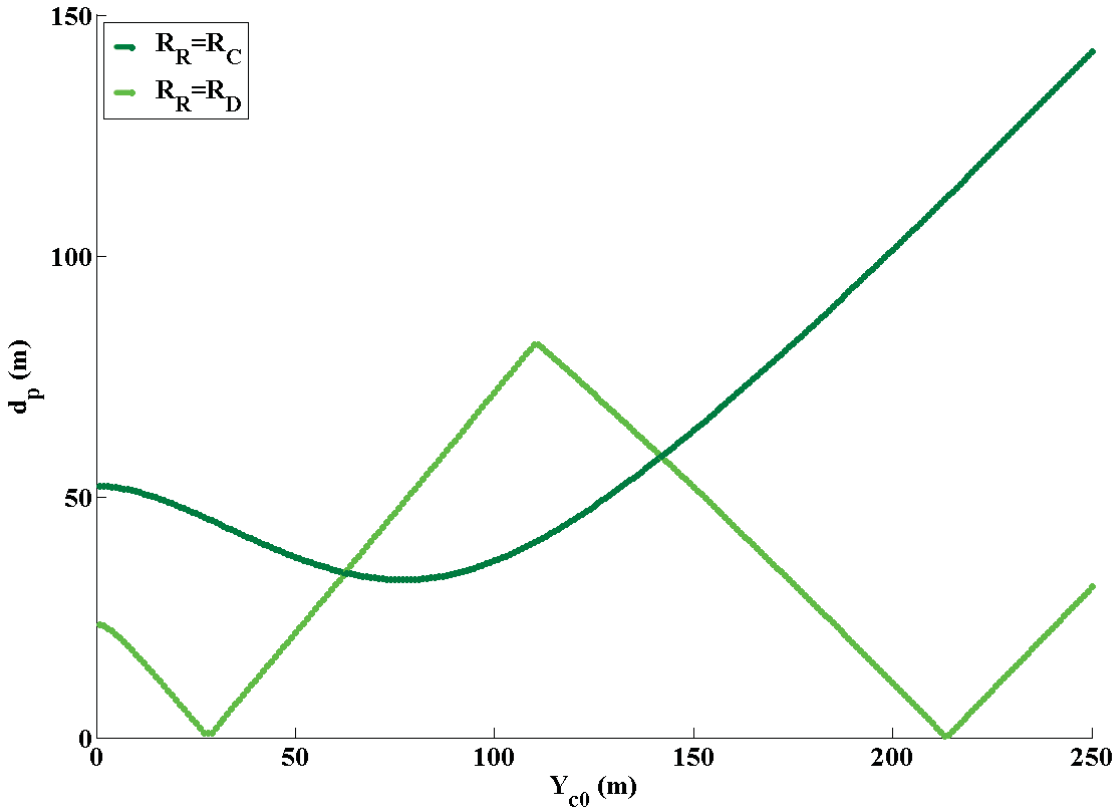

b) Distance of the waypoint from the map

Figure 3.8 Waypoints and their distance from the map

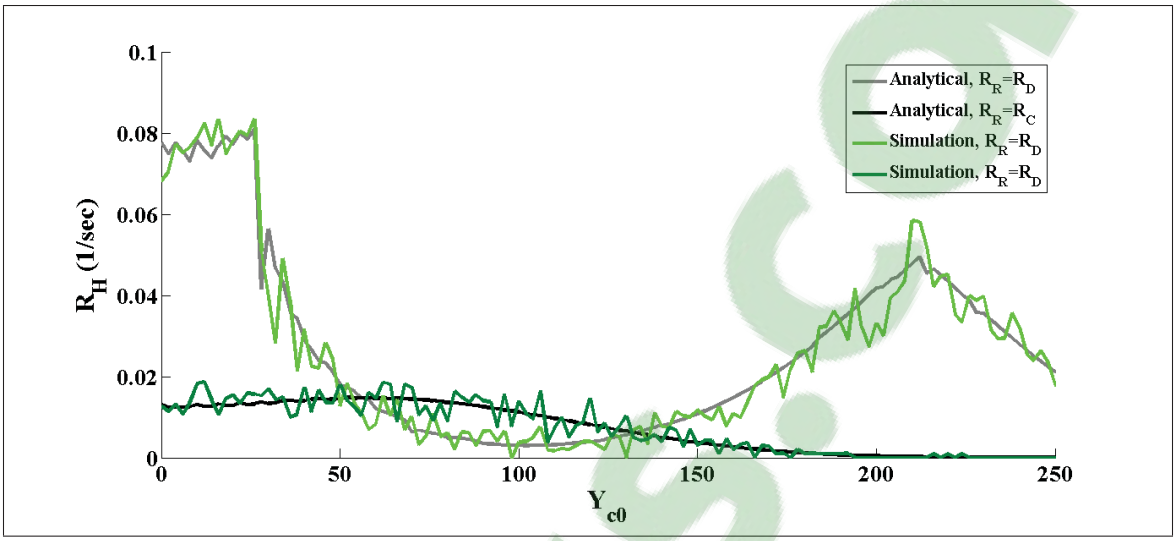

Figure 3.9 Handover rate

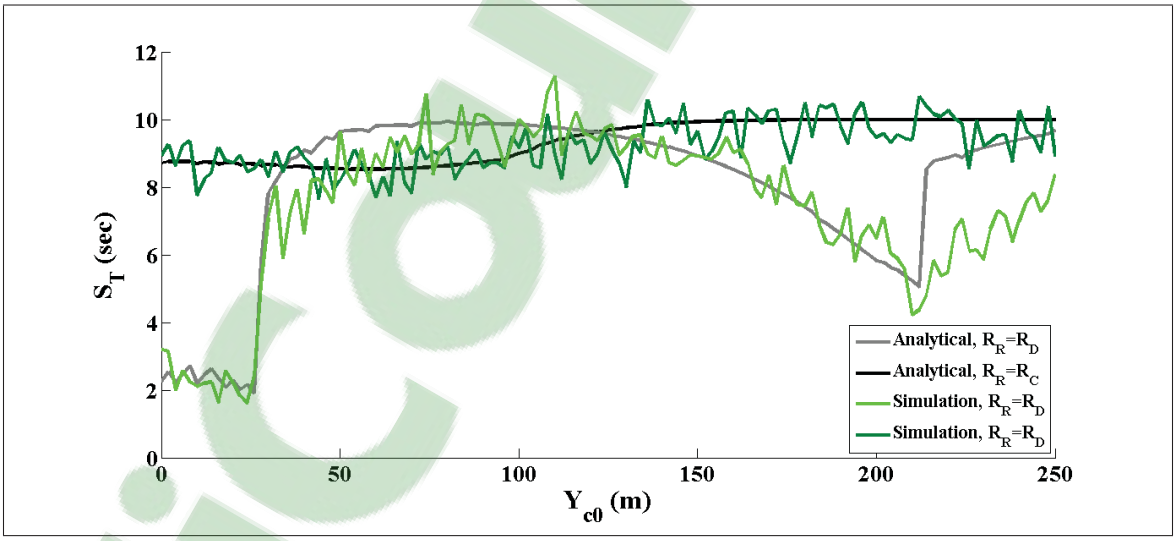

Figure 3.10 Sojourn time

opposite changes in handover rate. In other words, when handover rate increases the sojourn time decreases and vice versa. This behavior can be explained also from Fig. 3.8b. When d_p decreases it means that the waypoint gets closer to the map, therefore the handover rate increases but the sojourn time decreases since the average time that UE_c moves without TM change to the D2D UEs is reduced. However when d_p increases, the handover rate decreases

and the sojourn time increases. This is because with higher distance form the map, when the velocity is constant, UE_c moves further without intersecting with the map.

To validate our analytical calculation of the handover rate and sojourn time, for each specific point on the blue line in Fig. 3.8a, we place UE_c there and we generate a random direction, θ and transition distance, L based on their distribution and the probabilistic characteristics as summarized in Table 3.1. Then using (3.17) we calculate the intersection points and their total number. Having these values, the handover rate and sojourn time are calculated using (3.23) and (3.25) respectively. We iterate this procedure for the current location 10^6 times and then we average out over the resulted values for handover rate and sojourn time. Applying these steps for all points on the blue line, the results are shown in Fig. 3.9 and Fig. 3.10. As could be seen the results from the simulation as discussed above validates the analytical results.

3.8 Conclusion

In this paper, we address the problem of vertical handover in D2D enabled 5G networks. Due to cellular UE's movement transmission mode between the D2D UEs might be change in order to maximize the overall network throughput. We use the mode selection map of a D2D enabled network and find distance from the map and intersection with the map, as decision parameters in the handover algorithm. Using these parameters, we develop a vertical handover algorithm. We apply this algorithm on a sample network to check its functionality. Then to evaluate the performance of the handover, we analytically derive handover rate and sojourn time for a D2D enabled network. We consider a scenario where the first waypoint of the moving cellular UE is located on the y-axis and present the performance metrics when the first waypoint changes. We noticed that the handover rate increases as the first waypoint gets closer to the map and decreases as the first waypoint gets farther from the map. The behavior of the sojourn time is opposite of the handover rate and has a direct relation to the distance of the waypoint from the map.

CONCLUSION AND RECOMMENDATIONS

The D2D transmission, being one of the features of LTE-A, brings proximity gain, hop gain, reuse gain, and pairing gain to the network. However there are many issues that should be resolved to optimally use it in cellular networks. In this work, we study problem of mode selection map derivation and its application to mobility management. Our first main objective is to develop an analytical framework to find the mode selection map of a simple D2D enabled network for two different channel conditions: 1) LoS path-loss channel; 2) fading channel. The second main objective is the development of a vertical handover mechanism using the mode selection map.

4.1 General Conclusions

For mode selection derivation, the overall throughput of the network for the reuse, dedicated, and cellular modes is calculated and presented in three different equations. When the channel's model is LoS path-loss, to find the mode selection map, these equations are equalized two by two and the resulted equation is solved. For the fading channel scenario, due to the probabilistic variation of the channels the expectation of the network overall throughput is calculated for three TMs and the resulted functions are equalized two by two and solved. For the LoS path-loss scenario we derive the map for three different cases when UE_c, UE_s, and UE_d are moving. For the fading scenario we develop our analytical approach for the case of UE_c moving in the network.

We also study the vertical handover issue in D2D enabled network and propose a handover algorithm for the case when UE_c moves in the network assuming fixed LoS channels. The algorithm is relying on two decision parameters, i.e. distance from the map and intersection with the map, which are analytical computed. To evaluate the performance of the handover mech-

anism we present handover rate and sojourn time and we calculate them for a D2D enabled network analytically using the mode selection map derived earlier.

In Chapter 1 we propose an analytical solution to find the mode selection map of a single cell D2D enabled 5G network consisting of two paired D2D UEs, one cellular UE, and one eNB. D2D UEs select their TM among the reuse, dedicated, and cellular modes by choosing the one that results in the highest overall throughput of the network; However, the cellular UE communicates with eNB in UL. We show that for fixed transmission power and noise power while having LoS channel, the selected TM for the communication between D2D UEs, depends on each UE's location. Moreover, we find that there are disjoint regions in the network where if a moving UE stays inside that region, the TM mode between D2D UEs will not change. We realized that, depending on which UE moves in the network, there are three different cases to formulate the mode selection map problem were two of them have been discussed in this chapter. Using specific analytical approaches for each case, we find a set of geometrical functions that explicitly define the mode selection map. Using the results from our analytical solutions we develop simulation scenarios for each case on a specific network and we realize that there are certain regions defined by equirate boundaries where if UE_s or UE_d is located there, one of the TMs would be the best mode for the transmission between the paired D2D UEs.

In Chapter 2 we propose an analytical solution to find the mode selection map of a single cell D2D enabled 5G network over fading channels consisting of two paired D2D UEs, one cellular UE, and one eNB. D2D UEs can select their TM among the reuse, dedicated, and cellular modes; However, the cellular UE communicates with eNB in UL. We show that there are disjoint regions in the network where if a moving UE stays inside that region, the TM mode between D2D UEs will not change. Using the proposed analytical approaches, we find geometrical functions that are dependent on the transmission power and location of entities, noise power, and standard deviation of fading and shadowing variables, that explicitly define

the mode selection map. We use the results from our analytical solutions to develop simulation scenarios for each case on a specific network. Although the fast fading and shadowing effect causes changes in communication channels, their statistics remains unchanged. Therefore, the resulted map is constant, in spite of channel fluctuations and it can be a reliable source for applications such as mode selection, resource allocation, mobility management and handover.

Finally in Chapter 3 we address the problem of vertical handover in D2D enabled 5G networks. Due to cellular UE's movement, transmission mode between the paired D2D UEs might be required to change to keep the overall network throughput at the highest possible. We use the mode selection map of a D2D enabled network to find distance from the boundaries of the map and intersection with these boundaries, as decision parameters of the handover algorithm. Using these parameters, we present the vertical handover algorithm in a flowchart that shows how the handover mechanism works. We apply this algorithm on a sample network to check its functionality. Then to evaluate the performance of the handover algorithm, we derive handover rate and sojourn time for a D2D enabled network analytically. We consider a scenario where the first waypoint of the moving cellular UE is located on y-axis and present the performance metrics when the first waypoint changes. We realized that the handover rate increases as the first waypoint gets closer to the boundary and its value decreases as the first waypoint gets further from the boundary. For the sojourn time its changing behavior is opposite with the handover rate and has a direct relation to the distance of the waypoint from the boundary of the map.

4.2 Future Works

This research work addressed the mode selection map derivation and vertical handover mechanisms issues in D2D enabled networks. Some perspectives for the continuation of this thesis are listed below:

- The derivation of the mode selection map for the case of having fading channels between involved entities in the network when 1) UE_s moves in the network but UE_d and UE_c are fixed, 2) UE_d moves in the network but UE_s and UE_c are fixed;
- Study the D2D transmission range for different modes in LoS path-loss and fading scenarios;
- Development of possible handover mechanisms for D2D enabled networks considering QoS parameters in addition to mode selection map;
- Study off-loading and resource allocation techniques in D2D enabled network using the mode selection map.

APPENDIX I

AN OPTIMAL MIMO MODE SELECTION METHOD FOR D2D TRANSMISSION IN CELLULAR NETWORKS

Armin Morattab[1], Zbigniew Dziong[1], Kazem Sohraby[2], Md. Habibul Islam[3]

[1] Department of Electrical Engineering, École de Technologie Supérieure,
1100 Notre-Dame Ouest, Montreal, Quebec, Canada, H3C 1K3
[2] Department of Electrical and Computer Engineering, South Dakota School of Mines & Technology, Rapid City, SD 57701, USA
& an Adjunct in Computer Science Department, Sand Diego State University, USA
[3] School of Information and Communications Technologies, Southern Alberta Institute of Technology, Calgary, Canada

Article submitted for review in January 2017.

Abstract

Device-to-Device (D2D) communication is one of the new features introduced for Long Term Evolution-Advanced (LTE-A) and beyond networks. In this paper, we address the problem of communication mode selection for a pair of User Equipments (UEs). In particular we assume that the paired UEs can choose from the reuse, dedicated, and cellular modes. While this problem was treated in the literature for Single-Input-Single-Output (SISO) case, we derive models for networks where UEs and evolved-Node-Bs (eNBs) exploit Multiple-Input-Multiple-Output (MIMO) techniques with four antennas at each side. This approach requires design of the pre-coding matrices at each node which poses a challenge in the reuse mode due to the non-convexity problem. To solve this issue we propose a distributed iterative algorithm. The numerical study compares the performance of the MIMO based approach with that of the SISO case, and the results show that the presented MIMO based mode selection method provides significantly higher network throughput than that of the SISO based mode selection method for the same D2D transmission range.

Introduction

In LTE-A and 5G, existence of the ad-hoc networks as an underlying platform for the cellular networks which could share the same radio resources is the D2D transmission alternative. Allowing direct communication between UEs, D2D enhances the spectrum utilization, increases the cellular capacity, improves user throughput, and extends the battery lifetime of UEs.

To maximize the throughput, the transmission between the D2D enabled paired UEs, should be able to operate in multiple modes. The direct D2D transmission can be done either in the reuse mode or the dedicated mode. In the reuse mode D2D UEs and cellular UEs (i.e. the UEs which transmit data to their pair device through eNB) share some resources in Uplink (UL) or Downlink (DL) of the cellular network. However in the dedicated mode, a portion of the cellular network resources is reserved for D2D devices which cellular UEs are not allowed to use it. In addition to these two modes, the transmission between D2D enabled paired UEs can also be arranged in cellular mode which the traffic is relayed through the eNB as in traditional cellar communications.

The reuse mode should provide better spectrum efficiency since multiple users would be able to share the same resources to transmit their data. On the other hand, the dedicated mode and cellular mode ease the task of interference management. However, these two modes may not utilize the resources efficiently to maximize the overall network throughput. Therefore, the major issue in D2D transmission is how to select the best transmission mode for D2D enabled paired UEs so that the overall network throughput is maximized and the QoS requirements are satisfied. In (Zulhasnine *et al.*, 2010; Doppler *et al.*, 2010; Yu *et al.*, 2011) the authors have presented different approaches to deal with this issue of mode selection. The D2D and cellular link quality and the interference situation of each possible sharing mode has been considered in (Zulhasnine *et al.*, 2010) and finally here, the authors consider the selection of a mode that provides the highest sum-rate while satisfying the Signal-to-Noise-and-Interference-Ratio (SINR) constraint of the cellular network in both single-cell and multiple-cell is considered. In their model each cell includes one D2D pair and one cellular user. In (Doppler *et al.*, 2010)

the authors have presented a mode selection scheme with power control in a single-cell and multi-cell scenarios where one D2D link and one cellular user reuse the same resources. In that work, the users are subject to spectral efficiency restrictions and maximum transmission power or energy constraints. Their method enables a more reliable D2D transmission with limited interference to the cellular network compared to simpler mode selection procedures which forces all D2D terminals to reuse the same resources as the cellular communication. In (Yu *et al.*, 2011) a joint optimum resource allocation and power control between the cellular and D2D connections that share the same resources have been analyzed for different resource sharing modes in both single-cell and multi-cell scenarios. In their method the cellular user with a higher channel quality will share the resource with a D2D link which causes lower interference.

As LTE-A UEs, D2D transceivers can use multiple antennas and MIMO schemes to increase data throughput and link coverage without increasing transmission power or bandwidth. MIMO technique spreads the transmission power over multiple antennas to achieve an array gain with more bits per second per hertz of bandwidth and a diversity gain to mitigate the effect of fading. A major requirement for using MIMO technology in D2D transmissions is the design of efficient precoders. The design should minimize transmission power in order to minimize the interference caused to the neighbors while guaranteeing the QoS requirements. In (Janis *et al.*, 2009), some interference-avoiding precoding schemes have been proposed for downlink MIMO transmissions in the presence of intra-cell D2D links. In (Min *et al.*, 2011), a new interference management strategy is proposed to enhance the overall capacity of cellular networks and D2D systems when the eNB equipped with multiple antennas enables multiple cellular UEs to communicate simultaneously with the help of MIMO spatial multiplexing techniques. In (Fodor and Reider, 2011) the authors propose a new distributed power control algorithm that iteratively determines the SINR targets in a mixed cellular and D2D environment for MIMO and SISO scenarios and allocates transmit powers such that the overall power consumption is minimized subject to a sum-rate constraint.

In this paper, we study the mode selection problem in an LTE-A cellular network where the UEs and eNBs are exploiting multiple antennas. Previous works which considered MIMO for D2D transmission, either have discussed the power control issue without precoder design, or have applied precoding just for the eNB. In our study, since four by four MIMO is allowed in LTE-A for UEs and eNBs, we apply a precoding strategy for four antennas. The value of the precoding matrices is determined in the mode selection problem, which gives the highest throughput among all transmission modes after solving the optimization problem for each mode. Although the solutions of the optimization problems for dedicated and cellular modes are straightforward, the solution for the reuse mode is complex because of the non-convexity problem. Therefore, a convex approximation of the throughput function, based on the method presented in (Zhao *et al.*, 2012) is given, which leads to a distributed iterative algorithm to find the efficient precoders. Comparing with SISO transmission, by designing efficient precoders and applying our mode selection algorithm, the overall throughput of the network is shown to significantly increase while the same SINR target is achieved with higher D2D range.

This paper is organized as follows: Section 3 describes the system model and formulates problem of mode selection considering multiple antennas at UEs and eNB. In Section 4, a convex approximation of the optimization problem for the reuse mode is presented and an iterative algorithm to solve it is discussed. Simulation results are presented in Section 5, and Section 6 highlights our findings.

3. System Model

We consider a single cell scenario with one pair of D2D enabled UEs (UE_{TX} and UE_{RX}) and a single cellular UE (UE_C). These nodes in addition to the eNB are assumed equipped with four antennas which enable them to use precoding/decoding techniques. The precoders are also designed for efficient transmission. However, in this paper, we only use spatial multiplexing, and do not apply MIMO coding scheme such as Space-Time Block Codes (STBC). Hence the codeword covariance matrix (Q) is equal to the identity matrix, i.e. $Q = I$.

The transmission between UE_{TX} and UE_{RX} can be done in reuse, dedicated, or cellular mode, while communication between UE_C and eNB is always in cellular mode. For simplicity we only considered one way transmission for (UE_{TX},UE_{RX}) and (eNB,UE_C) pairs. The notation (a,b) implies that transmission occurs from (a) to (b) only.

A quasi-static Rayleigh flat fading model is applied to determine Channel State Information (CSI) matrices in an urban area. Another important assumption is that each transmitter knows the CSI matrix of all the channels between it and the receiving nodes using the feedback provided by its paired receiver (UE or eNB).

Fig.I-1 represents a cellular network with UE_{TX} and UE_{RX} as D2D pair, and UE_C as the cellular user. Note that the interference channel, which is shown in the model by black dashed arrows, is present only in the reuse mode, in which case the resources are shared between (UE_{TX},UE_{RX}) and (eNB,UE_C) for transmission. The desired signal flow is shown by solid arrows.

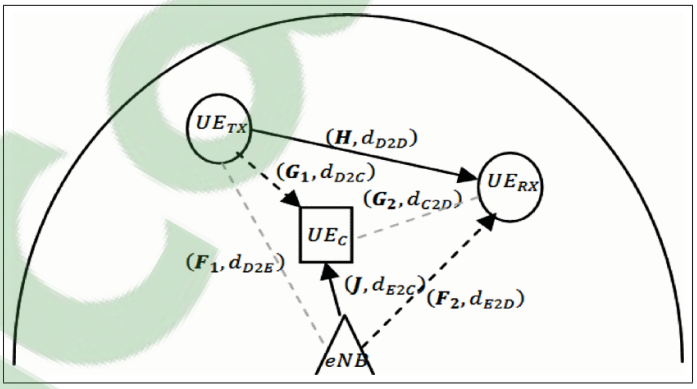

Figure-A I-1 Transmission in a D2D enabled LTE-A network

As discussed before the precoding is applied in all transmission modes, at the transmitters i.e. UE_{TX}, and eNB. The received signals at receivers, i.e. UE_{RX}, and UE_C, for different transmission modes are expressed as follows:

$$y_{D2D}^{Re} = HW_{Re}x_{D2D} + F_2U_{CRe}x_{E2C} + N_D^{Re} \qquad \text{(A I-1a)}$$

$$y_{E2C}^{Re} = JU_{CRe}x_{E2C} + G_1W_{Re}x_{D2D} + N_c^{Re} \quad \text{(A I-1b)}$$

$$y_{D2D}^{Ded} = HW_{Ded}x_{D2D} + N_D^{Ded} \quad \text{(A I-2a)}$$

$$y_{E2C}^{Ded} = JU_{CDed}x_{E2C} + N_c^{Ded} \quad \text{(A I-2b)}$$

$$y_{D2E}^{Cell} = F_1U_{D2D}^{UL}x_{D2E} + N_E^{Cell} \quad \text{(A I-3a)}$$

$$y_{E2D}^{Cell} = F_2U_{D2D}^{DL}x_{E2D} + N_D^{Cell} \quad \text{(A I-3b)}$$

$$y_{E2C}^{Cell} = JU_cx_{E2C} + N_c^{Cell} \quad \text{(A I-3c)}$$

The description for transmit and receive signals in the above equations for different modes, is summarized as follows:

Table-A I-1 Description and furmulaiton notation of the transmit and receive signals

Description	**Formulation Notation**		
	Reuse	***Dedicated***	***Cellular***
Received signal at UE_{RX}	$\boldsymbol{y}_{D2D}^{Re}$	$\boldsymbol{y}_{D2D}^{Ded}$	$\boldsymbol{y}_{E2D}^{Cell}$
Received signal at UE_C	$\boldsymbol{y}_{E2C}^{Re}$	$\boldsymbol{y}_{E2C}^{Ded}$	$\boldsymbol{y}_{E2C}^{Cell}$
Received signal at eNB	-	-	$\boldsymbol{y}_{D2E}^{Cell}$
Transmitted signal from UE_{TX}	$\boldsymbol{x}_{D2D}$	$\boldsymbol{x}_{D2D}$	$\boldsymbol{x}_{D2E}$
Transmitted signal from eNB	$\boldsymbol{x}_{E2C}$	$\boldsymbol{x}_{E2C}$	$\boldsymbol{x}_{E2C}, \boldsymbol{x}_{E2D}$
Received noise at UE_{RX}	$\boldsymbol{N}_D^{Re}$	$\boldsymbol{N}_D^{Ded}$	$\boldsymbol{N}_D^{Cell}$
Received noise at UE_C	$\boldsymbol{N}_C^{Re}$	$\boldsymbol{N}_C^{Re}$	$\boldsymbol{N}_C^{Re}$
Received noise at eNB	-	-	$\boldsymbol{N}_E^{Cell}$
Precoding matrix at UE_{TX}	$\boldsymbol{W}_{Re}$	$\boldsymbol{W}_{Ded}$	$\boldsymbol{U}_{D2D}^{UL}$
Precoding matrix at eNB	$\boldsymbol{U}_{CRe}$	$\boldsymbol{U}_{CDed}$	$\boldsymbol{U}_C, \boldsymbol{U}_{D2D}^{DL}$

For the cellular mode since transmission between UE_{TX} and UE_{RX} is done in UL and DL, for each link we have $\boldsymbol{U}_{D2D}^{UL}$ and $\boldsymbol{U}_{D2D}^{DL}$ precoding matrices applied to $\boldsymbol{x}_{D2E}$ at UE_{TX} and to $\boldsymbol{x}_{E2D}$ at eNB, respectively, and for the DL link of the UE_C we have applied $\boldsymbol{U}_C$ in eNB. All the precod-

ing matrices are four by four with their values determined during the mode selection procedure. As shown in Fig.I-1, $\boldsymbol{H}$, $\boldsymbol{G}_1$, $\boldsymbol{G}_2$, $\boldsymbol{F}_1$, $\boldsymbol{F}_2$, and $\boldsymbol{J}$ are the four by four CSI matrices of the MIMO channels between the nodes in the network. We have considered a quasi-static Rayleigh flat fading channel model as discussed in [8] to generate the CSI matrices. For example for the $\boldsymbol{H}$ matrix the value of its elements $\left[h_{ij}\right]$, are as follows:

$$h_{ij} = \sqrt{c\frac{1}{d_{ij}^{\alpha}}}\sqrt{s_{ij}}z_{ij} \tag{A I-4}$$

In this expression, d_{ij} is the distance between i'th antenna at the transmitter and j'th antenna at the receiver. We assume d_{ij}s are constant. The d_{ij}s corresponding to the CSI matrices $\boldsymbol{H}$, $\boldsymbol{G}_1$, $\boldsymbol{G}_2$, $\boldsymbol{F}_1$, $\boldsymbol{F}_2$, and $\boldsymbol{J}$, are d_{D2D}, d_{D2C}, d_{C2D}, d_{D2E}, d_{E2D}, and d_{E2C} respectively. α is the pathloss exponent; c is the propagation constant. $S_{ij} = 10^{\frac{s_{ij}}{10}}$ is a log normal shadow fading variable, where s_{ij} is a zero mean Gaussian random variable with standard deviation v. z_{ij} is modeled as a set of normalized Gaussian random variables, assumed to be independent for each transmit-receive link.

Equations (A I-1a) and (A I-1b), represent the received signals at reuse mode. In these equations, the first term is the desired signal, the second term is the interference from the other transmitter, and the third term is the Gaussian noise vector. Since there is no interference in dedicated and cellular modes, in equations (A I-2a) and (A I-2b), and (A I-3a)–(A I-3b), only the desired signal term and the Gaussian noise term appear in the formulation.

The approach to find the overall rate of transmission in different modes having SISO nodes is discussed in (Doppler *et al.*, 2010). Here we generalize those formulations considering UEs and eNB having multiple antennas and the transmitters applying precoding:

$$R_{Re} = \log_2 |I_4 + \frac{(HW_{Re}W_{Re}^T H^T)P_{UE}}{(F_2 U_{CRe}U_{CRe}^T F_2^T)P_{eNB} + N_0 I_4}|$$

$$+\log_2|I_4+\frac{(JU_{CRe}U_{CRe}^T J^T)P_{eNB}}{(G_1W_{Re}W_{Re}^T G_1^T)P_{UE}+N_0I_4}| \quad \text{(A I-5a)}$$

$$R_{Ded}=\frac{1}{2}\log_2|I_4+\frac{(HW_{Ded}W_{Ded}^T H^T)P_{UE}}{N_0I_4}$$

$$+\frac{1}{2}\log_2|I_4+\frac{(JU_{CDed}U_{CDed}^T J^T)P_{eNB}}{N_0I_4}| \quad \text{(A I-5b)}$$

$$R_{Cell}=\min\left(\frac{1}{4}\log_2|I_4+\frac{(F_1U_{D2D}^{UL}U_{D2D}^{UL\ T}F_1^T)P_{UE}}{N_0I_4}|,\frac{1}{4}\log_2|I_4+\frac{(F_2U_{D2D}^{DL}U_{D2D}^{DL^T}F_2^T)P_{eNB}}{N_0I_4}|\right)$$

$$+\frac{1}{2}\log_2|I_4+\frac{(JU_CU_C^T J^T)P_{eNB}}{N_0I_4}| \quad \text{(A I-5c)}$$

R_{Re}, R_{Ded}, and R_{Cell} stands for the overall rate of the network in reuse, dedicated, and cellular mode respectively. P_{UE} and P_{eNB} are the total transmit powers at UEs and eNB respectively, and $\boldsymbol{I}_n$ is an $(n\times n)$ identity matrix. To formulate the rate equations the resource allocation strategy in Fig.I-2 has been considered for different modes.

<table>
<tr><td rowspan="4">Available resources</td><td>1</td><td rowspan="4">D2D + E2C</td><td rowspan="2">D2D</td><td>E2D</td></tr>
<tr><td>0.75</td><td>D2E</td></tr>
<tr><td>0.5</td><td rowspan="2">E2C</td><td rowspan="2">E2C</td></tr>
<tr><td>0.25</td></tr>
<tr><td></td><td></td><td>Reuse mode</td><td>Dedicated mode</td><td>Cellular mode</td></tr>
</table>

Figure-A I-2 Resource allocation strategy for different transmission modes

In equations (A I-5a) and (A I-5b), the first term is the rate of the D2D transmission, and the second term stands for the rate of the cellular transmission. In (A I-5c) since the D2D transmission works in cellular mode, which is happening in UL and DL in cascade, the first term derived as $min\,(a,b)$ which a and b are UL and DL rates respectively, and the second term is for the DL link of UE_C.

Having the overall rate for each mode, the optimization problem determines the proper precoding matrices which are formulated as follows:

$$\max(R_{Re})$$

$$s.t. \quad \begin{cases} \gamma_{\min}^{UE} \leq SINR_{UE_C}^{Re} \\ \gamma_{\min}^{UE} \leq SINR_{UE_{RX}}^{Re} \\ tr(W_{Re}W_{Re}^{T}) = 1 \\ tr(U_{CRe}U_{CRe}^{T}) = 1 \end{cases} \tag{A I-6a}$$

$$\max(R_{Ded})$$

$$s.t. \quad \begin{cases} \gamma_{\min}^{UE} \leq SINR_{UE_C}^{Ded} \\ \gamma_{\min}^{UE} \leq SINR_{UE_{RX}}^{Ded} \\ tr(W_{Ded}W_{Ded}^{T}) = 1 \\ tr(U_{CDed}U_{CDed}^{T}) = 1 \end{cases} \tag{A I-6b}$$

$$\max(R_{Cell})$$

$$s.t. \quad \begin{cases} \gamma_{\min}^{UE} \leq SINR_{UE_C}^{Cell} \\ \gamma_{\min}^{UE} \leq SINR_{UE_{RX}}^{Cell} \\ \gamma_{\min}^{eNB} \leq SINR_{eNB}^{Cell} \\ tr(U_{D2D}^{UL}U_{D2D^T}^{UL}) = 1 \\ tr(U_{D2D}^{DL}U_{D2D^T}^{DL}) = 1 \\ tr(U_cU_c^{T}) = 1 \end{cases} \tag{A I-6c}$$

The formulations presented in (A I-6a)–(A I-6c) contain two type of constraints: the SINR constraints of the UEs and eNB which are in the form of $\gamma_{min}^{RX\ type} < SINR_{RX}^{Mode}$, and constant average sum of transmit power constraints which for a desired precoding matrix $\boldsymbol{W}$ are in the form of $tr\left(\boldsymbol{W}\boldsymbol{W}^{T}\right) = 1$. $\gamma_{min}^{RX\ type}$ is the minimum acceptable SINR at each *RX type* (UE or eNB), $SINR_{RX}^{Mode}$ is the SINR of each *RX* (UE_C, UE_{RX}, or eNB) for a determined transmission *Mode*. The function $tr(\boldsymbol{A})$ represents trace of the matrix $\boldsymbol{A}$.

Solving (A I-6a) is straightforward since it is a convex optimization problem. To solve (A I-6c), a small reasonable modification such as $\min(a,b) \approx \frac{(a+b)}{2}$ is applied to make it concave. However the optimization problem in (A I-6a) is non-convex problem as discussed in (Zhao *et al.*, 2012). Later, we present an iterative algorithm to find the efficient precoding matrixes in the reuse mode.

As soon as the optimum rates for different modes are determined, the mode selection algorithm chooses the optimum mode - the one with the highest rate as follows:

$$Optimum\ mode = \arg \max_{\text{i=Re,Ded,Cell}} (R_i) \tag{A I-7}$$

4. Distributed convex approximation and the iterative algorithm

As discussed in the previous section, efficient design of precoders in the reuse mode leads to a non-convex optimization problem which is hard to solve. In this section we investigate this problem, by a convex approximation of (A I-6a) and present an iterative solution.

The network model in the reuse mode can be considered as a MIMO interference channel as shown in Fig.I-3.

Based on the formulation in (Zhao *et al.*, 2012) the rate for different links in the network for the reuse mode is as follows:

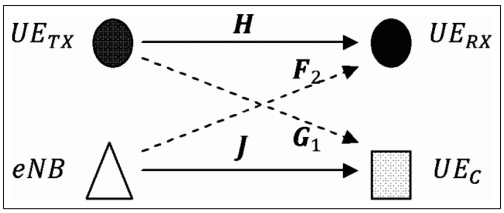

Figure-A I-3 MIMO interference channel in reuse mode

$$R_1 = \log\det(I_4 + (W_{Re}^T H^T B_1^{-1} H W_{Re}) P_{UE}) \tag{A I-8a}$$

$$R_2 = \log\det(I_4 + (U_{CRe}^T J^T B_2^{-1} J U_{CRe}) P_{eNB}) \tag{A I-8b}$$

Where R_1 is the rate of the D2D transmission, and R_2 is the rate of the eNB to UE_C link. $\boldsymbol{B}_1$ and $\boldsymbol{B}_2$ are the noise plus inter-user interference terms defined as:

$$B_1 = (F_2 U_{CRe} U_{CRe}^T F_2^T) P_{eNB} + N_0 I_4 \tag{A I-9a}$$

$$B_2 = (G_1 W_{Re} W_{Re}^T G_1^T) P_{UE} + N_0 I_4 \tag{A I-9b}$$

Following (A I-9a) and (A I-9b), the optimization problem in (A I-6a) can be reformulated as:

$$\max(R_1 + R_2)$$
$$s.t. \quad \begin{cases} \gamma_{\min}^{UE} \le SINR_{UE_{RX}}^{Re} \\ \gamma_{\min}^{UE} \le SINR_{UE_C}^{Re} \\ tr(W_{Re} W_{Re}^T) = 1 \\ tr(U_{CRe} U_{CRe}^T) = 1 \end{cases} \tag{A I-10}$$

As discussed in (Zhao *et al.*, 2012) a convex approximation of (A I-10) which lead to a distributed iterative algorithm is achieved by introducing linear receiver filters, $\boldsymbol{U}_1$ and $\boldsymbol{U}_2$, as auxiliary optimization variables, i.e. $\mathrm{UE_{RX}}$ and eNB respectively. Then the rates of the two receivers becomes:

$$R_1 = \log\det(I_4 + (W_{Re}^T H^T U_1^T (U_1^T B_1 U_1)^{-1} U_1 H W_{Re}) P_{UE}) \tag{A I-11a}$$

$$R_2 = \log\det(I_4 + (U_{CRe}^T J^T U_2^T (U_2^T B_2 U_2)^{-1} U_2 J U_{CRe}) P_{eNB}) \tag{A I-11b}$$

And the SINR formulas, having the decoders therefore would be as follows:

$$SINR_{UE_{RX}}^{Re\ \ l} = \frac{U_1^{[l]^T} (H W_{Re}^{[l]} W_{Re}^{[l]^T} H^T) U_1^{[l]} P_{UE}}{U_1^{[l]^T} (\Sigma_{\substack{n=1 \\ n\neq 1}}^{L} (H W_{Re}^{[n]} W_{Re}^{[n]^T} H^T) P_{UE} + B_1) U_1^{[l]}} \tag{A I-12a}$$

$$SINR_{UE_C}^{Re\ \ l} = \frac{U_2^{l^T} (J U_{CRe}^{[l]} U_{CRe}^{[l]^T} J^T) U_2^l P_{eNB}}{U_2^{[l]^T} (\Sigma_{\substack{n=1 \\ n\neq l}}^{L} (J U_{CRe}^{[n]} U_{CRe}^{[n]^T} J^T) P_{eNB} + B_2) U_2^{[l]}} \tag{A I-12b}$$

Where $SINR_{UE_{RX}}^{Re\ \ l}$ and $SINR_{UE_C}^{Re\ \ l}$ stands for the SINR of the received signal at $\mathrm{UE_{RX}}$ and $\mathrm{UE_C}$'s l'th layer after applying the decoders. The SINR constraints should be satisfied for all L MIMO layers. It should be noted that for dedicated and cellular transmission the inter-user interference terms appear in $SINR$ formulas should be canceled out. $\boldsymbol{M}^{[l]}$ is the l'th column of the matrix $\boldsymbol{M}$.

There would be no capacity loss i.e. the R_1 and R_2 terms in (A I-8a) and (A I-8b), and (A I-11a) and (A I-11b) would be equal as long as the following optimal linear receiver filters are applied:

$$U_1 = B_1^{-1} H W_{Re} \tag{A I-13a}$$

$$U_2 = B_2^{-1} J U_{CRe} \tag{A I-13b}$$

By presenting the receiver filters, the non-concave optimization problem in (A I-10) is approximated with the following two new distributed convex problems which should be iteratively solved at the corresponding transmitters.

$$\max(\log\det((\tilde{H}^T W_1 \tilde{H})P_{UE}) - tr(I_4 + N_2^{-1}(\tilde{G}_1^T W_1 \tilde{G}_1)P_{UE}))$$

$$s.t. \quad \begin{cases} U_1^{[l]}\left((H((\sum_{\substack{n=1\\n\neq l}}^{L} W_{Re}^{[n]} W_{Re}^{[n]^T})\gamma_{\min}^{UE} - W_{Re}^{[l]} W_{Re}^{[l]^T})H^T)P_{UE}\right)U_1^{[l]} \\ \quad + ((F_2 W_2^p F_2^T)P_{eNB} + N_0 I_4)\gamma_{\min}^{UE} < 0,\ for\ l = 1,\ldots,L \\ U_2^{[l]^T}\left((J((\sum_{\substack{n=1\\n\neq l}}(U_{CRe}^{p\ [n]}\ U_{CRe}^{p\ [n]^T}))\gamma_{\min}^{UE} - U_{CRe}^{p\ [l]})J^T)P_{eNB}\right)U_2^{[l]} \\ \quad + ((G_1 W_1 G_1^T)P_{UE} + N_0 I_4)\gamma_{\min}^{UE} \le 0,\ for\ l = 0,\ldots,L \\ tr(U_{CRe}U_{CRe}^T) = 1 \end{cases} \qquad \text{(A I-14a)}$$

$$\max(\log\det((\tilde{J}^T W_2 \tilde{J})P_{eNB}) - tr(I_4 + N_1^{-1}(\tilde{F}_2^T W_2 \tilde{F}_2)P_{eNB}))$$

$$s.t. \quad \begin{cases} U_2^{[l]^T}\left((J((\sum_{\substack{n=1\\n\neq l}}^{L} U_{Re}^{[n]} U_{Re}^{[n]^T})\gamma_{\min}^{UE} - U_{Re}^{[l]} U_{Re}^{[l]^T})J^T)P_{eNB}\right)U_2^{[l]} \\ \quad + ((G_1 W_2^p G_2^T)P_{UE} + N_0 I_4)\gamma_{\min}^{UE} < 0,\ for\ l = 1,\ldots,L \\ U_1^{[l]^T}\left((H((\sum_{\substack{n=1\\n\neq l}}(W_{Re}^{p\ [n]}\ W_{Re}^{p\ [n]^T}))\gamma_{\min}^{UE} - W_{Re}^{p\ [l]})H^T)P_{UE}\right)U_1^{[l]} \\ \quad + ((F_2 W_2 F_2^T)P_{eNB} + N_0 I_4)\gamma_{\min}^{UE} \le 0,\ for\ l = 0,\ldots,L \\ \mathrm{tr}(\mathrm{W}_2) = 1 \end{cases} \qquad \text{(A I-14b)}$$

In the above equations $\boldsymbol{W}_1 = \boldsymbol{W}_{Re}\boldsymbol{W}_{Re}^T$, $\boldsymbol{W}_2 = \boldsymbol{U}_{CRe}\boldsymbol{U}_{CRe}^T$. $\boldsymbol{W}_1^p = \boldsymbol{W}_{Re}^p \boldsymbol{W}_{Re}^{p\ T}$ and $\boldsymbol{W}_2^p = \boldsymbol{U}_{CRe}^p \boldsymbol{U}_{CRe}^{p\ T}$ are positive semi-definite matrixes defined by the optimum achieved precoding matrices at the previous iteration, $\boldsymbol{N}_1 = N_0\boldsymbol{U}_1^T\boldsymbol{U}_1$, $\boldsymbol{N}_2 = N_0\boldsymbol{U}_2^T\boldsymbol{U}_2$, $\widetilde{\boldsymbol{H}} \triangleq \boldsymbol{H}^T\boldsymbol{U}_1$, $\widetilde{\boldsymbol{J}} \triangleq \boldsymbol{J}^T\boldsymbol{U}_2$, $\widetilde{\boldsymbol{F_2}} \triangleq \boldsymbol{F}_2^T\boldsymbol{U}_1$, $\widetilde{\boldsymbol{G_1}} \triangleq \boldsymbol{G}_1^T\boldsymbol{U}_2$.

The algorithm to find the proper values based on (Zhao *et al.*, 2012), is summarized in Table AI-2.

Table-A I-2 Iterative distributed convex optimization algorithm to find precoding matrices in reuse mode

Initialize $\boldsymbol{W}_{Re}^p$ and $\boldsymbol{U}_{CRe}^p$, that should be feasible in their corresponding constraints.
Repeat
Stage 1: Find the optimal value for the receiver filters $\boldsymbol{U}_k$, using (A I-13a) and (A I-13b), given $\left\{\boldsymbol{W}_{Re}^p \text{ and } \boldsymbol{U}_{CRe}^p\right\}$.
Stage 2: To find the precoding matrixes, first solve $\boldsymbol{W}_{Re}$ and $\boldsymbol{U}_{CRe}$ from (A I-14) and (A I-15) given the current $\{\boldsymbol{U}_k\ ,\ k = 1,2\}$ and $\left\{\boldsymbol{W}_{Re}^p \text{ and } \boldsymbol{U}_{CRe}^p\right\}$, and then substitute $\boldsymbol{W}_{Re}^p = \boldsymbol{W}_{Re}$ and $\boldsymbol{U}_{CRe}^p = \boldsymbol{U}_{CRe}$.
Until approximate convergence.
Find the R_k values using (A I-8a) and (A I-8b), then calculate $R_{Re} = R_1 + R_2$.

Although the convergence of the proposed algorithm is not analytically proved in [7], its convergence is observed in all the simulated cases. In the next section we will discuss the simulation results of the presented mode selection method for MIMO nodes and we compare with the SISO case.

5. Simulation Results

We evaluate the performance of the mode selection algorithm for the MIMO and SISO cases for the network scenario from Fig.I-1 where we have one pair of D2D enabled UEs and a cellular UE which is connected to eNB, and all equipments have four antennas in the MIMO mode. The parameter values used in the simulation are summarized in Table AI-3.

Table-A I-3 Simulation parameters

Parameter	Value
Bandwidth	1.25 MHz
Cell radius	3Km
N_0	-142.88 dB (at 25°C)
P_{UE}	23 dBm
P_{eNB}	46 dBm
α	3 (for urban area)
v	7 dB
$\gamma_{\min}^{UE}$	-9 dB
$\gamma_{\min}^{eNB}$	-7 dB

UE_{TX} and UE_{RX} are fixed in the network with the normalized distance of L from each other and both are at the normalized distance of D from eNB. The mode selection map of the network is as follows: we calculated the network performance for UE_C location at each point of a position matrix inside the cell, where the points have 200m distance in x, and y directions. For each point the rate optimization in all modes is executed for 50 different realization of the channel, and the mode selection is applied on the mean rate value of each mode. For the SISO transmission the mode selection is applied without precoding at transmitters. The mode selection map of the MIMO and SISO, for the case of $D = 0.7$, and $L = 0.5$ is depicted in Fig.I-4a, and I-4b.

By comparing visually the mode selection maps of MIMO and SISO scenarios, it can be seen that when the UE_C is far from the D2D UEs, for example when it is located at the bottom of the cell, the reuse mode is best. As soon as the UE_C gets closer to the D2D UEs the mode selection policy changes for MIMO and SISO cases. Namely, as seen from Fig.I-4b, a very close UE_C to UE_{RX} distance will lead to cellular mode selection and as the distance of the UE_C from UE_{RX} increases, the mode changes into dedicated and then reuse mode.

To further investigate the effect of using MIMO techniques for D2D transmission, the mean rate of the network for different values of normalized distances, D and L, is depicted in Fig.I-5a, and I-5b.

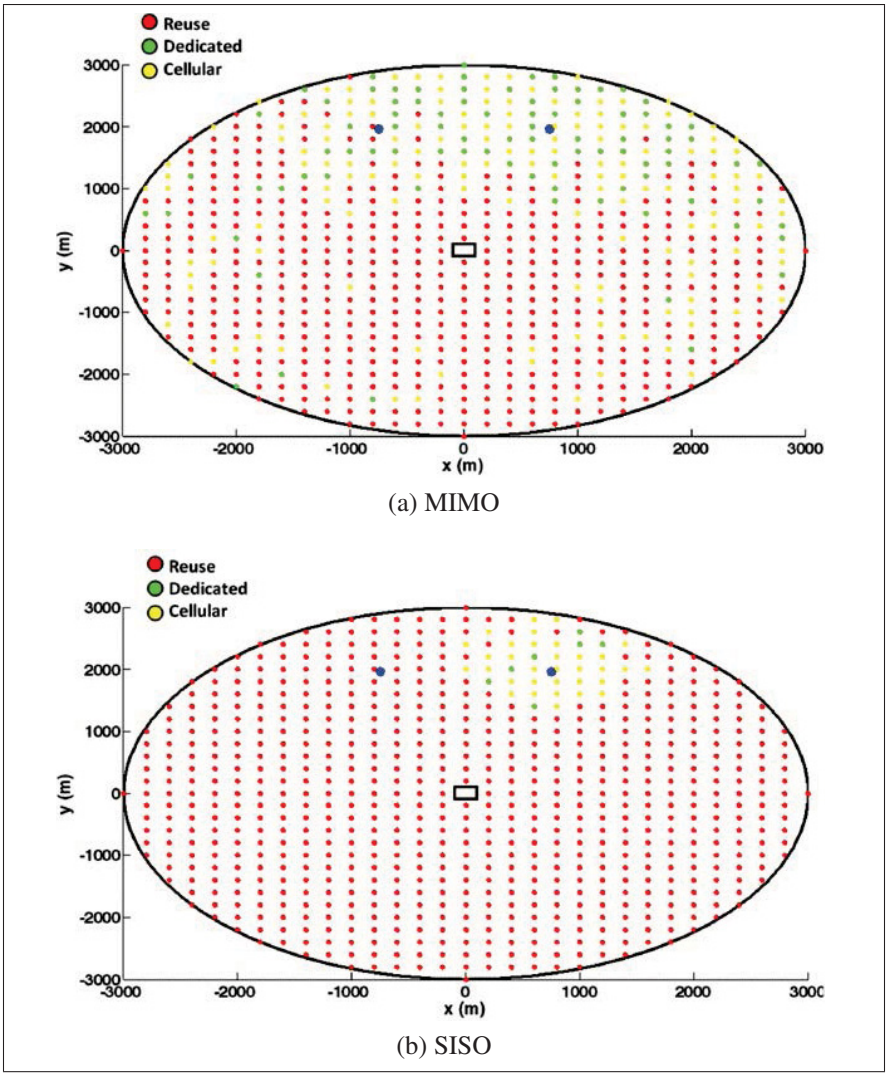

(a) MIMO

(b) SISO

Figure-A I-4 Mode selection map for $D = 0.7$, and $L = 0.5$

As these figures show and as expected, for the same amount of transmit power, the overall throughput of the network for MIMO case is considerably higher than the SISO scenario. The higher performance comes from the spatial multiplexing gain which achieved by designing efficient precoders at the transmitter and applying the proposed mode selection algorithm.

Fig.I-6 shows the mean overall MIMO to SISO rate ratio, which represents the gain of using MIMO precoding in D2D. For this simulation, using the MIMO mode selection algorithm results in a linear gain of 5.9-6.3 in the best case of $L = 0.1$, depending on the different values of D. As could be seen for close D2D range the gain of using MIMO is higher and it decreases

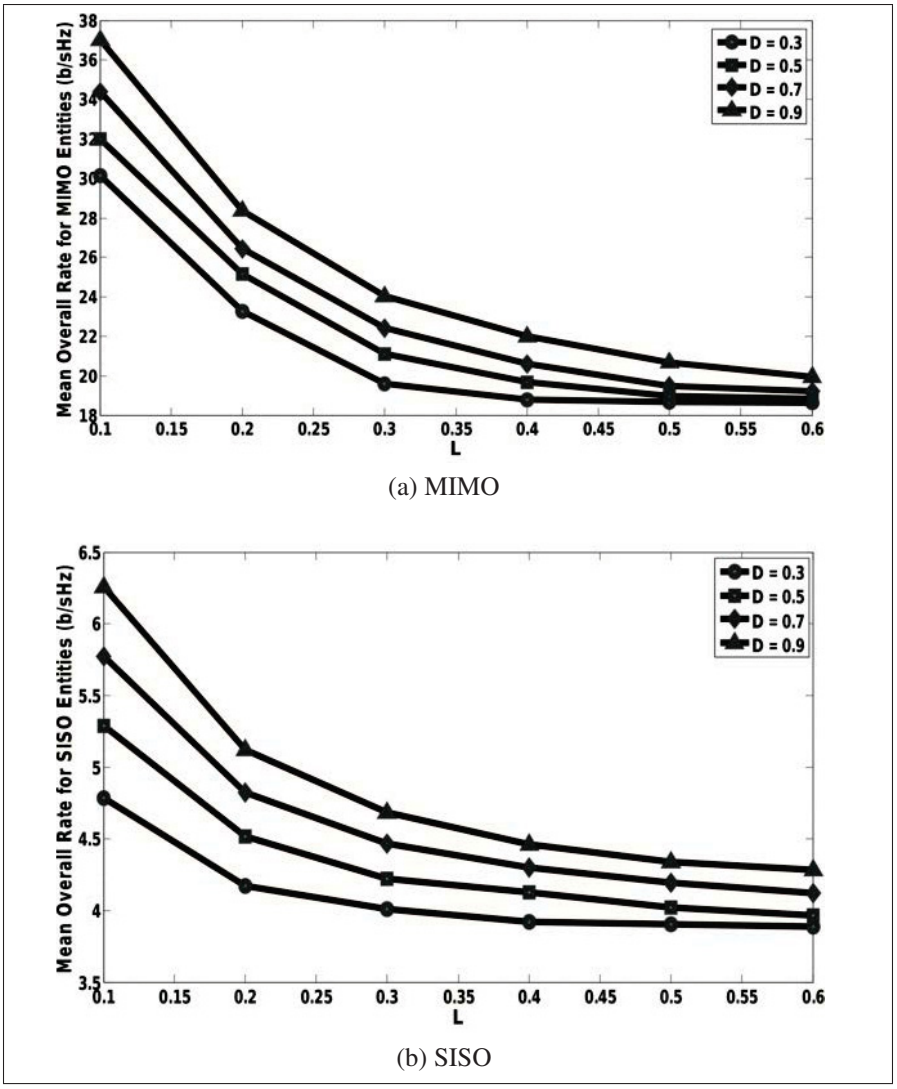

(a) MIMO

(b) SISO

Figure-A I-5 Achievable rate of the network

as L increases. Moreover, as L becomes larger, the value of gain stabilizes in the range 4.6-4.8 for all values of D.

As could be seen in Fig.I-6 the different MIMO to SISO gain curves for different Ds intersect. It shows that at first which L has small value, the MIMO to SISO gain is higher for smaller Ds, then at certain point for L, the gain for greater values of D is higher, and by increasing L again the gain for smaller values of D would be higher.

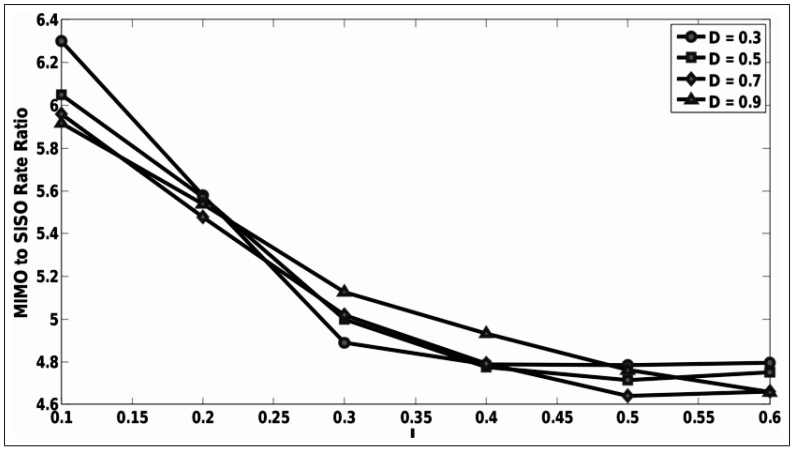

Figure-A I-6 Rate ratio of MIMO and SISO scenarios

6. Conclusions

In this paper, we studied the mode selection problem in a cellular network where UEs and eNBs exploit MIMO techniques with four antennas at each node. The approach presented here required the design of the precoding matrixes at each node, which is a challenge in the reuse mode due to the non-convexity of the optimization problem. We proposed a distributed iterative algorithm to solve this problem. Numerical studies show that using the proposed method for MIMO mode selection the overall network throughput can increase 5.9-6.3 times in some cases depending on D2D range and their distance to eNB.

APPENDIX II

MOBILITY IMPACT ON MODE SELECTION MAP IN D2D NETWORKS – AN ANALYTICAL APPROACH

Armin Morattab[1], Zbigniew Dziong[1], Kazem Sohraby[2], Md. Habibul Islam[3]

[1] Department of Electrical Engineering, École de Technologie Supérieure,
1100 Notre-Dame Ouest, Montreal, Quebec, Canada, H3C 1K3
[2] Department of Electrical and Computer Engineering, South Dakota School of Mines & Technology, Rapid City, SD 57701, USA
& an Adjunct in Computer Science Department, Sand Diego State University, USA
[3] School of Information and Communications Technologies, Southern Alberta Institute of Technology, Calgary, Canada

Article submitted for review in January 2017.

Abstract

Device-to-Device (D2D) transmission is a promising technology which enables the User Equipments (UE) in 5G cellular networks to directly communicate without going through the evolved Node-B (eNB). In such networks UEs should select a Transmission Mode (TM) amongst reuse, dedicated, and cellular modes by maximizing the overall transmission throughput or referring to a mode selection map. The selection map identifies the mode which results in the highest data rate given the current state of the network. This paper presents a new analytical framework for the derivation of the selection map of D2D enabled cellular networks. While this problem was treated in the literature through numerical simulations, our approach is analytical and consequently fast and precise.

Introduction

In a conventional cellular system, all communications take place through the base stations. Device-to-Device (D2D) transmission is a promising technology which enables the User Equipment (UE) in 5G cellular networks to directly communicate without going through the evolved

Node-B (eNB). This technique would result in lower power and latency and as result higher overall network throughput.

To achieve the maximum overall throughput, D2D enabled UEs are allowed to operate in different TMs which includes, reuse, dedicated, and cellular modes. To better understand these TMs Fig.II-1. presents a D2D enabled 5G network , which includes a pair of D2D enabled UEs,(UE_s and UE_d) and a pair of cellular devices, i.e. UE_c, with eNB working in cellular Up-Link (UL). Referring to Fig.II-2. in the cellular mode, the transmission between UEs is indirect, through the eNB, however in the reuse and dedicated modes, transmission is direct between UE_s and UE_d. Moreover in the dedicated and cellular modes, both transmitters in the network, i.e. UE_s and UE_c, do not share channel resources, however in the reuse mode, they share channels . Therefore in the reuse mode, interference at UE_d would be from UE_c and at eNB from UE_s while in the cellular and dedicated modes there would be no interference at the receivers. Hence reuse mode is preferred in terms of spectrum efficiency. On the other hand, the dedicated and cellular modes ease the task of interference management since the transmitters do not interfere with the unpaired receivers.

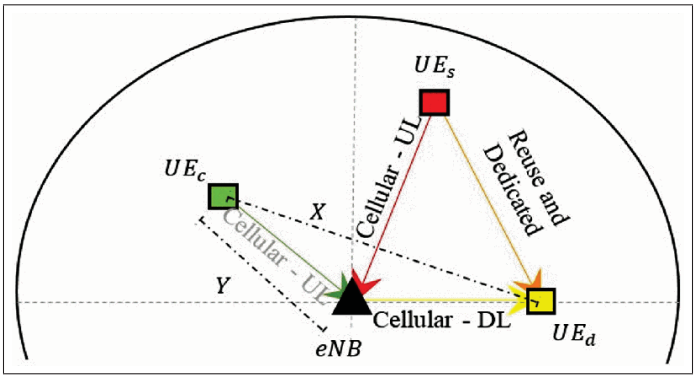

Figure-A II-1 D2D enabled 5G network

The main issue in a D2D enabled network is to select the optimal mode for transmission between the D2D enabled UEs. For a fixed power scenario, this selection strongly depends on the location of the UE_c, as an interferer. Assuming that the position of UE_s and UE_d is fixed, the optimal mode at UE_s depends on the relative position of UE_c as well as its power. The

collection of such positions labeled with their optimal mode is called the mode selection map of the D2D enabled network. Such a mode selection map can be derived periodically and used by the Mobility Management Entity (MME) or eNBs to decide on vertical handover.

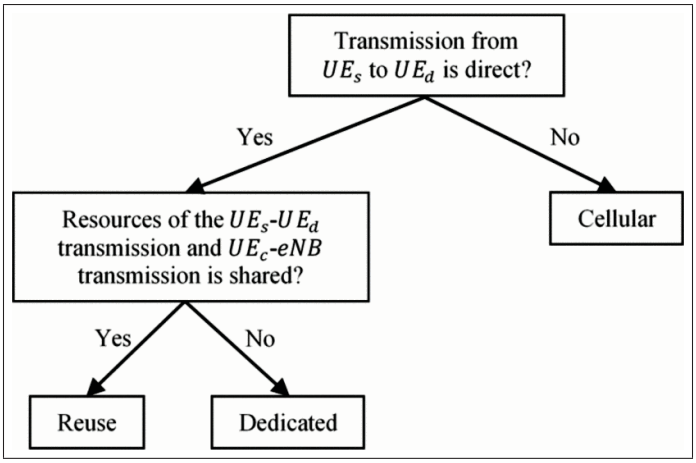

Figure-A II-2 Modes in D2D enabled 5G networks

There are several studies dedicated to the issue of mode selection in D2D enabled networks. The D2D and cellular link quality and the interference of each possible sharing mode has been considered in (Zulhasnine *et al.*, 2010). In that paper, the mode which results in the highest sum-rate is selected. They have considered a Signal-to-Noise-and-Interference-Ratio (SINR) constraint to ensure having the required Quality of Service (QoS) of the cellular network for single-cell and multiple-cell scenarios. Authors in (Doppler *et al.*, 2010) have presented a mode selection scheme with power control where the same resources are reused by one cellular user and one D2D pair in a single-cell and multi-cell scenario. Maximum transmission power or energy constraints and spectral efficiency restrictions applied to the users. A more reliable D2D transmission with limited interference to the cellular network is reached using the presented method compared to a simpler mode selection procedure which forces all D2D terminals to reuse resources used by the cellular users. In (Yu *et al.*, 2011) a joint optimum resource allocation and power control between the cellular and D2D users that share the same resources have been analyzed for different resource sharing modes in both single-cell and multi-cell scenarios. In their method a cellular user with higher channel quality shares the resource with a D2D

link which causes lower interference. In (Liu *et al.*, 2012b) the authors analyze the underlay and overlay mode selection of D2D communication in the LTE-A single-cell scenario in the presence of a relay node. They show that whether D2D users can reuse the cellular uplink resource or not is affected by the system parameters. Specifically the underlay mode is preferred when the cellular user is closer to the eNB (or relay node) than the D2D user. In (Yu *et al.*, 2014) a joint mode selection, channel assignment, and power control in D2D communications are addressed. Authors in (Yu *et al.*, 2014) aim at maximizing the overall system throughput while guaranteeing the SINR of both D2D and cellular links by developing low-complexity algorithms according to the network load. Finally in (Morattab *et al.*, 2015) the authors have addressed the problem of mode selection based on the highest rate for a pair of users equipped with multiple antennas. The users exploit Multiple Input Multiple Output (MIMO) precoding to achieve higher data rates in all modes and to reduce the interference. A mode selection map in [6] has been achieved using numerical simulations which specifies the best transmission mode between paired users for different positions of the cellular user. It has been shown that MIMO D2D reaches significantly higher rates using the precoding technique and mode selection method.

The mode selection algorithms presented above are based on numerical simulations which are somewhat complex, time consuming, and inefficient. Moreover the aforementioned researches are focused on the problem of mode selection without discussing the mode selection map. In this paper, we present a comprehensive and tractable analytical framework to derive the mode selection map of a D2D enabled 5G network. To the best of our knowledge this is the first proposal of such an analytical framework. We then use this framework to develop an algorithm which results in the detailed mode selection map with high precision.

The remainder of this paper is organized as follows: Section 3 describes the system model and formulates the overall throughput of the network for reuse, dedicated, and cellular TMs. Section 4, consists of two parts. In Section 4.1 we develop an analytical solution to the problem of finding the mode selection map. In the Section 4.2 an algorithm for developing the mode

selection map based on the results of previous section is presented. Simulation results are presented in Section 5. Section 6 highlights our findings.

3. System Model

We consider a single cell scenario with one pair of UEs (UE_s as the source UE and UE_d as the destination UE) and a single cellular UE (UE_c) which operates in cellular Up-Link (UL) mode, as shown in Fig.II-1. For simplicity it is assumed that all UEs and the eNB use a single antenna for transmission, however our model can be extended for entities with multiple antennas.

A quasi-static Rayleigh flat fading model, as discussed in (Dai *et al.*, 2004), is applied to determine fading channel gain coefficients, i.e. h_{ij}s between transmitter i and receiver j, as follows:

$$h_{ij} = \sqrt{c\frac{1}{d_{ij}^{\alpha}}}\sqrt{s_{ij}}z_{ij} = \sqrt{\frac{K_{ij}}{d_{ij}^{\alpha}}} \tag{A II-1}$$

In the above expression, d_{ij} is the distance between transmitter i and receiver$j$, which i is either s or c representing UE_s and UE_c , respectively. Likewise j is either d or e for UE_d and eNB, respectively; $K_{ij} = cs_{ij}z_{ij}^2$ is a random number; α is the pathloss exponent; c is the propagation constant; $S_{ij} = 10^{s_{ij}/10}$ is a log normal shadow fading variable, where s_{ij} is a zero mean Gaussian random variable with standard deviation v. z_{ij} is modeled as a set of normalized Gaussian random variables, assumed to be independent for each transmit-receive link.

The received signals, y, at UE_d and eNB, from the transmitters with power P for different modes are as follows:

$$y_d^R = \sqrt{P_s}h_{ds}x_s^R + \sqrt{P_c}h_{cs}x_c^R + n \tag{A II-2}$$

$$y_e^R = \sqrt{P_c}h_{ce}x_c^R + \sqrt{P_s}h_{se}x_x^R + n \tag{A II-3}$$

$$y_d^D = \sqrt{P_s} h_{ds} x_s^R + n \tag{A II-4}$$

$$y_e^D = \sqrt{P_c} h_{ce} x_c^R + n \tag{A II-5}$$

$$y_{e1}^c = \sqrt{P_s} h_{se} x_s^R + n \tag{A II-6}$$

$$y_d^c = \sqrt{P_e} h_{es} x_e^R + n \tag{A II-7}$$

$$y_{e2}^c = \sqrt{P_c} h_{ce} x_c^R + n \tag{A II-8}$$

where x is the unit power of transmitted signal, n is the white Gaussian noise with power N_0, R, D, and C as superscripts representing reuse, dedicated, and cellular modes, respectively, and s, d, c, and e are subscripts which represent UE_s, UE_d, UE_c, and eNB, respectively.

We assume that the transmitters exploit near capacity channel coding, therefore the data rate, would be almost equal to the capacity. Then the overall throughput of the network for each mode is as follows:

$$R_R = \log_2\left(1 + \frac{|h_{sd}|^2 P_s}{|h_{cd}|^2 P_c + N_0}\right) + \log_2\left(1 + \frac{|h_{ce}|^2 P_c}{|h_{se}|^2 P_s + N_0}\right) \tag{A II-9}$$

$$R_D = \frac{1}{2}\left(\log_2\left(1 + \frac{|h_{sd}|^2 P_s}{N_0}\right) + \log_2\left(1 + \frac{|h_{ce}|^2 P_c}{N_0}\right)\right) \tag{A II-10}$$

$$R_c = \frac{1}{2}\left(\min\left(\log_2\left(1 + \frac{|h_{se}|^2 P_s}{N_0}\right), \log_2\left(1 + \frac{|h_{ed}|^2 P_e}{N_0}\right)\right) + \log_2\left(1 + \frac{|h_{ce}|^2 P_c}{N_0}\right)\right) \tag{A II-11}$$

Having the overall throughput for different modes, we develop an analytical approach to find the mode selection map. In the following section we present the approach.

4. Analytical Solution and TM Selection Map Algorithm

In Part A, we develop an analytical approach to find the exact formulations and conditions to specify the mode selection map of the D2D enabled 5G network. In part B, we use these

results to propose an algorithm for developing the mode selection map. The map is a set of contours that specify the border of the regions where a specific mode gives the highest overall throughput.

4.1 Analytical Approach to Find the Mode Selection Map

For simplicity we assume that the locations of UE_s and UE_d are fixed while UE_c location can vary. Assume $d_{cd} = X$ and $d_{ce} = Y$. We want to find the geometrical areas inside the cell that, if UE_c is located there, a specific mode between UE_s and UE_d would result in the highest overall throughput. To address this issue we need to find the locus for points which satisfy the following equations:

$$R_R = R_D \tag{A II-12}$$

$$R_R = R_C \tag{A II-13}$$

We rewrite the equations (A II-9)–(A II-11) as follows:

$$R_R = \log_2\left(\left(1+\frac{a_1}{a_2 x+1}\right)(1+a_3 y)\right) \tag{A II-14}$$

$$R_D = \frac{1}{2}\log_2(a_1'(1+a_4 y)) \tag{A II-15}$$

$$R_C = \frac{1}{2}\log_2(a_5(1+a_4 y)) \tag{A II-16}$$

where a_1, a_1', a_2, a_3, a_4, and a_5 are constant parameters, while x and y are variables defined as follows:

$$a_1 = \frac{K_{sd}P_s}{d_{sd}^{\alpha}N_0} \tag{A II-17}$$

$$a_1' = 1 + a_1 \tag{A II-18}$$

$$a_2 = \frac{K_{cd} P_c}{N_0} \tag{A II-19}$$

$$a_3 = \frac{K_{ce} P_c}{d_{ce}^{\alpha} \left(\frac{K_{se} p_S}{d_{se}^{\alpha}} + N_0 \right)} \tag{A II-20}$$

$$a_4 = \frac{K_{ce} P_c}{N_0} \tag{A II-21}$$

$$a_5 = min\left(1 + \frac{K_{se} P_s}{d_{se}^{\alpha} N_0}, 1 + \frac{K_{ed} P_e}{d_{ed}^{\alpha} N_0}\right) \tag{A II-22}$$

$$x = \frac{1}{X^{\alpha}} \tag{A II-23}$$

$$y = \frac{1}{Y^{\alpha}} \tag{A II-24}$$

By defining x and y in (A II-23) and (A II-24) as a function of variable distances X and Y, shown in Fig.II-1, they both should have positive values.

We notice that R_D and R_C in equations (A II-15) and (A II-16) have the same form. In fact R_D's equation in (A II-15) is a special case of R_D in (A II-16) where a_1' is substituted instead of a_5. Therefore we need to find the locus only for equation (A II-13) and then the results can be applied to equation (A II-12) by substituting a_1' with a_5. It should be noticed that R_D and R_C intersect only if $a_5 = a_1'$ otherwise if $a_5 > a_1'$ then $R_C > R_D$ and if $a_5 < a_1'$ then $R_C < R_D$.

Based on (A II-13), we have the following relations:

$$\log_2\left(\left(1 + \frac{a_1}{a_2 x + 1}\right)(1 + a_3 y)\right) = \frac{1}{2}\log_2(a_5(1 + a_4 y)) \tag{A II-25}$$

$$\left(\left(1 + \frac{a_1}{a_2 x + 1}\right)(1 + a_3 y)\right)^2 = a_5(1 + a_4 y) \tag{A II-26}$$

which becomes:

$$a_3^2(a_1'+a_2x)^2y^2+(2a_3(a_1'+a_2x)^2-a_4a_5(1+a_2x)^2)y + ((a_1'+a_2x)^2-a_5(1+a_2x)^2)=0 \quad \text{(A II-27)}$$

and be simplified as:

$$f(x,y)=ay^2+by+c=0 \quad \text{(A II-28)}$$

$$a=a_3^2(a_1'+a_2x)^2 \quad \text{(A II-29)}$$

$$b=2a_3(a_1'+a_2x)^2-a_4a_5(1+a_2x)^2 \quad \text{(A II-30)}$$

$$c=(a_1'+a_2x)^2-a_5(1+a_2x)^2 \quad \text{(A II-31)}$$

For equation (A II-31) to have a solution, the following inequality should be satisfied:

$$0<\Delta=b^2-4ac \quad \text{(A II-32)}$$

$$0<a_4^2a_5^2(1+a_2x)^4-4a_3a_5(a_4-a_3)(a_1'+a_2x)^2(1+a_2x)^2 \quad \text{(A II-33)}$$

Developing this inequality with substitutions from (A II-23), leads to the following conditions and constraints on X:

- if $a_4 < a_3$, for all $X > 0$
- if $a_4 > a_3$
  - if $\frac{a_4\sqrt{a_5}}{2\sqrt{a_3(a_4-a_3)}} < 1$, for no $X > 0$

- if $1 < \frac{a_4\sqrt{a_5}}{2\sqrt{a_3(a_4-a_3)}} < a_1'$, for $0 < X < \sqrt[\alpha]{\frac{a_2a_4\sqrt{a_5}-2a_2\sqrt{a_3(a_4-a_3)}}{2a_1'\sqrt{a_2(a_4-a_3)}-a_4\sqrt{a_5}}}$
- if $a_1' < \frac{a_4\sqrt{a_5}}{2\sqrt{a_3(a_4-a_3)}}$, for all $X > 0$

As long as there is an x which satisfies (A II-33), the implicit function in (A II-31), i.e. $f(x,y)$, would have two roots as follows:

$$y = \frac{-b \pm \sqrt{\Delta}}{2a} \tag{A II-34}$$

Since $y=\frac{1}{Y^{\alpha}}$ and Y is the distance between UE_c and eNB which is positive, only values of x that satisfy the following constraint are accepted:

$$y > 0 \tag{A II-35}$$

For the roots presented in equation (A II-34), depending on the number of positive roots, there are four different possibilities that are illustrated in Fig.II-3 and summarized below:

if $b < 0$

$$\begin{cases} \text{if } c < 0, y = \dfrac{-b+\sqrt{\Delta}}{2a} & \text{(A II-36a)} \\ \text{if } c > 0, y = \dfrac{-b\pm\sqrt{\Delta}}{2a} & \text{(A II-36b)} \end{cases}$$

if $b > 0$

$$\begin{cases} \text{if } c < 0, y = \dfrac{-b+\sqrt{\Delta}}{2a} & \text{(A II-36c)} \\ \text{if } c > 0, \text{No positive solution} & \text{(A II-36d)} \end{cases}$$

To be able to use the proper equation from (A II-36a)–(A II-36d) we should figure out how the sign of b and c would change for different values of x. For the sign of b the results are summarized as follows:

- if $\sqrt{\frac{a_4 a_5}{2a_3}} < 1$, for all $X > 0$, $b > 0$
- if $1 < \sqrt{\frac{a_4 a_5}{2a_3}} < a'_1$
  - for $0 < X < \sqrt[\alpha]{\frac{a_2(\sqrt{2a_3}-\sqrt{a_4 a_5})}{\sqrt{a_4 a_5}-a'_1\sqrt{2a_3}}}$, $b < 0$
  - for $\sqrt[\alpha]{\frac{a_2(\sqrt{2a_3}-\sqrt{a_4 a_5})}{\sqrt{a_4 a_5}-a'_1\sqrt{2a_3}}} < X$, $b > 0$
- if $a'_1 < \sqrt{\frac{a_4 a_5}{2a_3}}$, for all $X > 0$, $b < 0$

and for the sign of c:

- if $a'_1 > \sqrt{a_5}$
  - for $0 < X < \sqrt[\alpha]{\frac{a_2(\sqrt{a_5}-1)}{a'_1-\sqrt{a_5}}}$, $c < 0$
  - for $\sqrt[\alpha]{\frac{a_2(\sqrt{a_5}-1)}{a'_1-\sqrt{a_5}}} < X$, $c > 0$
- if $a'_1 < \sqrt{a_5}$, for all $X > 0$, $c < 0$

Although by using the presented equations and inequalities we are able to find proper y (or Y), there are two more constraints based on triangle inequality theorem that should be satisfied:

$$X + Y \geq d_{ed} \tag{A II-37}$$

$$X - Y \leq d_{ed} \tag{A II-38}$$

It should be noticed that since the locus for mode selection map is just dependent on X and Y, it would be symmetric to the line connecting eNB and UE_d. Hence for simplicity we let UE_d to be on the horizontal axis as the symmetric line.

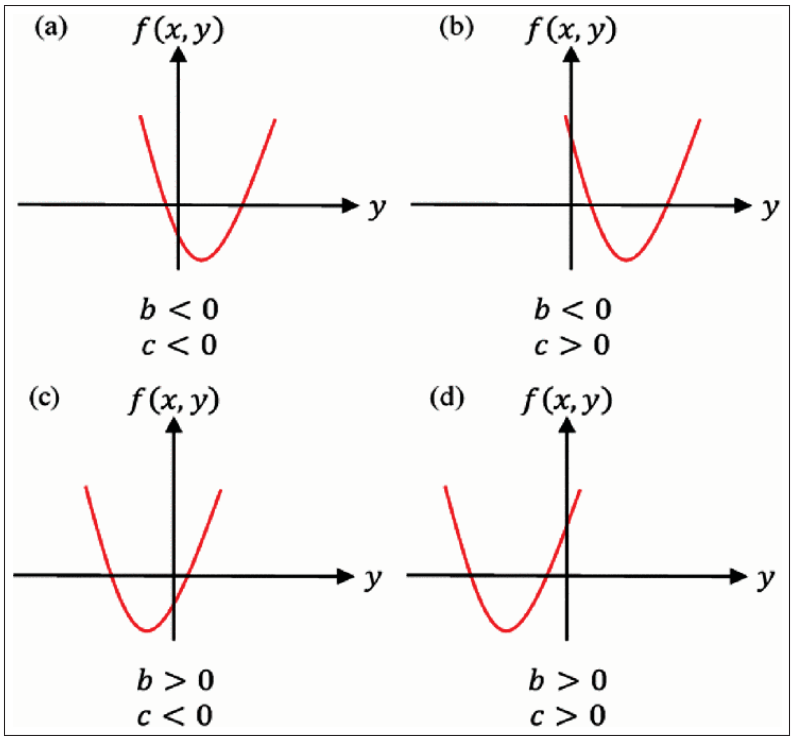

Figure-A II-3 Four possible cases for the solutions of (A II-31)

For values of X that *Delta* in (A II-32) is positive, using equations (A II-36a)–(A II-36d) we can find proper y (or Y) if it exists. Finally the calculated (X,Y) is accepted if they satisfy inequalities (A II-37) and (A II-38). Then UE_c's position, i.e. (X_c, Y_c), at points where R_R=R_C (or R_R=R_D) is calculated as follows:

$$X_c = -\frac{(X^2 - Y^2 - d_{ed}^2)}{2d_{ed}} \qquad \text{(A II-39)}$$

$$Y_c = \pm\sqrt{Y^2 - X_c^2} \qquad \text{(A II-40)}$$

4.2 Algorithm for developing the mode selection map

Based on the analytical solution for the mode selection map in part A, our mode selection map algorithm is as follows:

Calculate a_1, a_1', a_2, a_3, and a_4 using the equations in (A II-17)–(A II-21).

To draw the locus (A II-13), calculate a_5 as presented in (A II-22), and for locus (A II-12) substitute a_5 with a_1'.

If $a_4 < a_3$

Set $X_{dl} = 0$ and $X_{du} = \infty$.

Else

If $\frac{a_4\sqrt{a_5}}{2\sqrt{a_3(a_4-a_3)}} < 1$, there is no solution to $f(x,y) = 0$

If $1 < \frac{a_4\sqrt{a_5}}{2\sqrt{a_3(a_4-a_3)}} < a_1'$, set $X_{dl} = 0$ and $X_{du} = \sqrt[\alpha]{\frac{a_2a_4\sqrt{a_5}-2a_2\sqrt{a_3(a_4-a_3)}}{2a_1'\sqrt{a_3(a_4-a_3)}-a_4\sqrt{a_5}}}$.

If $a_1' < \frac{a_4\sqrt{a_5}}{2\sqrt{a_3(a_4-a_3)}}$, set $X_{dl} = 0$ and $X_{du} = \infty$.

End

If $X_{du} = \infty$

If $\sqrt{\frac{a_4a_5}{2a_3}} < 1$ and $a_1' > \sqrt{a_5}$, set $X_{du} = \sqrt[\alpha]{\frac{a_2(\sqrt{a_5}-1)}{a_1'-\sqrt{a_5}}} + r_M$

If $1 < \sqrt{\frac{a_4a_5}{2a_3}} < a_1'$ and $a_1' > \sqrt{a_5}$, set $X_{du} = \max\left(\sqrt[\alpha]{\frac{a_2(\sqrt{2a_3}-\sqrt{a_4a_5})}{\sqrt{a_4a_5}-a_1'\sqrt{2a_3}}}, \sqrt[\alpha]{\frac{a_2(\sqrt{a_5}-1)}{a_1'-\sqrt{a_5}}}\right) + r_M$

If $a_1' < \sqrt{\frac{a_4a_5}{2a_3}}$ and $a_1' > \sqrt{a_5}$, set $X_{du} = \sqrt[\alpha]{\frac{a_2(\sqrt{a_5}-1)}{a_1'-\sqrt{a_5}}} + r_C$

If $\sqrt{\frac{a_4a_5}{2a_3}} < 1$ or $a_1' < \sqrt{\frac{a_4a_5}{2a_3}}$, and $a_1' < \sqrt{a_5}$, set $X_{du} = r_C + r_M$

If $1 < \sqrt{\frac{a_4a_5}{2a_3}} < a_1'$ and $a_1' < \sqrt{a_5}$, set $X_{du} = \sqrt[\alpha]{\frac{a_2(\sqrt{2a_3}-\sqrt{a_4a_5})}{\sqrt{a_4a_5}-a_1'\sqrt{2a_3}}} + r_C$

End

Set $sz = 10^{-4}$

$X_d = X_{dl} : s : X_{du}$

For $n = 1 : length(X)$

Set $X = X_d(n)$

Find $sign(b)$ for X using the conditions presented in Section 4.1

Find $sign(c)$ for X using the conditions presented in Section 4.1

Set $x = \frac{1}{X^{\alpha}}$

Knowing $sign(b)$ and $sign(c)$, find proper y, if there is any, for x referring to (A II-36a)–(A II-36d)

If y exists, set $Y = \sqrt[\alpha]{1/y}$

If (X,Y) satisfy inequalities (A II-37) and (A II-38)

Calculate (X_c,Y_c) using (A II-39) and (A II-40)

Plot (X_c,Y_c)

end

end

In the next section, we use our algorithm to develop the mode selection map of example 5G networks.

5. Simulation Results

We evaluate the performance of the mode selection algorithm presented in previous section, for the network scenario from Fig.II-1 where there is one pair of D2D enabled UEs (UE_s and UE_d) and a cellular UE (UE_c). We assume that all the entities use a single antenna for their transmission/receiving. The parameter values used in the simulation are summarized in Table AII-1.

Positions of the UE_s and UE_d are assumed fixed as shown in Table AII-1. Using the algorithm presented in the previous section, first we develop the $X-Y$ curves for different P_cs, as shown in Fig.II-4 without considering the constraints (A II-37) and (A II-38). These constraints shown in Fig.II-4 as red dashed lines, cuts the curves into pieces, indicated by bold lines, of valid (X,Y)s.

Using the equations (A II-39) and (A II-40), we map the selected cuts to the contours which define the locus defined by (A II-12) and (A II-13). The results are shown in Fig.II-5.

Table-A II-1 Simulation Parameters

Parameter	**Value**
Cell radius (r_C)	1Km
Margin radius (r_M)	500m
UE_s's position (X_s,Y_s)	(250,250)
UE_d's position (X_d,Y_d)	(300,0)
Step size (sz)	1e-4m
UE's maximum power (P_{UE})	23 dBm
eNB's maximum power (P_{eNB})	46 dBm
P_s and P_d	P_{UE}
P_e	P_{eNB}
P_c	0.05 dBm to P_{UE} with steps = 0.05 dBm
Path-loss exponent (α)	3 (for urban area)
Shadow fading's standard deviation (v)	7 dB

In our simulation scenario we achieved $a_1' > a_5$ so we have $R_R > R_C$. This means that if UE_c moves from infinity toward eNB, as long as it is outside the locus defined by $R_R = R_D$, the transmission between UE_s and UE_d happens in reuse mode and as soon as it is inside the contour, the R_D would be larger than R_R. Therefore the mode between UE_s and UE_d changes from reuse to dedicated mode.

Another important aspect is the number of cuts on each curve, as illustrated in Fig.II-4. This number actually specifies the number of closed contours for a specific P_c, as illustrated in Fig.II-5. For example applying the algorithm for $R_R = R_D$, and $P_c = 0.05$, $P_c = 0.1$leads to a single cut on the curve, as shown in Fig.II-4, which maps to a single part contour in Fig.II-5. However for $P_c = 0.15$ and $P_c = 0.2$ there are two cuts on each curve for each P_c, which maps into a contour which consists of two closed parts.

Finally it can be seen from Fig.II-5 that increasing P_c extends the area of the region limited by a contour. This is because increasing P_c leads to an increase in the amount of interference from UE_c to UE_d in the reuse mode, which itself reduces R_R and causes $R_R = R_C$ and $R_R = R_D$ to happen in further distances.

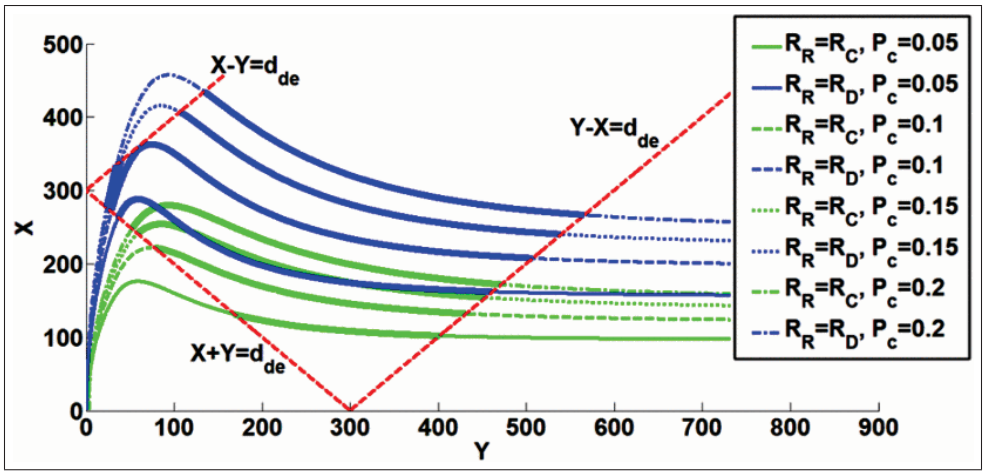

Figure-A II-4 X-Y curves without considering the constraints (A II-37) and (A II-38)

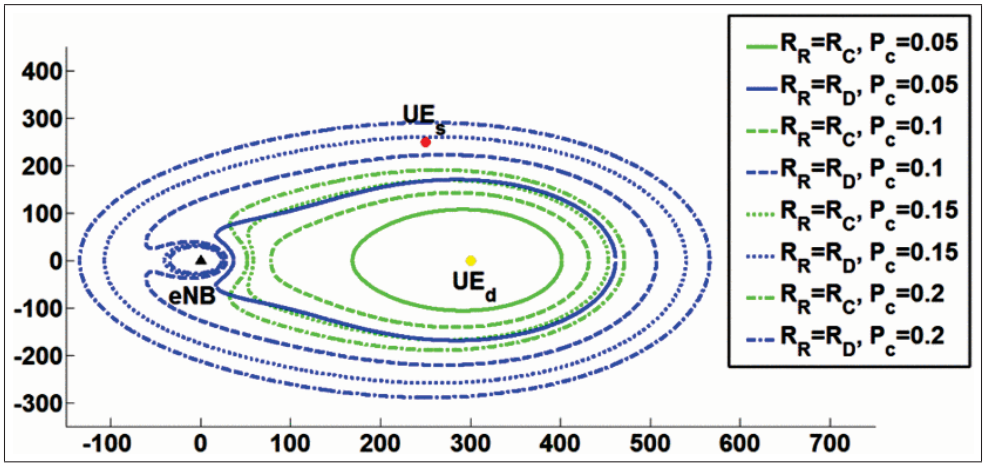

Figure-A II-5 TM selection map of a D2D enabled 5G network

6. Conclusions

In this paper, we first model the transmission between a pair of D2D enabled UEs in the reuse, dedicated, and cellular modes. Based on this model we develop an analytical approach to derive the mode selection map. Depending on the network parameters, there are several scenarios, each of which brings a subset of constraints and conditions for the variables and parameters of the problem. The exact solution to this problem for each scenario is discussed in the paper. Finally we present simulation results using the proposed analytical approach. We showed that the triangle inequality constraints affect the mode selection map by cutting the curves resulting

from the algorithm. These constraints can cut a specific curve into two pieces which maps into a contour consisting of two parts. Moreover we showed that increasing the transmission power of the cellular user extends the region limited by contour.

clicours.com

BIBLIOGRAPHY

3GPP. (1999). *3GPP TSG RAN WG2 TR 25.924 V0.1.0: on "opportunity driven multiple access (ODMA)"*.

3GPP. (2012). Global initiatives for M2M standardization. Consulted at http://www.3gpp.org/Global-Initiative-for-M2M.

Akyildiz, I. F., McNair, J., Ho, J. S. M., Uzunalioglu, H. & Wang, W. (1999). Mobility management in next-generation wireless systems. *Proceedings of the IEEE*, 87(8), 1347-1384. doi: 10.1109/5.775420.

Andrews, J. G., Buzzi, S., Choi, W., Hanly, S. V., Lozano, A., Soong, A. C. K. & Zhang, J. C. (2014). What will 5G be? *IEEE Journal on Selected Areas in Communications*, 32(6), 1065-1082. doi: 10.1109/JSAC.2014.2328098.

Asadi, A., Wang, Q. & Mancuso, V. (2014). A survey on device-to-device communication in cellular networks. *IEEE Communications Surveys Tutorials*, 16(4), 1801-1819. doi: 10.1109/COMST.2014.2319555.

Ashton, K. (2009). That 'internet of things' thing. *RFiD Journal*, 22(7), 97–114.

Bar-Noy, A., Kessler, I. & Sidi, M. (1994, Jun). Mobile users: to update or not to update? *INFOCOM '94. networking for global communications., 13th proceedings IEEE*, pp. 570-576 vol.2. doi: 10.1109/INFCOM.1994.337685.

Belleschi, M., Fodor, G. & Abrardo, A. (2011, Dec). Performance analysis of a distributed resource allocation scheme for D2D communications. *2011 ieee globecom workshops (gc wkshps)*, pp. 358-362. doi: 10.1109/GLOCOMW.2011.6162471.

Chandrasekhar, V., Andrews, J. G. & Gatherer, A. (2008). Femtocell networks: a survey. *IEEE Communications Magazine*, 46(9), 59-67. doi: 10.1109/MCOM.2008.4623708.

Chen, H. Y., Shih, M. J. & Wei, H. Y. (2015, Oct). Handover mechanism for device-to-device communication. *Standards for communications and networking (CSCN), 2015 IEEE conference on*, pp. 72-77. doi: 10.1109/CSCN.2015.7390423.

Cho, S., Jang, E. W. & Cioffi, J. M. (2009). Handover in multihop cellular networks. *IEEE Communications Magazine*, 47(7), 64-73. doi: 10.1109/MCOM.2009.5183474.

CISCO. (2015). Cisco Visual Networking Index: Global Mobile Data Traffic Forecast Update 2014-2019 White Paper.

Claussen, H., Ho, L. T. W. & Samuel, L. G. (2008). An overview of the femtocell concept. *Bell Labs Technical Journal*, 13(1), 221-245. doi: 10.1002/bltj.20292.

Cotton, S. L. (2015). Human body shadowing in cellular device-to-device communications: Channel modeling using the shadowed $\kappa - \mu$ fading model. *IEEE Journal on Selected Areas in Communications*, 33(1), 111-119. doi: 10.1109/JSAC.2014.2369613.

Cotton, S. L. (2016). Second-order statistics of $kappa - mu$ shadowed fading channels. *IEEE Transactions on Vehicular Technology*, 65(10), 8715-8720. doi: 10.1109/TVT.2015.2506260.

da S. Rêgo, M. G., Maciel, T. F., d. H. M. Barros, H., Cavalcanti, F. R. P. & Fodor, G. (2012, Aug). Performance analysis of power control for device-to-device communication in cellular MIMO systems. *2012 international symposium on wireless communication systems (ISWCS)*, pp. 336-340. doi: 10.1109/ISWCS.2012.6328385.

Dai, H., Molisch, A. F. & Poor, H. V. (2004). Downlink capacity of interference-limited mimo systems with joint detection. *IEEE Transactions on Wireless Communications*, 3(2), 442-453. doi: 10.1109/TWC.2003.821168.

Damnjanovic, A., Montojo, J., Wei, Y., Ji, T., Luo, T., Vajapeyam, M., Yoo, T., Song, O. & Malladi, D. (2011). A survey on 3GPP heterogeneous networks. *IEEE Wireless Communications*, 18(3), 10-21. doi: 10.1109/MWC.2011.5876496.

Doppler, K., Rinne, M., Wijting, C., Ribeiro, C. & Hugl, K. (2009). Device-to-device communication as an underlay to LTE-advanced networks. *Communications Magazine, IEEE*, 47(12), 42-49. doi: 10.1109/MCOM.2009.5350367.

Doppler, K., Yu, C.-H., Ribeiro, C. & Janis, P. (2010, April). Mode selection for device-to-device communication underlaying an LTE-advanced network. *Wireless communications and networking conference (wcnc), 2010 ieee*, pp. 1-6. doi: 10.1109/WCNC.2010.5506248.

Doppler, K., Ribeiro, C. B. & Janis, P. (2011). *Device-to-device communication in mobile and wireless communications for IMT-advanced and beyond (eds a. osseiran j. f. monserrat and w. mohr)*. John Wiley Sons, Ltd, Chichester, UK. doi: 10.1002/9781119976431.ch9.

ElSawy, H., Hossain, E. & Alouini, M. S. (2014). Analytical modeling of mode selection and power control for underlay D2D communication in cellular networks. *IEEE Transactions on Communications*, 62(11), 4147-4161. doi: 10.1109/TCOMM.2014.2363849.

Elshaer, H., Vlachos, C., Friderikos, V. & Dohler, M. (2016, May). Interference-aware decoupled cell association in device-to-device based 5G networks. *2016 IEEE 83rd vehicular technology conference (VTC spring)*, pp. 1-5. doi: 10.1109/VTCSpring.2016.7504298.

Feng, D., Lu, L., Yuan-Wu, Y., Li, G. Y., Feng, G. & Li, S. (2013, Dec). Optimal resource allocation for device-to-device communications in fading channels. *2013 IEEE global communications conference (GLOBECOM)*, pp. 3673-3678. doi: 10.1109/GLOCOM.2013.6831644.

Feng, D., Yu, G., Xiong, C., Yuan-Wu, Y., Li, G. Y., Feng, G. & Li, S. (2015). Mode switching for energy-efficient device-to-device communications in cellular networks. *IEEE Transactions on Wireless Communications*, 14(12), 6993-7003. doi: 10.1109/TWC.2015.2463280.

Fodor, G. & Reider, N. (2011, Dec). A distributed power control scheme for cellular network assisted D2D communications. *Global telecommunications conference (GLOBECOM 2011), 2011 IEEE*, pp. 1-6. doi: 10.1109/GLOCOM.2011.6133537.

Gruber, I. & Li, H. (2004, May). Cellular-ad hoc network interoperation for coverage extension. *Emerging technologies: Frontiers of mobile and wireless communication, 2004. proceedings of the IEEE 6th circuits and systems symposium on*, 2, 513-516 Vol.2. doi: 10.1109/CASSET.2004.1321938.

Gu, J., Bae, S. J., Choi, B.-G. & Chung, M. Y. (2011, June). Dynamic power control mechanism for interference coordination of device-to-device communication in cellular networks. *2011 third international conference on ubiquitous and future networks (ICUFN)*, pp. 71-75. doi: 10.1109/ICUFN.2011.5949138.

Halperin, D., Ammer, M. J., Anderson, T. E. & Wetherall, D. (2007). Interference cancellation: Better receivers for a new wireless MAC. *Hotnets*.

Huang, Y., Nasir, A. A., Durrani, S. & Zhou, X. (2016). Mode selection, resource allocation, and power control for D2D-enabled two-tier cellular network. *IEEE Transactions on Communications*, 64(8), 3534-3547. doi: 10.1109/TCOMM.2016.2580153.

Irmer, R., Droste, H., Marsch, P., Grieger, M., Fettweis, G., Brueck, S., Mayer, H. P., Thiele, L. & Jungnickel, V. (2011). Coordinated multipoint: Concepts, performance, and field trial results. *IEEE Communications Magazine*, 49(2), 102-111. doi: 10.1109/MCOM.2011.5706317.

Janis, P., Yu, C.-H., Doppler, K., Ribeiro, C., Wijting, C., Hugl, K., Tirkkonen, O. & Koivunen, V. (2009). Device-to-device communication underlaying cellular communications systems. *International Journal of Communications, Network and System Sciences*, Vol.02No.03, 10. doi: 10.4236/ijcns.2009.23019.

Jarray, C. & Giovanidis, A. (2016, May). The effects of mobility on the hit performance of cached D2D networks. *2016 14th international symposium on modeling and optimization in mobile, ad hoc, and wireless networks (WiOpt)*, pp. 1-8. doi: 10.1109/WIOPT.2016.7492958.

Kaufman, B. & Aazhang, B. (2008, Oct). Cellular networks with an overlaid device to device network. *2008 42nd asilomar conference on signals, systems and computers*, pp. 1537-1541. doi: 10.1109/ACSSC.2008.5074679.

Kaufman, B., Lilleberg, J. & Aazhang, B. (2013). Spectrum sharing scheme between cellular users and ad-hoc device-to-device users. *IEEE Transactions on Wireless Communications*, 12(3), 1038-1049. doi: 10.1109/TWC.2012.011513.120063.

Le, L. & Hossain, E. (2007). Multihop cellular networks: Potential gains, research challenges, and a resource allocation framework. *IEEE Communications Magazine*, 45(9), 66-73. doi: 10.1109/MCOM.2007.4342859.

Lee, D., Kim, S. I., Lee, J. & Heo, J. (2012, Oct). Performance of multihop decode-and-forward relaying assisted device-to-device communication underlaying cellular networks. *Information theory and its applications (ISITA), 2012 international symposium on*, pp. 455-459.

Lei, L., Zhong, Z., Lin, C. & Shen, X. (2012). Operator controlled device-to-device communications in LTE-advanced networks. *IEEE Wireless Communications*, 19(3), 96-104. doi: 10.1109/MWC.2012.6231164.

Li, P. & Guo, S. (2014). *Cooperative device-to-device communication in cognitive radio cellular networks*. Springer. doi: 10.1007/978-3-319-12595-4.

Li, Y., Li, J., Jiang, J. & Peng, M. (2013, Dec). Performance analysis of device-to-device underlay communication in Rician fading channels. *2013 IEEE global communications conference (GLOBECOM)*, pp. 4465-4470. doi: 10.1109/GLOCOMW.2013.6855654.

Liang, Y. C., Zeng, Y., Peh, E. C. Y. & Hoang, A. T. (2008). Sensing-throughput tradeoff for cognitive radio networks. *IEEE Transactions on Wireless Communications*, 7(4), 1326-1337. doi: 10.1109/TWC.2008.060869.

Lin, X., Ganti, R. K., Fleming, P. J. & Andrews, J. G. (2013). Towards understanding the fundamentals of mobility in cellular networks. *IEEE Transactions on Wireless Communications*, 12(4), 1686-1698. doi: 10.1109/TWC.2013.022113.120506.

Lin, Y.-D. & Hsu, Y.-C. (2000, Mar). Multihop cellular: a new architecture for wireless communications. *INFOCOM 2000. nineteenth annual joint conference of the IEEE computer and communications societies. proceedings. IEEE*, 3, 1273-1282 vol.3. doi: 10.1109/INFCOM.2000.832516.

Liu, Z., Peng, T., Chen, H. & Wang, W. (2012a, Dec). Optimal D2D user allocation over multibands under heterogeneous networks. *Global communications conference (GLOBECOM), 2012 IEEE*, pp. 1339-1344. doi: 10.1109/GLOCOM.2012.6503299.

Liu, Z., Peng, T., Lu, Q. & Wang, W. (2012b, June). Transmission capacity of D2D communication under heterogeneous networks with dual bands. *Cognitive radio oriented wireless networks and communications (CROWNCOM), 2012 7th international ICST conference on*, pp. 169-174.

Liu, Z., Peng, T., Xiang, S. & Wang, W. (2012c, June). Mode selection for device-to-device (d2d) communication under LTE-advanced networks. *Communications (icc), 2012 ieee international conference on*, pp. 5563-5567. doi: 10.1109/ICC.2012.6364738.

Mahmoud, M. E. & Shen, X. (2012). FESCIM: Fair, efficient, and secure cooperation incentive mechanism for multihop cellular networks. *IEEE Transactions on Mobile Computing*, 11(5), 753-766. doi: 10.1109/TMC.2011.92.

Middleton, G. B. & Lilleberg, J. (2007). An algorithm for efficient resource allocation in realistic wide area cellular networks. *The 10th international symposium on wireless personal multimedia communications (wpmc)*.

Min, H., Seo, W., Lee, J., Park, S. & Hong, D. (2011). Reliability improvement using receive mode selection in the device-to-device uplink period underlaying cellular networks. *IEEE Transactions on Wireless Communications*, 10(2), 413-418. doi: 10.1109/TWC.2011.122010.100963.

Mitola, J. & Maguire, G. Q. (1999). Cognitive radio: making software radios more personal. *IEEE Personal Communications*, 6(4), 13-18. doi: 10.1109/98.788210.

Morattab, A., Dziong, Z., Sohraby, K. & Islam, M. (2015, Oct). An optimal MIMO mode selection method for D2D transmission in cellular networks. *Wireless and mobile computing, networking and communications (WiMob), 2015 IEEE 11th international conference on*, pp. 392-398. doi: 10.1109/WiMOB.2015.7347989.

Morattab, A., Dziong, Z., Sohraby, K. & Islam, M. H. (2016, April). Mobility impact on mode selection map in D2D networks – an analytical approach. *2016 IEEE wireless communications and networking conference*, pp. 1-6. doi: 10.1109/WCNC.2016.7564729.

Mumtaz, S. & Rodriguez, J. (2014). *Smart device to smart device communication*. Springer. doi: 10.1007/978-3-319-04963-2.

Orsino, A., Gapeyenko, M., Militano, L., Moltchanov, D., Andreev, S., Koucheryavy, Y. & Araniti, G. (2015, Dec). Assisted handover based on device-to-device communications in 3GPP LTE systems. *2015 IEEE globecom workshops (GC Wkshps)*, pp. 1-6. doi: 10.1109/GLOCOMW.2015.7414095.

Osseiran, A., Doppler, K., Ribeiro, C., Xiao, M., Skoglund, M. & Manssour, J. (2009). Advances in device-to-device communications and network coding for IMT-advanced. *ICT Mobile Summit*.

Osseiran, A., Monserrat, J. F. & Mohr, W. (2011). *Mobile and wireless communications for IMT-advanced and beyond*. John Wiley & Sons.

Panagopoulos, A. D. (2015). *Handbook of research on next generation mobile communication systems*. IGI Global.

Papoulis, A. & Pillai, S. U. (2002). *Probability, random variables, and stochastic processes*. Tata McGraw-Hill Education.

Pekka Kyösti,Juha Meinilä, L. H. X. Z. T. J. C. S. M. N. M. M. A. H. J. Y. V.-M. H. M. A. R. B. Y. d. J. T. R. (2008). IST-4-027756 WINNER II D1.1.2 V1.2 WINNER II Channel Models. 82.

Peng, M., Li, Y., Quek, T. Q. S. & Wang, C. (2014). Device-to-device underlaid cellular networks under Rician fading channels. *IEEE Transactions on Wireless Communications*, 13(8), 4247-4259. doi: 10.1109/TWC.2014.2314115.

Phunchongharn, P., Hossain, E. & Kim, D. I. (2013). Resource allocation for device-to-device communications underlaying LTE-advanced networks. *IEEE Wireless Communications*, 20(4), 91-100. doi: 10.1109/MWC.2013.6590055.

Qiao, C. & Wu, H. (2000). iCAR: an integrated cellular and ad-hoc relay system. *Computer communications and networks, 2000. proceedings. ninth international conference on*, pp. 154-161. doi: 10.1109/ICCCN.2000.885485.

Qiao, C., Wu, H. & Tonguz, O. (2000). Load balancing via relay in next generation wireless systems. *Mobile and ad hoc networking and computing, 2000. MobiHOC. 2000 first annual workshop on*, pp. 149-150. doi: 10.1109/MOBHOC.2000.869231.

Raghothaman, B., Deng, E., Pragada, R., Sternberg, G., Deng, T. & Vanganuru, K. (2013, Jan). Architecture and protocols for LTE-based device to device communication. *Computing, networking and communications (ICNC), 2013 international conference on*, pp. 895-899. doi: 10.1109/ICCNC.2013.6504208.

Rappaport, T. S. et al. (1996). *Wireless communications: principles and practice*. Prentice Hall PTR New Jersey.

Rodziewicz, M. (2012, April). Network coding aided device-to-device communication. *European wireless, 2012. EW. 18th european wireless conference*, pp. 1-5.

Sadr, S. & Adve, R. S. (2015). Handoff rate and coverage analysis in multi-tier heterogeneous networks. *IEEE Transactions on Wireless Communications*, 14(5), 2626-2638. doi: 10.1109/TWC.2015.2390224.

Salem, M., Adinoyi, A., Rahman, M., Yanikomeroglu, H., Falconer, D., Kim, Y. D., Kim, E. & Cheong, Y. C. (2010). An overview of radio resource management in relay-enhanced OFDMA-based networks. *IEEE Communications Surveys Tutorials*, 12(3), 422-438. doi: 10.1109/SURV.2010.032210.00071.

Shen, Y., Zhou, W., Wu, P., Toni, L., Cosman, P. C. & Milstein, L. B. (2013, Dec). Device-to-device assisted video transmission. *2013 20th international packet video workshop*, pp. 1-8. doi: 10.1109/PV.2013.6691441.

Shin, S., Lee, U., Dressler, F. & Yoon, H. (2016). Analysis of cell sojourn time in heterogeneous networks with small cells. *IEEE Communications Letters*, 20(4), 788-791. doi: 10.1109/LCOMM.2016.2516003.

Sklar, B. (1997). Rayleigh fading channels in mobile digital communication systems. I. characterization. *Communications Magazine, IEEE*, 35(9), 136-146. doi: 10.1109/35.620535.

Song, L., Niyato, D., Han, Z. & Hossain, E. (2015). *Wireless device-to-device communications and networks*. Cambridge University Press. Consulted at http://dx.doi.org/10.1017/CBO9781107478732.

Tang, H. & Ding, Z. (2016). Mixed mode transmission and resource allocation for D2D communication. *Wireless Communications, IEEE Transactions on*, 15(1), 162-175. doi: 10.1109/TWC.2015.2468725.

Teh, Y. W., Newman, D. & Welling, M. (2007). A collapsed variational Bayesian inference algorithm for latent Dirichlet allocation. In Schölkopf, B., Platt, J. C. & Hoffman, T. (Eds.), *Advances in Neural Information Processing Systems 19* (pp. 1353–1360). MIT Press. Consulted at http://papers.nips.cc/paper/3113-a-collapsed-variational-bayesian-inference-algorithm-for-latent-dirichlet-allocation.pdf.

Tehrani, M. N., Uysal, M. & Yanikomeroglu, H. (2014). Device-to-device communication in 5G cellular networks: challenges, solutions, and future directions. *IEEE Communications Magazine*, 52(5), 86-92. doi: 10.1109/MCOM.2014.6815897.

Tse, D. & Viswanath, P. (2005). *Fundamentals of wireless communication*. Cambridge university press.

Wang, B., Chen, L., Chen, X., Zhang, X. & Yang, D. (2011, May). Resource allocation optimization for device-to-device communication underlaying cellular networks. *Vehicular technology conference (VTC spring), 2011 IEEE 73rd*, pp. 1-6. doi: 10.1109/VETECS.2011.5956157.

Wang, L. & Tang, H. (2016). *Device-to-device communications in cellular networks*. Springer.

Xiao, X., Tao, X. & Lu, J. (2011, Sept). A QoS-aware power optimization scheme in OFDMA systems with integrated device-to-device (D2D) communications. *Vehicular technology conference (VTC fall), 2011 IEEE*, pp. 1-5. doi: 10.1109/VETECF.2011.6093182.

Xu, X., Zhang, Y., Sun, Z., Hong, Y. & Tao, X. (2016). Analytical modeling of mode selection for moving D2D-enabled cellular networks. *IEEE Communications Letters*, 20(6), 1203-1206. doi: 10.1109/LCOMM.2016.2552171.

Yang, K., Wu, Y., Huang, J., Wang, X. & Verdu, S. (2008, April). Distributed robust optimization for communication networks. *INFOCOM 2008. the 27th conference on computer communications. IEEE*. doi: 10.1109/INFOCOM.2008.171.

Yilmaz, O. N. C., Li, Z., Valkealahti, K., Uusitalo, M. A., Moisio, M., Lundén, P. & Wijting, C. (2014, April). Smart mobility management for D2D communications in 5G networks. *Wireless communications and networking conference workshops (WCNCW), 2014 IEEE*, pp. 219-223. doi: 10.1109/WCNCW.2014.6934889.

Yu, C. H., Tirkkonen, O., Doppler, K. & Ribeiro, C. (2009a, April). On the performance of device-to-device underlay communication with simple power control. *Vehicular technology conference, 2009. VTC spring 2009. IEEE 69th*, pp. 1-5. doi: 10.1109/VETECS.2009.5073734.

Yu, C. H., Tirkkonen, O., Doppler, K. & Ribeiro, C. (2009b, June). Power optimization of device-to-device communication underlaying cellular communication. *2009 IEEE international conference on communications*, pp. 1-5. doi: 10.1109/ICC.2009.5199353.

Yu, C. H., Doppler, K., Ribeiro, C. B. & Tirkkonen, O. (2011). Resource sharing optimization for device-to-device communication underlaying cellular networks. *IEEE Transactions on Wireless Communications*, 10(8), 2752-2763. doi: 10.1109/TWC.2011.060811.102120.

Yu, G., Xu, L., Feng, D., Yin, R., Li, G. Y. & Jiang, Y. (2014). Joint mode selection and resource allocation for device-to-device communications. *IEEE Transactions on Communications*, 62(11), 3814-3824. doi: 10.1109/TCOMM.2014.2363092.

Yuan, G., Zhang, X., Wang, W. & Yang, Y. (2010). Carrier aggregation for LTE-Advanced mobile communication systems. *IEEE Communications Magazine*, 48(2), 88-93. doi: 10.1109/MCOM.2010.5402669.

Zhao, Y., Diggavi, S. N., Goldsmith, A. & Poor, H. V. (2012, Oct). Convex optimization for precoder design in mimo interference networks. *2012 50th annual allerton conference on communication, control, and computing (allerton)*, pp. 1213-1219. doi: 10.1109/Allerton.2012.6483356.

Zulhasnine, M., Huang, C. & Srinivasan, A. (2010, Oct). Efficient resource allocation for device-to-device communication underlaying LTE network. *2010 IEEE 6th international conference on wireless and mobile computing, networking and communications*, pp. 368-375. doi: 10.1109/WIMOB.2010.5645039.